Chemical Physics 565 (2023) 111766

Contents lists available at ScienceDirect

Chemical Physics

journal homepage: www.elsevier.com/locate/chemphys

Electron impact inelastic molecular processes for deuterated compounds

Smruti Parikh [a,*], Minaxi Vinodkumar [b], Chetan Limbachiya [a]

[a] The M. S. University of Baroda, Vadodara 390 001, India
[b] V.P. and R.P.T.P. Science College, Vallabh Vidyanagar 388 120, India

ARTICLE INFO

Keywords:
Electron Scattering
Spherical Complex Optical Potential
Complex Scattering Potential-ionisation contribution
Deuterated molecules
Ionisation

ABSTRACT

In this theoretical work, electron induced inelastic molecular processes for deuterated molecules HD, D_2, D_2O, SiD_x (x = 1–3), ND_x (x = 1–3) and CD_x (x = 2–4) are studied and quantified from ionisation threshold to 5 keV. The total inelastic cross section (Q_{inel}) are computed using Spherical Complex Optical Potential (SCOP) and total ionisation cross sections (Q_{ion}) and total electronic excitation cross sections ($\sum Q_{exc}$) have been evaluated through the Complex Spherical Potential – ionisation contribution (CSP-ic) method. Electron driven inelastic effects for deuterated hydrogen (HD) are investigated for the first time in this study. This is the first report of total Q_{ion} for HD, SiD_x (x = 1–3), ND_x (x = 1,2), CD_x (x = 2,3) molecules and maiden study of Q_{inel} and $\sum Q_{exc}$ for all these molecules. Further, isotope effect is studied for these targets and using various correlation analyses, dipole polarizability for ND and SiD_x (x = 1–3) molecules are predicted.

1. Introduction

A salient feature of deuterated compounds that without radioactivity they can be stable, allows them to play a prominent role and they become increasingly used in the fields of energy and military, mainly in nuclear weapons, DF-laser (deuterium-fluoride) weapons, nuclear energy industries, nuclear fusion research, high-power lasers, microwaves, cryogenic superconductivity, intense electron beam technology etc. Also, they are widely utilized as special applicable elements in fields of biomedical, agriculture, pharmaceutical, new material development research, chemical research, semiconductor industries, earth science, etc. [1].

The electron impact collisions with deuterated molecules is studied through elastic and inelastic processes. These processes include excitation processes, with shape, core excited and Feshbach resonances and Ramsauer-Townsend minimum at very low energies. The ionisation process dominates beyond the ionisation threshold. Estimation of the total cross sections plays an important role in a variety of applications such as, astrophysics, plasma physics, planetary sciences, radiation sciences etc. [2–5]. Therefore, for the present study some deuterated molecules, HD, D_2, D_2O, ND_x (x = 1–3), SiD_x (x = 1–3) and CD_x (x = 2–4) have been chosen because of their wide spread of applications in various fields as discussed below.

In planetary atmospheres and star formation HD and D_2, the singly and doubly deuterated hydrogen molecules, respectively are known to play a significant role. HD is the third most abounding molecule in the interstellar medium (ISM). Also, HD has been found to be present in the atmospheres of Jupiter, Saturn, Uranus, and Neptune [5]. HD and D_2 also are key materials in the tokamak edge plasmas [6–9]. So, the well-validated database of the cross-sections for electron interaction with HD and D_2 molecules are required to distil the understanding of various processes that occur in edge plasma of tokamak.

The "heavy water" molecule D_2O is an interesting 'sister' of conventional H_2O molecule [10]. Due to the broad technological application of D_2O molecule as a coolant in nuclear power plants, also used in NMR spectroscopy and chemical studies using synchrotron radiation, where D atoms are used in place of H atoms in some compounds, etc., has made us to find it as the crucial and fascinating compound. D_2O has been also detected in astronomical environment [11]. So, the study of electron collision with D_2O is needed to understand the processes that take place in the terrestrial environment. Besides being a special functional material, the lack of cross-section data inspired us to perform these calculations.

The effects linked with the de-passivation of the hot carrier effects (e.g., electrons) is the major weak point in silicon hydrogenated films. However, deuterium conditioning of semiconductor devices has been proven to be effective in decreasing those effects. Rather than hydrogen, when deuterium is used in passivation of the devices, drastic reduction in degradation of threshold voltage and transconductance are found, which in turn enhances the practical lifetime of the devices by factor of

* Corresponding author.
E-mail address: smruti.parikh84@gmail.com (S. Parikh).

https://doi.org/10.1016/j.chemphys.2022.111766
Received 6 September 2022; Received in revised form 1 November 2022; Accepted 3 November 2022
Available online 8 November 2022

Table 1
Literature survey relevant to present work (IE - ionisation energy).

Sr	Target	Quantity	Energy (eV)	Method of investigation	Reference
1	HD	–	–	–	–
2	D_2	Total Q_{ion}	IE-1000	Experimental method	Rapp *et.al.* [23]
			IE-500	Experimental method	Cowling and Fletcher [24]
			600–20000	Experimental (Condenser technique)	Schram *et.al.* [25]
3	D_2O	Parent Q_{ion}	IE-170	Experimental (crossed molecule-electron beam apparatus)	Märk and Egger [26]
			IE-120	Experimental (quadrupole mass-spectrometric technique)	Snegursky and Zavilopulo [10]
		Parent Q_{ion}, Partial Q_{ion}	IE-200	Experimental (Fast-neutral-beam-technique)	Tarnovsky *et. al.* [27]
		Partial and Total Q_{ion}	IE-1000	Experimental method	Straub *et.al.* [28a]
		Total Q_{ion}	15–150	Experimental method	N. Lj. Djuric *et al.* [28b]
4	ND_3	Parent Q_{ion}	IE-200	Experimental (Fast-neutral-beam-technique)	Tarnovsky *et. al.* [29]
		Total Q_{ion}	IE-1000	Theoretical (using DM formalism, BEB method and calculation of Saksena)	Rejoub *et.al.* [30]
		Partial Q_{ion}		Experimental method	
5	ND, ND_2	Partial Q_{ion}	IE-200	Experimental (Fast-neutral-beam-technique)	Tarnovsky *et. al.* [29]
6	SiD, SiD_2, SiD_3	Partial Q_{ion}	IE-200	Experimental (Fast-neutral-beam-technique)	Tarnovsky *et. al.* [31]
7	CD_4	Total Q_{ion}	600–20000	Experimental (Condenser technique)	Schram *et.al.* [32]
		Partial Q_{ion}	IE-200	Experimental (Fast-neutral-beam-technique)	Tarnovsky *et. al.* [33]
8	CD_2, CD_3	Partial Q_{ion}	IE-200	Experimental (Fast-neutral-beam-technique)	Tarnovsky *et. al.* [33]
				Experimental (Crossed-beams apparatus)	Baiocchi *et. al.* [34]

10–50 and offers the possibility to operate the semiconductor devices at higher voltages [12–14]. Thus, a systematic study of small clusters of Si and D (e.g. SiD_x (x = 1–3)) is required to attained detailed knowledge of deposition process of deuterated amorphous silicon films, which are generally produced by Chemical Vapour Deposition (CVD) processes.

The use of amorphous carbon materials containing deuterium offers optical waveguide devices with low loss light transmission at characteristic wavelengths, which are considered to be accepted standard for optical telecommunication frequencies. Amorphous deuterated carbon material is deposited by Plasma Enhanced Chemical Vapour Deposition (PECVD) processes, which utilizes volatile deutero-carbon precursors, e.g., CD_4 etc., [15]. Also, an extensive modelling of transport of hydrocarbon in divertor plasmas in tokamak needs a full database of cross-sections for all interaction processes influencing the fragmentation of hydrocarbons. Among all existing molecular ions, the family of deutero-methane CD_x (x = 1–4) plays a crucial role [16,17].

Table 2
Molecular properties of present targets.

Target	IE (eV)	**Bond length (A°)**	**Target**	**IE (eV)**	**Bond length (A°)**
HD	15.44 [48]	0.7410 [48]	SiD	07.89 [31]	–
D_2	15.47 [48]	0.7420 [48]	SiD_2	08.92 [31]	–
D_2O	12.64 [48]	0.9687 [49]	SiD_3	08.14 [31]	–
ND	13.49 [29]	1.0367 [50]	CD_2	10.40 [34]	–
ND_2	11.45 [48]	1.0240 [48]	CD_3	09.85 [33]	–
ND_3	10.08 [48]	1.0026 [48]	CD_4	12.51 [33]	–

Different isotopes of ammonia, including ND_3 has been observed in dense cores of clouds (Barnad 1 [18] and NGC 1333 [19]) in interstellar medium (ISM). In ISM towards young solar mass protostar IRAS16293 [20] and in prestellar core 16293E [21], ND has also been discovered [20]. Also, as the source of nitrogen atoms, ammonia is used for the fabrication of nitride films. But, due to advancement in semiconductor devices with deuterium, ND_3 is also being used in place of NH_3 [22].

Even though there is a stupendous interest in D-molecules within the science society, less work has been undertaken for electron interaction with these molecules, as can be seen from Table 1. This has triggered us to carry out this work throughout the broad energy spectrum.

2. Theoretical methodology

When the incoming electrons approach the target atom/molecule, loss or removal of the incident flux is occurred which encompasses into the inelastic processes in the presence of elastic ones. The probability of occurrence of these elastic and inelastic processes are calculated through the elastic cross-sections (Q_{el}) and inelastic cross-sections (Q_{inel}), respectively. To consider all the inelastic events taking place along with the elastic processes, complex potential termed as Spherical Complex Optical Potential (SCOP) [35,36] is formulated as,

$$V_{opt}(r, E_i) = (V_{static} + V_{exc} + V_{pol}) + iV_{abs} \quad (1)$$

The undistorted molecular charge cloud is measured by the static potential (V_{static}), which can be computed using the Hartree-Fock wave functions [42,43]. Also, the exchange effect, occurred between the incoming electrons and target electrons is considered by the exchange potential (V_{exc}). The target electron cloud is seen as the Fermi gas by Hara, where the complete wave function is anti-symmetrized and the exchange energy is calculated from all the momentum states up to the fermi level [44,45]. The polarisation potential (V_{pol}) accounts for the transitory deformation of the target charge cloud in the presence of the projectile electron, which is caused by induced multipole moments. V_{abs} is the absorption potential takes care of all the inelastic effects (mainly electronic excitations and ionizations) occurring during the collision event of projectile and target. The modified expression for V_{abs} used here is given by in a.u. as [39,46],

$$V_{abs}(E_i, r) = -\frac{1}{2}\rho(r)v_{loc}\sigma_{ee} \quad (2)$$

where v_{loc} is incident electron velocity and σ_{ee} being the mean cross-section for the collision taking place between the projectile and molecular target.

It is essential to represent the target charge density because all of these potentials are built using it. In order to construct the total $\rho(r)$ of the molecule under study, which is then fed to construct the optical potential, we introduced parameterized charge densities of constituent atoms through Hartree Fock wave functions [42] and used single-centre

(SC) approximation for HD, D_2, D_2O, and ND_x (x = 1–3) and modified additivity rule (MAR) for SiD_x (x = 1–3) and CD_x (x = 2–4). In the case of SC and MAR, the atomic charge densities are superimposed on the molecule's centre of mass. In Table 2, necessary molecular inputs are listed.

The SCOP formalism employs a partial wave method with a spherical approximation, leading to the complex phase shifts (δ_l) that contain the hallmark of the incident electron-molecule interaction. Now, to calculate the elastic and inelastic cross-sections, the complex scattering amplitude is employed from the scattering matrix $S_l(k)$ [37,51],

$$S_l(k) = \eta_l(k) exp(2iRe(\delta_l)) \quad (3)$$

Here, $\eta_l(k) = exp(-2Im(\delta_l))$ is called the inelasticity or absorption factor responsible for all the possible inelastic effects leading to the inelastic cross-section (Q_{inel}).

The quantity Q_{inel} can be partitioned into its two major parts, viz. all the allowed electronic excitations and ionization processes, such as.

$$Q_{inel}(E_i) = \sum Q_{exc}(E_i) + Q_{ion}(E_i) \quad (4)$$

where, $\sum Q_{exc}$ represents the sum of all possible electronic excitations and Q_{ion} represents the total ionizations induced by the projectiles. Among all the terms of cross-sections, Q_{ion} is the most applied one in the market. Hence, to calculate the Q_{ion}, complex scattering potential-ionization contribution (CSP-iC), a semi-empirical approach is employed [39,40]. The basis of this method is based on the fact that at higher energies the quantity $\sum Q_{exc}$, which arises mainly from low-lying dipole allowed transitions, decreases rapidly. For the projectile energy higher from the ionization energy (IE) of the target,

$$Q_{inel} \geq Q_{ion} \quad (5)$$

Which implies to the energy dependent ratio,

$$R(E_i) = \frac{Q_{ion}}{Q_{inel}} = 1 - C_1\left[\frac{C_2}{U+a} + \frac{\ln U}{U}\right] \quad (6)$$

With, $U = E_i/IE$. The dimensionless parameters C_1, C_2 and a are evaluated imposing the three conditions on the ratio,.$R(E_i)$

$$R(E_i) = \begin{cases} 0, for E_i \leq IE \\ R_P, for E_i = E_P \\ 1, for E_i \gg IE \end{cases} \quad (7)$$

At the target's ionization threshold energy, the inelastic channel starts to take place, which includes the allowed total ionization and summed electronic excitations. At higher projectile energies, however, ionization takes over and excitation cross sections decrease dramatically, as indicated by the last condition in Eq. (7). The second condition indicates that when the incoming energy reaches the value, E_P (energy value where the Q_{inel} have its maxima), the ratio $R(E_i) = R_P$ will be in between 0.7 and 0.8 as found from both the theoretical and experimental [37,52–56] results of the stable target systems. This aspect introduces uncertainty of 10–15 % and gives the theory a semi-empirical character [37,38,41,56,57]. Computation of Eq. (7) allows to calculate the Q_{ion} and $\sum Q_{exc}$ [39,47].

3. Results and discussion

Here, we report the probability of three main inelastic events during electron collisions with D-molecules through calculation of the cross-section data, i.e., Q_{inel} (for total inelastic effects), Q_{ion} (for total ionisation effects) and $\sum Q_{exc}$ (for total electronic excitation effects) for families of deuterated compounds viz., HD, D_2, D_2O, ND_x (x = 1–3), SiD_x (x = 1–3) and CD_x (x = 2–4) along with comparisons with other work wherever available in Section 3.1. We further report the isotope effect in Section 3.2 and correlation of Q_{ion} with dipole polarizability (α) in Section 3.3 leading to prediction of α for ND and SiD_x (x = 1–3) which is not available in literature.

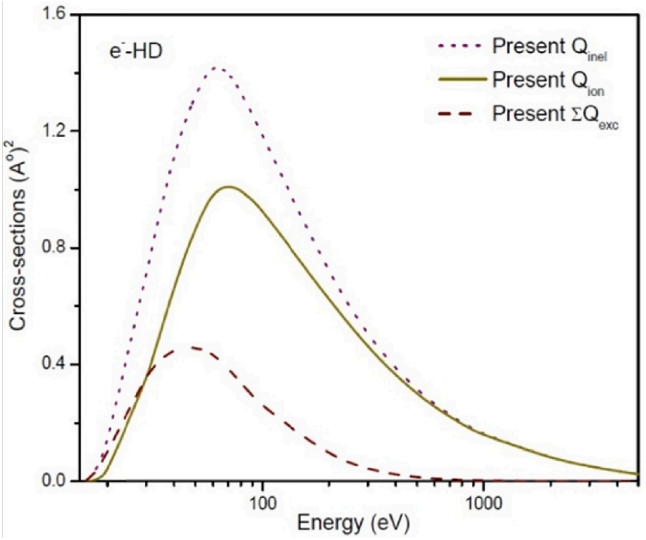

Fig. 1. E^--HD collision cross-section data. Dots: Present Q_{inel}; Solid: Present total Q_{ion}; Dash: Present $\sum Q_{exc}$.

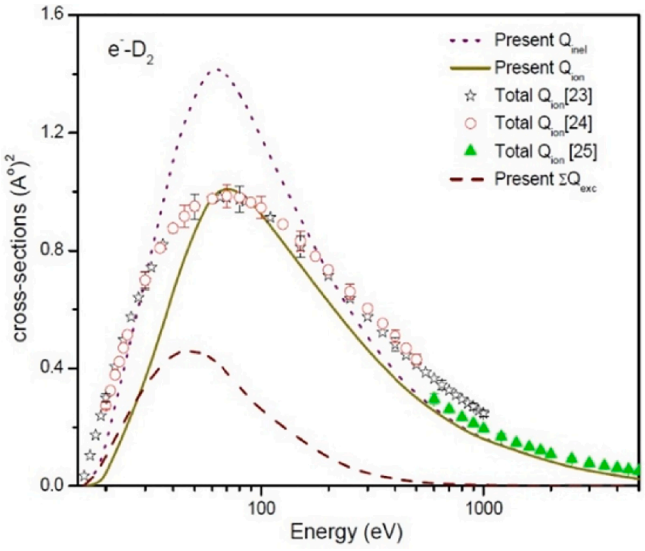

Fig. 2. E^--D_2 collision cross-section data. Dot: Present Q_{inel}; Solid: Present total Q_{ion}; Stars: total Q_{ion} [23]; Open circles: total Q_{ion} [24]; Filled triangle: total Q_{ion} [25]; Dash: Present $\sum Q_{exc}$.

3.1. Inelastic effects

Figs. 1 and 2 show the plots of the cross-section data against incident electron energy (E_i) ranging from IE to 5000 eV for the molecules HD and D_2, respectively. The upper most and the lower most curves in both the figures shows the Q_{inel} and $\sum Q_{exc}$ for HD and D_2 molecules, respectively. To the best of our knowledge, this is the maiden attempt to report cross-section data for HD molecule. In Fig. 1, present total Q_{ion} data for the electron collision with HD molecule is plotted. There is also a void for the theoretical cross-section data for the electron impact on D_2 molecule. Rapp and Englander-Golden [23], Cowling and Fletcher [24], Schram *et.al.* [25], reported the total ionisation cross-section data for D_2 molecule experimentally. At the peak region, our Q_{ion} data shows good agreement with the data of Rapp and Englander-Golden [23], and Cowling and Fletcher [24]. At higher energy regime, the present total Q_{ion} matches well with the experimental results of Schram *et.al.* [25]. Yoon *et.al.* [58] also has reviewed the cross-section data for HD and D_2.

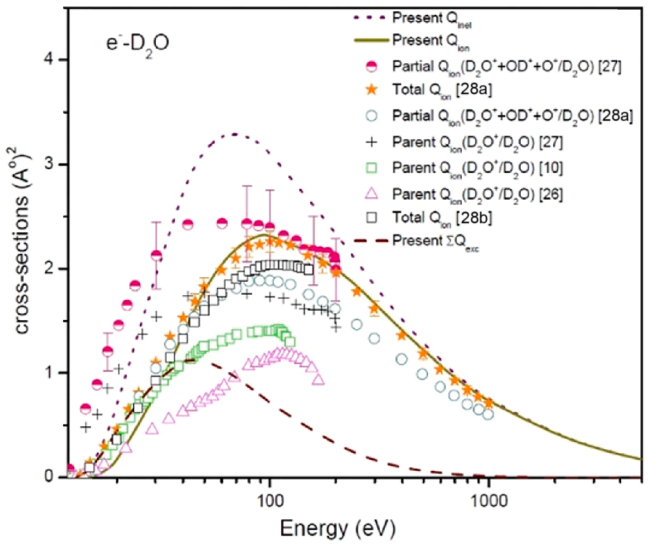

Fig. 3. E^--D_2O collision cross-section data. Dots: Present Q_{inel}; Solid: Present total Q_{ion}; Half-filled circles: Partial Q_{ion} (D_2O^++OD^++O^+/D_2O) [27]; Filled stars: Total Q_{ion} [28]; Open circles: Partial Q_{ion} (D_2O^++OD^++O^+/D_2O) [28a]; Plus: Parent Q_{ion} (D_2O^+/D_2O) [27]; Open squares: Parent Q_{ion} (D_2O^+/D_2O) [10]; Open triangle: Parent Q_{ion} (D_2O^+/D_2O) [26]; Open square: Total Q_{ion} [28b]; Dash: Present $\sum Q_{exc}$.

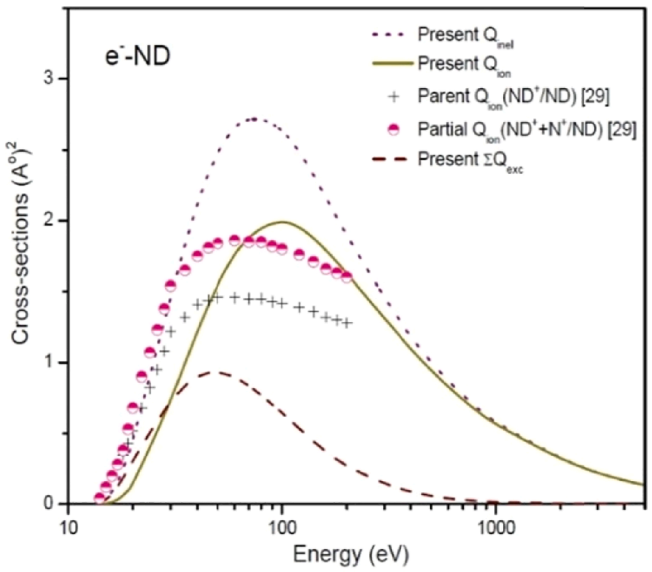

Fig. 4. E^--ND collision cross-section data. Dots: Present Q_{inel}; Solid: Present total Q_{ion}; Plus: Parent Q_{ion} (ND^+/ND) [29]; Half-filled circles: Partial Q_{ion} (ND^++N^+/ND) [29]; Dash: Present $\sum Q_{exc}$.

In Fig. 3, the present cross-sections for D_2O molecule are shown along with the available experimental data. No theoretical cross-section data are available for this molecule. An excellent agreement between the present total Q_{ion} and the experimental total Q_{ion} of Straub *et.al.* within the quoted uncertainty of 4.5 % can be seen in Fig. 3 [28a]. The experimental results for total Q_{ion} using parallel plate ionization chamber, measured by N. J. Djuric *et.al.* [28b] is observed to be of lower values compared to present one at the peak region. The good matching is found at the lower energy regime. The partial Q_{ion} (D_2O^++OD^++O^+/D_2O) was measured by Straub *et.al.* [28a] and Tarnovsky *et.al.* [27]. Present Q_{ion} compares well around the peak value with the partial Q_{ion} of Tarnovsky *et.al.* [27] measured within 15 % uncertainty, whereas partial Q_{ion} [28a] data underestimates the present Q_{ion} since the present

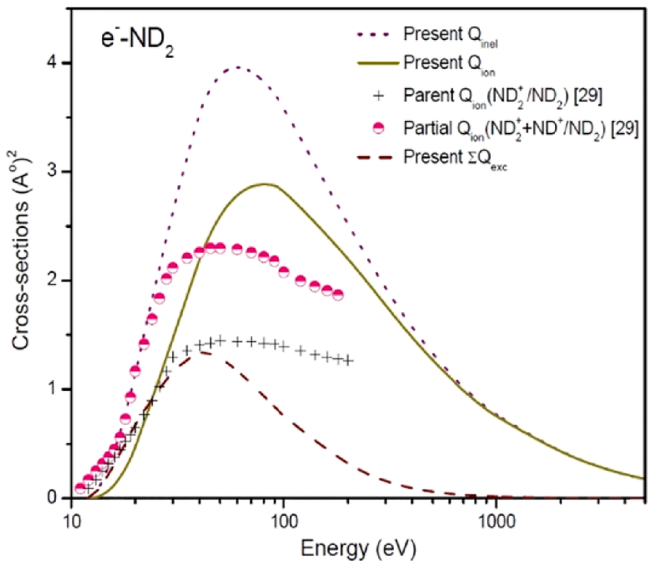

Fig. 5. E^--ND_2 collision cross-section data. Dots: Present Q_{inel}; Solid: Present total Q_{ion}; Plus: Parent Q_{ion} (ND_2^+/ND_2) [29]; Half-filled circles: Partial Q_{ion} (ND_2^++ND^+/ND_2) [29]; Dash: Present $\sum Q_{exc}$.

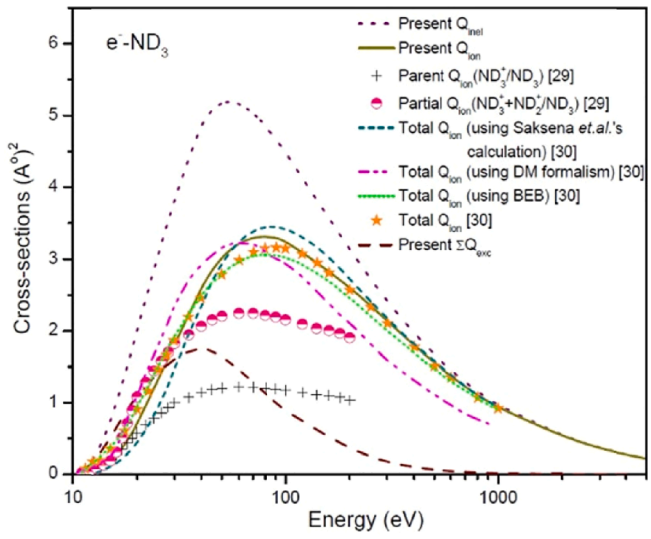

Fig. 6. E^--ND_3 collision cross-section data. Dots: Present Q_{inel}; Solid: Present total Qion; Plus: Parent Q_{ion} (ND_3^+/ND_3) [29]; Half-filled circles: Partial Q_{ion} (ND_3^++ND_2^+/ND_3) [29]; Short Dash line: Total Q_{ion} (Saksena et.al.) [30]; Dash-Dot-Dot line: Total Q_{ion} (DM formalism) [30]; Short Dot line: Total Q_{ion} (BEB method) [30]; Filled stars: Total Q_{ion} [30]; Dash: Present $\sum Q_{exc}$.

total Q_{ion} includes all ionisation channels. Märk and Egger [26], Tarnovsky *et.al.* [27], Snegursky and Zavilopulo [10] measured the absolute parent ionisation cross-sections (D_2O^+/D_2O). All these absolute parent Q_{ion} (D_2O^+/D_2O) [10,26,27] are lower than present Q_{ion}, as expected. The total Q_{inel} and $\sum Q_{exc}$ using present methodology is also plotted in Fig. 3 for which no comparison is available.

Figs. 4, 5 and 6 display the present Q_{inel}, total Q_{ion} and $\sum Q_{exc}$ data for the ND_x (x = 1–3) molecules respectively along with the available comparisons. Here, also there is a scarcity of the theoretical and experimental cross-section data for ND and ND_2 radicals. Only Tarnovsky *et.al.* [29] measured the absolute parent (ND^+/ND and ND_2^+/ND_2) and partial (ND^++N^+/ND and ND_2^++ND^+/ND_2) ionisation cross-sections for ND and ND_2 radicals shown in Figs. 4 and 5, respectively. The partial Q_{ion} shown in Figs. 4 and 5 are obtained by summing the

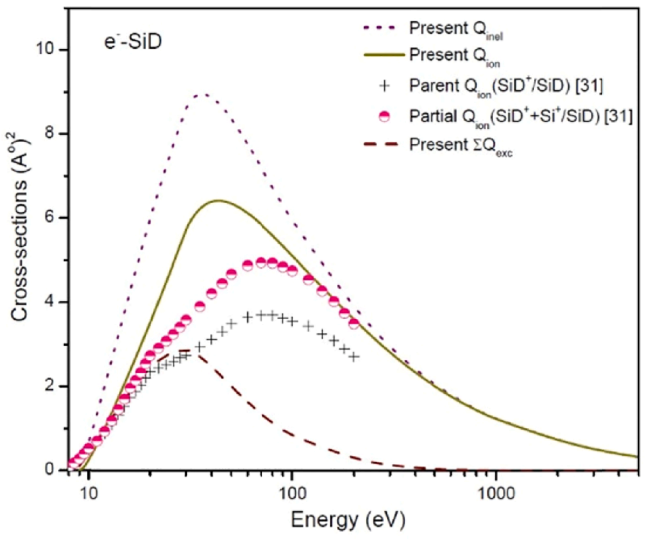

Fig. 7. e^--SiD collision cross-section data. Dots: Present Q_{inel}; Solid: Present total Q_{ion}; Plus: Parent Q_{ion} (SiD^+/SiD) [31]; Half-filled circles: Partial Q_{ion} ($SiD^+ + Si^+/SiD$) [31]; Dash: Present $\sum Q_{exc}$.

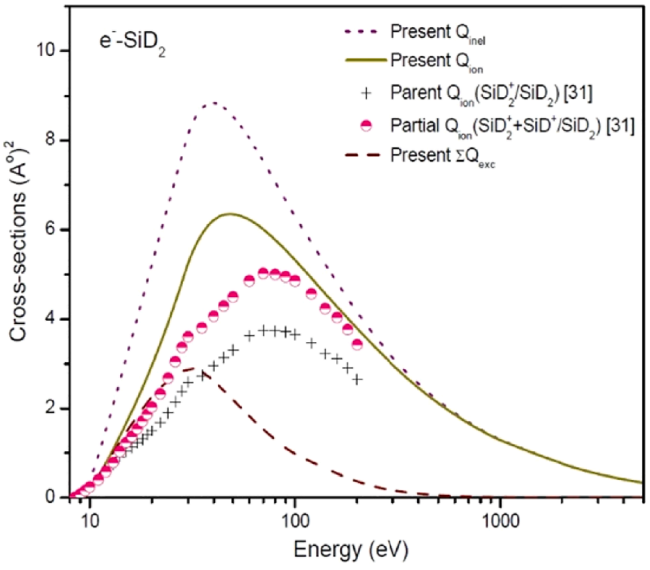

Fig. 8. e^--SiD_2 collision cross-section data. Dots: Present Q_{inel}; Solid: Present total Q_{ion}; Plus: Parent Q_{ion} (SiD_2^+/SiD_2) [31]; Half-filled circles: Partial Q_{ion} ($SiD_2^+ + SiD^+/SiD_2$) [31]; Dash: Present $\sum Q_{exc}$.

absolute Q_{ion} data for ND^+ and N^+ fragment ions from ND radical and ND_x^+ (x = 1,2) fragment ions from ND_2 radical [29]. All these partial Q_{ion} and parent Q_{ion} data show lower values than that of present total Q_{ion} data as expected.

Fig. 6 reports the cross-sections data for ND_3 molecule. Rejoub *et.al.* [30] measured the absolute partial and parent ionisation cross-section data for the formation of different fragment ions from ND_3 parent molecule. They are not shown in Fig. 6 to maintain the brevity. Also, total Q_{ion} was measured and reported by them [30]. Theoretically Q_{ion} was reported using the calculations of Saksena *et.al.* [30], Deutsch-Märk formalism [30] and Binary-encounter-Bethe model by Rejoub *et.al.* [30]. Our Q_{ion} data shows excellent matching with the experimental and theoretical data of Rejoub *et.al.* [30] throughout the energy range of present study. The measured absolute parent (ND_3^+/ND_3) and partial Q_{ion} ($ND_3^+ + ND_2^+/ND_3$) (which was obtained by summing the two absolute single Q_{ion} data for the formation of ND_x^+ (x = 2–3) fragment ions

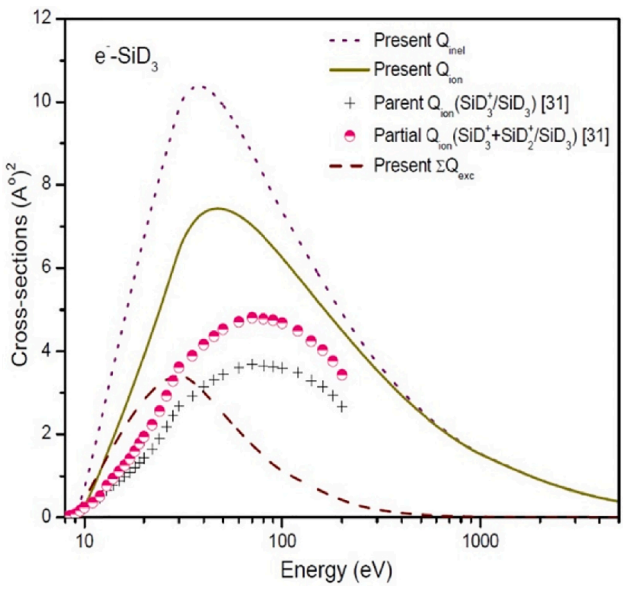

Fig. 9. e^--SiD_3 collision cross-section data. Dots: Present Q_{inel}; Solid: Present Q_{ion}; Plus: Parent Q_{ion} (SiD_3^+/SiD_3) [31]; Half-filled circles: Partial Q_{ion} ($SiD_3^+ + SiD_2^+/SiD_3$) [31]; Dash: Present $\sum Q_{exc}$.

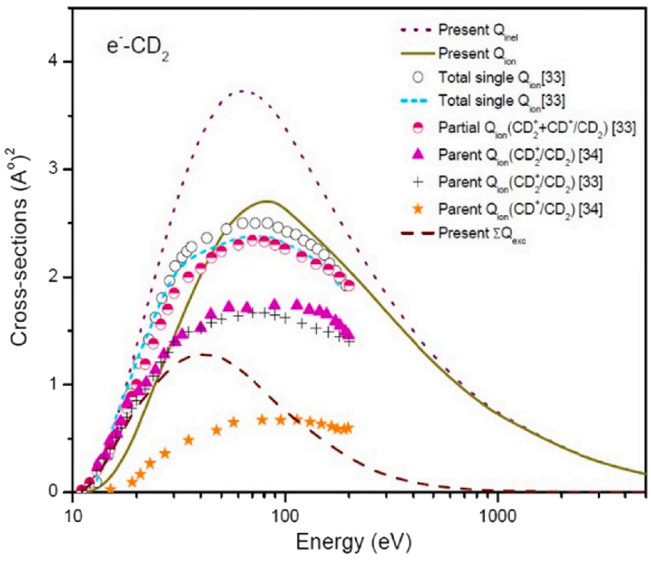

Fig. 10. e^--CD_2 collision cross-section data. Dots: Present Q_{inel}; Solid: Present Q_{ion}; Open circle: Total single Q_{ion} [33]; Short Dash line: Total single Q_{ion} [33]; Half-filled circles: Partial Q_{ion} ($CD_2^+ + CD^+/CD_2$) [33]; Filled triangles: Parent Q_{ion} (CD_2^+/CD_2) [34]; Plus: Parent Q_{ion} (CD_2^+/CD_2) [33]; Filled stars: Parent Q_{ion} (CD^+/CD_2) [34]; Dash: Present $\sum Q_{exc}$.

from ND_3 parent molecule) data of Tarnovsky *et.al.* [29] underestimates the present total Q_{ion} data, as expected.

In Figs. 7, 8 and 9, we report the present calculated Q_{inel}, Q_{ion} and $\sum Q_{exc}$ cross-sections for SiD_x (x = 1–3) molecules, respectively. This is the maiden attempt for reporting the cross-section data for SiD_x (x = 1–3) molecules. The lone measurement of absolute parent (SiD^+/SiD, SiD_2^+/SiD_2 and SiD_3^+/SiD_3) and partial Q_{ion} ($SiD^+ + Si^+/SiD$, $SiD_2^+ + SiD^+/SiD_2$ and $SiD_3^+ + SiD_2^+/SiD_3$) for the formation of SiD_x^+ (x = 1–3) and Si^+ fragment ions from SiD_x (x = 1,2,3) molecules reported by Tarnovsky *et. al.* [31]. The partial Q_{ion} data [31] for SiD (summation of absolute single Q_{ion} for the formation of $SiD^+ + Si^+$ fragments from SiD), SiD_2 (summation of absolute single Q_{ion} for the formation of $SiD_2^+ + SiD^+$ from SiD_2) and SiD_3 (summation of absolute single Q_{ion} for the formation of

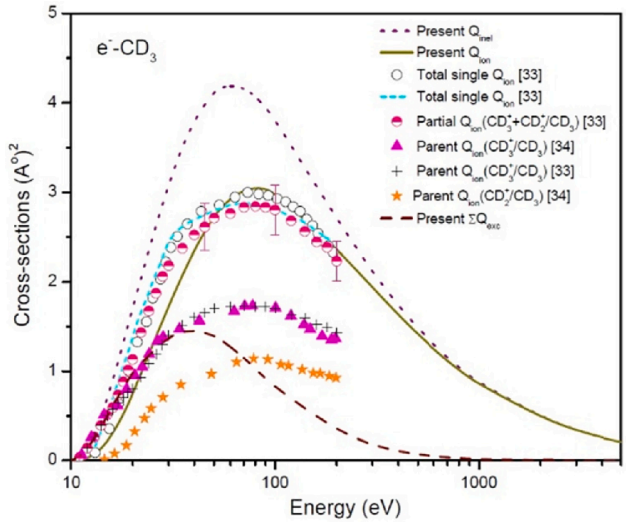

Fig. 11. e^--CD_3 collision cross-section data. Dots: Present Q_{inel}; Solid: Present total Q_{ion}; Open circle: Total single Q_{ion} [33]; Short Dash line: Total single Q_{ion} [33]; Half-filled circles: Partial Q_{ion} (CD_3^++CD_2^+/CD_3) [33]; Filled triangles: Parent Q_{ion} (CD_3^+/CD_3) [34]; Plus: Parent Q_{ion} (CD_3^+/CD_3) [33]; Filled stars: Parent Q_{ion} (CD_2^+/CD_3) [34]; Dash: Present $\sum Q_{exc}$.

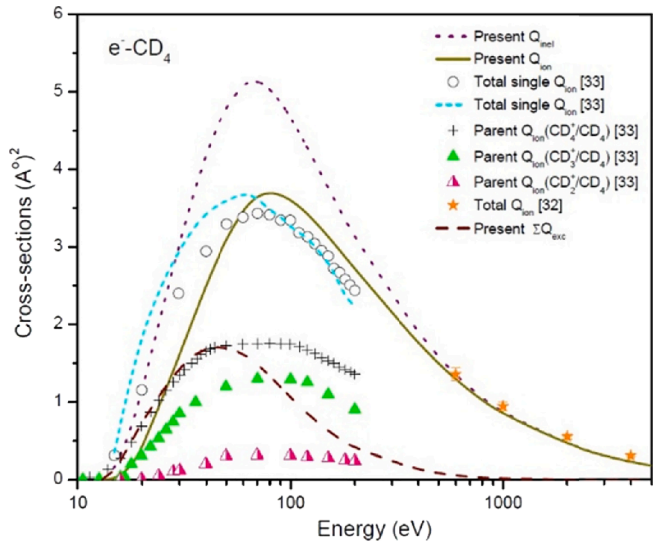

Fig. 12. e^--CD_4 collision cross-section data. Dots: Present Q_{inel}; Solid: Present total Q_{ion}; Open circle: Total single Q_{ion} [33]; Short Dash line: Total single Q_{ion} [33]; Plus: Parent Q_{ion} (CD_4^+/CD_4) [33]; Filled triangles: Parent Q_{ion} (CD_3^+/CD_4) [34]; Half-filled triangle: Parent Q_{ion} (CD_2^+/CD_4) [33]; Filled stars: Total Q_{ion} [32]; Dash: Present $\sum Q_{exc}$.

SiD_3^++SiD_2^+) [31] is also compared with the present Q_{ion} data. The present Q_{ion} data, because of encompassing all possible ionisation processes, overestimate the partial Q_{ion} and absolute parent Q_{ion} of Tarnovsky *et.al.* [31] for SiD_x (x = 1–3) molecules.

Figs. 10, 11 and 12, show the plots of the cross-section data for the CD_x (x = 2–4) molecules respectively for the energy ranging from IE to 5000 eV. There is a void for the cross-section data for these molecules. There are no total Q_{ion} data reported for CD_2 and CD_3 radicals as per our literature survey (Table 1). The absolute partial Q_{ion} (CD_2^++CD^+/CD_2 and CD_3^++CD_2^+/CD_3) for the formation of CD_x^+ (x = 1–2) from CD_2 radical and CD_x^+ (x = 2,3) from CD_3 radical were reported by Tarnovsky *et.al.* [33] and Baiochhi *et.al.* [34] experimentally. In Figs. 10 and 11, presently calculated total Q_{ion} is shown along with the partial and parent Q_{ion} data of Tarnovsky *et.al.* [33] and Baiochhi *et.al.* [34] for CD_2 and CD_3 radicals, respectively. Tarnovsky *et.al.* [33] also reported the total single Q_{ion} (measured partial Q_{ion} were added by them) for CD_2 and CD_3 radicals both theoretically and experimentally. We found these values of total single Q_{ion} close to present Q_{ion}. As noted by Tarnovsky *et.al.* [21] the cross section of formation of multiply charged parent or fragment ions are lower as compared with those of singly charged parent/fragment ions.

Therefore, the sum of cross section of all singly charged ions which is total single Q_{ion} is comparable with present total Q_{ion}. Partial Q_{ion} data for CD_2 (CD_2^++CD^+/CD_2), CD_3 (CD_3^++CD_2^+/CD_3) are also compared with the present one. All the absolute parent Q_{ion} and partial Q_{ion} data are of lower values than that of present total Q_{ion}.

Fig. 12 shows the plot of the cross-sections data for CD_4 molecule. The only measurement for absolute total Q_{ion} of CD_4 is done by Schram *et.al.* [32] experimentally for the energy range 600–20000 eV. Their data shows very good agreement with present Q_{ion} data. Tarnovsky *et.al.* [33] measured the absolute parent Q_{ion} for the formation of CD_x^+ (x = 2,3,4) fragment ions from CD_4 experimentally. We have plotted our results of total Q_{ion} against three varieties of parent Q_{ion} [33] in Fig. 12. As expected, all these parent Q_{ion} [33] are lower than our present total Q_{ion}. They also reported total single Q_{ion} experimentally as well as theoretically for CD_4 [33] and both of which compare well with present total Q_{ion} as specially in the peak region, as predicted by Tarnovsky *et.al.* [21].

Table 3
Ratio of Q_{ion} for deuterated and corresponding protonated molecules.

E_i (eV)	D_2/H_2	D_2O/H_2O	ND_3/NH_3	SiD_3/SiH_3	CD_4/CH_4
9	–	–	–	0.9231	–
11	–	–	1.0000	0.9932	–
13	–	0/0	1.0000	0.9968	0/0
16	0/0	1.0000	0.9943	0.9982	1.1194
18	1.0000	0.9987	0.9951	0.9983	1.0697
20	0.9394	1.0000	0.9945	0.9984	1.0537
60	0.9917	1.0027	0.9952	0.9995	1.0143
100	0.9942	1.0012	0.9967	0.9998	1.0104
500	0.9966	0.9992	0.9981	0.9996	1.0089
1000	0.9937	0.9986	0.9979	0.9993	1.0072
5000	1.0000	1.0000	1.0000	1.0000	1.0055

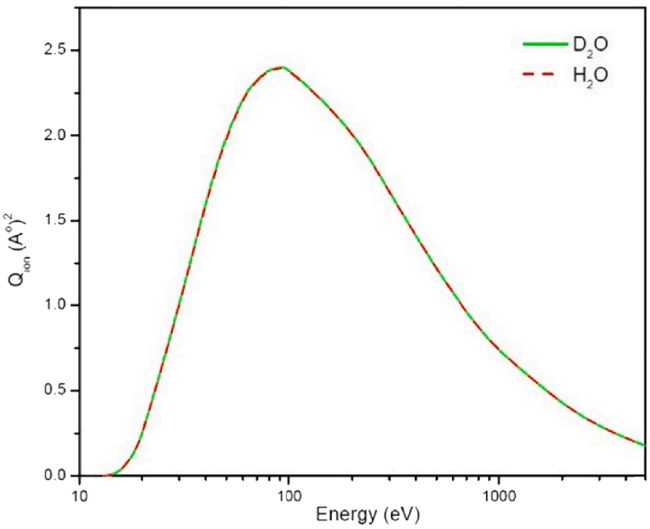

Fig. 13. Comparison of Q_{ion} between D_2O and H_2O.

3.2. Isotope effect

In this sub-section, we attempt to see the isotope effect for the electron driven ionisation process which is an applied quantity. In order

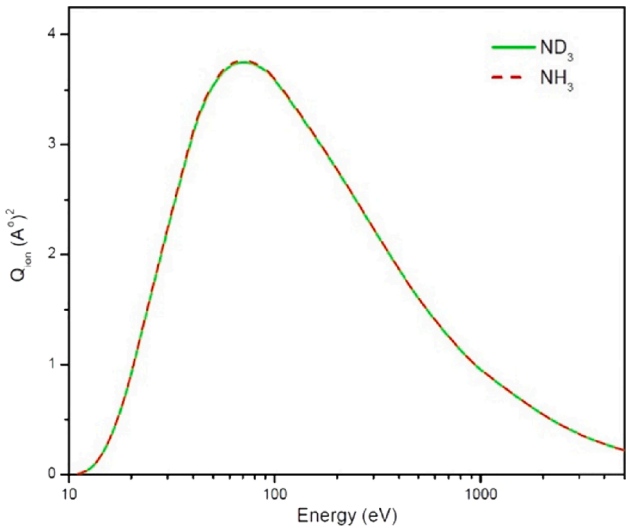

Fig. 14. Comparison of Q_{ion} between ND_3 and NH_3.

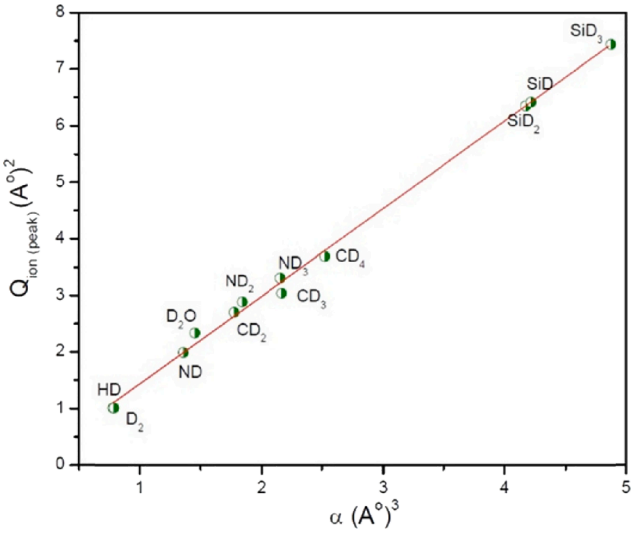

Fig. 15. Correlation between Q_{ion} (peak) and polarizability α.

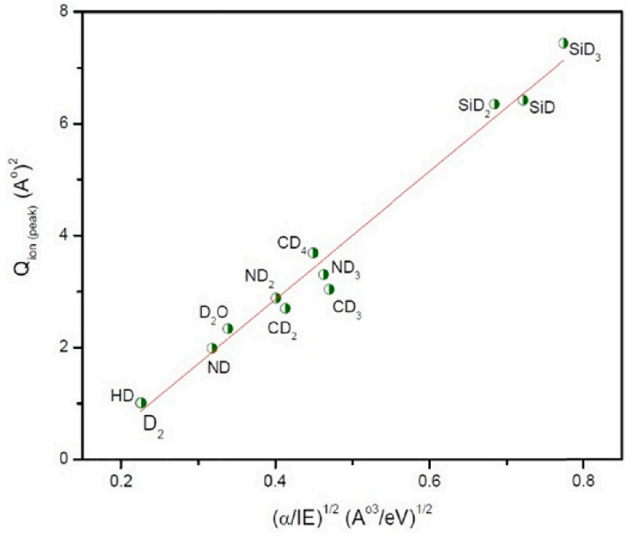

Fig. 16. Correlation between Q_{ion} (peak) and. $\sqrt{\alpha/IE}$

Table 4
Dipole polarizability (α).

Target	Available α $(A^o)^3$	Predicted α in this work $(A^o)^3$
HD	0.7910 [48]	–
D_2	0.7830 [48]	–
D_2O	1.4530 [48]	–
ND	–	1.3589
ND_2	1.8420 [48]	–
ND_3	2.1580 [48]	–
SiD	–	4.2157
SiD_2	–	4.1719
SiD_3	–	4.8701
CD_2	1.7750 [60]	–
CD_3	2.1700 [60]	–
CD_4	2.5230 [48]	–

to study this effect, we have computed Q_{ion} for H_2, H_2O, NH_3, SiH_3 and CH_4 and compared with the Q_{ion} for their deuterated counterpart. We display in Table 3 the ratio of Q_{ion} for deuterated to protonated molecules.

The Q_{ion} is sensitive to the size of the molecular charge cloud through number of electrons and the first ionisation energy. We observe that Q_{ion} does not depend on isotopes. This is expected since the computation involves the electronic charge density and the first ionisation energy. We note that the first ionisation energies for these deuterated molecules and their protonated counterparts are nearly the same. For the clear insight, the comparison of Q_{ion} values for D_2O and H_2O are shown in Fig. 13 and for ND_3 and NH_3 are shown in Fig. 14.

3.3. Prediction of polarizability from Q_{ion}

We have studied the correlation between the maximum Q_{ion} and the polarizability (α) for the present targets. In Fig. 15 the linear relationship between Q_{ion} (peak) and α can be seen as proposed by Harland and Vallance [59] with the following fitting equation,

$$Q_{ion}(peak) = 1.5510\alpha - 0.1178 (R^2 = 0.9968)$$

In Fig. 16, the maximum Q_{ion} is plotted against $\sqrt{\alpha/IE}$; the least squares fit shows a good degree of correlation with

$$Q_{ion}(peak) = 11.4475\sqrt{\alpha/IE} - 1.7195 (R^2 = 0.9813)$$

These correlations enabled us to predict the polarizability of ND, SiD, SiD_2 and SiD_3 molecules which is not available in literature to the best of our information (Table 4).

4. Conclusion

In this work of electron interactions with some deuterated molecules viz. HD, D_2, D_2O, ND_x (x = 1–3), SiD_x (x = 1–3) and CD_x (x = 2–4) we focussed on inelastic processes owing to their wide spread of applications in various fields of technology and applied sciences. We calculated various total cross sections, Q_{inel}, Q_{ion} and $\sum Q_{exc}$ for a wide energy starting from ionisation energy (IE) to 5000 eV using SCOP and CSP-ic method. Looking into previous work, we observed that experimental results for parent and partial Q_{ion} are reported for most of these molecules up to only 200 eV. Total Q_{ion} is available for D_2 and CD_4 by Schram *et.al.* [25,32] only for energy 600–20000 eV and hence, they have missed the important peak of Q_{ion}. Also, for D_2O experimental and for ND_3 experimental and theoretical total Q_{ion} data is reported [28,30] up to 1000 eV. The present work attempts to fill the void in terms of total Q_{ion} for all these molecules and for a wide energy range. The total Q_{ion} encompasses all the parent, partial and total single Q_{ion}. The deuterated hydrogen (HD) molecule is investigated for the first time in this work. Moreover, this is the maiden study of total inelastic cross sections, Q_{inel} and summed total excitation cross sections, $\sum Q_{exc}$ for all of these molecules. For most of these molecules $\sum Q_{exc}$ peak is seen at around 30 eV. We have examined the isotope effect for deuterated molecules and their protonated counterparts and found that Q_{ion} do not show any

Table 5
Inelastic cross-sections for HD, D_2 and D_2O $(A^o)^{2.}$

E_i (eV)	HD			D_2			D_2O		
	Q_{inel}	Q_{ion}	$\sum Q_{exc}$	Q_{inel}	Q_{ion}	$\sum Q_{exc}$	Q_{inel}	Q_{ion}	$\sum Q_{exc}$
13	–	–	–	–	–	–	0.002	0.000	0.002
16	0.002	0.000	0.002	0.002	0.000	0.002	0.186	0.039	0.147
20	0.127	0.032	0.095	0.126	0.031	0.095	0.682	0.238	0.444
40	0.982	0.578	0.404	0.979	0.573	0.406	2.704	1.602	1.102
60	1.220	0.838	0.382	1.218	0.833	0.385	3.242	2.202	1.040
80	1.197	0.887	0.310	1.195	0.882	0.313	3.238	2.370	0.868
100	1.101	0.857	0.244	1.099	0.852	0.247	3.106	2.391	0.715
500	0.310	0.295	0.015	0.309	0.294	0.015	1.285	1.219	0.066
1000	0.161	0.158	0.003	0.160	0.157	0.003	0.753	0.737	0.016
2000	0.077	0.077	0.000	0.077	0.077	0.000	0.420	0.417	0.003
3000	0.049	0.049	0.000	0.049	0.049	0.000	0.292	0.291	0.001
4000	0.036	0.036	0.000	0.036	0.036	0.000	0.222	0.221	0.001
5000	0.025	0.025	0.000	0.025	0.025	0.000	0.176	0.176	0.000

Table 6
Inelastic cross-sections for ND_x (x = 1–3) $(A^o)^{2.}$

E_i (eV)	ND			ND_2			ND_3		
	Q_{inel}	Q_{ion}	ΣQ_{exc}	Q_{inel}	Q_{ion}	ΣQ_{exc}	Q_{inel}	Q_{ion}	ΣQ_{exc}
11	–	–	–	–	–	–	0.031	0.003	0.028
12	–	–	–	0.006	0.000	0.006	0.138	0.022	0.116
14	0.003	0.000	0.003	0.156	0.029	0.127	0.511	0.139	0.373
20	0.445	0.138	0.307	1.145	0.461	0.684	2.001	0.900	1.105
60	2.659	1.761	0.898	3.960	2.784	1.176	5.154	3.707	1.454
100	2.634	1.990	0.644	3.597	2.842	0.755	4.490	3.608	0.885
500	0.999	0.942	0.057	1.327	1.268	0.059	1.666	1.599	0.067
1000	0.576	0.562	0.014	0.766	0.752	0.014	0.964	0.948	0.016
3000	0.219	0.218	0.001	0.290	0.289	0.001	0.366	0.365	0.001
4000	0.165	0.165	0.000	0.219	0.219	0.000	0.275	0.275	0.000
5000	0.133	0.133	0.000	0.177	0.177	0.000	0.219	0.219	0.000

Table 7
Inelastic cross-sections for SiD_x (x = 1–3) $(A^o)^{2.}$

E_i (eV)	SiD			SiD_2			SiD_3		
	Q_{inel}	Q_{ion}	ΣQ_{exc}	Q_{inel}	Q_{ion}	ΣQ_{exc}	Q_{inel}	Q_{ion}	ΣQ_{exc}
8	0.000	0.000	0.000	–	–	–	–	–	–
9	0.116	0.013	0.103	0.000	0.000	0.000	0.119	0.013	0.106
10	0.492	0.101	0.391	0.136	0.017	0.119	0.520	0.104	0.416
20	6.153	3.456	2.697	5.219	2.786	2.451	6.877	3.776	3.101
40	8.879	6.401	2.478	8.810	6.195	2.615	10.311	7.309	3.002
60	7.766	6.125	1.641	8.014	6.199	1.815	9.302	7.235	2.067
80	6.731	5.592	1.139	7.047	5.759	1.288	8.206	6.737	1.469
100	5.941	5.109	0.832	6.258	5.304	0.954	7.318	6.229	1.089
500	2.058	2.013	0.045	2.163	2.109	0.054	2.567	2.504	0.063
1000	1.238	1.229	0.009	1.288	1.277	0.011	1.522	1.509	0.013
3000	0.516	0.516	0.000	0.527	0.527	0.000	0.618	0.618	0.000
5000	0.325	0.325	0.000	0.330	0.330	0.000	0.390	0.390	0.000

Table 8
Inelastic cross-sections for CD_x (x = 2–4) $(A^o)^{2.}$

E_i (eV)	CD_2			CD_3			CD_4		
	Q_{inel}	Q_{ion}	ΣQ_{exc}	Q_{inel}	Q_{ion}	ΣQ_{exc}	Q_{inel}	Q_{ion}	ΣQ_{exc}
10	–	–	–	0.000	0.000	0.000	–	–	–
11	0.017	0.000	0.017	0.077	0.008	0.069	–	–	–
12	0.122	0.017	0.105	0.259	0.046	0.213	–	–	–
13	0.303	0.061	0.242	0.515	0.122	0.393	0.006	0.000	0.006
20	2.161	0.952	1.209	2.748	1.245	1.503	1.157	0.412	0.745
60	5.295	3.777	1.518	6.139	4.396	1.743	5.079	3.463	1.616
80	4.938	3.767	1.171	5.718	4.377	1.341	5.025	3.690	1.335
100	4.448	3.550	0.898	5.173	4.143	1.030	4.663	3.600	1.063
500	1.426	1.366	0.060	1.704	1.633	0.071	1.558	1.479	0.079
1000	0.796	0.782	0.014	0.951	0.935	0.016	0.861	0.842	0.019
3000	0.289	0.288	0.001	0.344	0.343	0.001	0.309	0.308	0.001
5000	0.173	0.173	0.000	0.206	0.206	0.000	0.182	0.182	0.000

dependence on isotopes owing to nearly same IEs for them. Further, the correlation of the Q_{ion} (peak) with dipole polarizability (α) and $\sqrt{\alpha/IE}$ as studied by Harland and Vallance [59] was verified and using that we predicted the α for ND and SiD_x (x = 1–3) family that can be confirmed by scientific groups.

Declaration of Competing Interest

The authors declare that they have no known competing financial interests or personal relationships that could have appeared to influence the work reported in this paper.

Data availability

Data will be made available on request.

Acknowledgements

The authors thank the Department of Science and Technology, Government of India (DST-SERB) for the major research project (No. CRG/2021/000253) for financial support under which part of this work is carried out.

Appendix A. Numeric data for electron interactions with the deuterated molecules

See Table 5, Table 6, Table 7, Table 8.

References

[1] Jiping Liu, Xiaobo Liu, Deuteride materials, Springer Singapore, Singapore, 2019, pages 231.
[2] W.Y. Baek, B. Grosswendt, J. Phys. B: Atomic Mol. Opt. Phys. 36 (4) (2003) 731.
[3] N.J. Manson, J.M. Gingell, N.C. Jones, L. Kaminski, Philosophical Transactions of the Royal Society of London, Series A: Math., Phys. Eng. Sci. 357 (1755) (1999) 1175.
[4] S.M. Younger, T.D. Märk, in: Electron Impact Ionization, Springer, Vienna, 1985, pp. 24–41.
[5] F. W. Taylor, S. K. Atreya, T. Encrenaz, D. H. Hunten, P. G. Irwin, and T. C. Owen, in Jupiter: The Atmosphere, Satellite and Magnetopshere, ed. F. Bagenal *et al.* (Cambridge: Cambridge Univ. Press), 59 (2004).
[6] S. Brezinsek, P.T. Greenland, P.h. Mertens, A. Pospieszczyk, U. Samm, B. Schweer, G. Sergienko, Phys. Scr. T103 (1) (2003) 63.
[7] A. Pospieszczyk, S. Brezinsek, A. Meigs, P.h. Mertens, G. Sergienko, M. Stamp, J. Nucl. Mater. 363–365 (2007) 811.
[8] A. Pospieszczyk, S. Brezinsek, G. Sergienko, P.T. Greenland, A. Huber, A. Meigs, Ph. Mertens, U. Samm, M. Stamp, S. Wiesen, J. Nucl. Mater. 337-339 500 (2005). PSI-16.
[9] E.M. Hollmann, S. Brezinsek, N.H. Brooks, M. Groth, A.G. McLean, A. Yu Pigarov, D.L. Rudakov, Plasma Phys. Controlled Fusion 48 (8) (2006) 1165.
[10] A.V. Snegursky, A.N. Zavilopulo, Scientific Herald of Uzhhorod University, Series Phys. 6 (2000) 207.
[11] H.M. Butner, S.B. Charnley, C. Ceccarelli, S.D. Rodgers, J.R. Pardo, B. Parise, J. Cernicharo, G.R. Davis, Astrophys J 659 (2007) L137.
[12] (a) Joseph W. Lyding, Karl Hess, Forming of deuterium containing nitride spacers and fabrication of semiconductor devices, November (2000). (b) J. W. Lyding, K. Hess and I.C. Kizilyalli, Appl. Phys. Lett. **68**:2526 (1996).
[13] Richard W. Gregor, Isik C. Kizilyalli, Deuterated dielectric and polysilicon film-based semiconductor devices and method of manufacture thereof, February (2000).
[14] William F. Clark, Thomas G. Ference, Terence B. Hook, Dale W. Martin, Use of deuterated materials in semiconductor processing, October 1999.
[15] Eric M. Breitung, Optical waveguide devices with deuterated amorphous carbon core structures, February 2006.
[16] J. Lecointre, S. Cherkani-Hassani, D.S. Belic, J.J. Jureta, K. Becker, H. Deutsch, T. D. Märk, M. Probst, R.K. Janev, P. Defrance, Journal of Physics B: Atomic, Mol. Opt. Phys. 40 (11) (2007) 2201.
[17] D.S. Belic, J.J. Jureta, R. Janev, P. Defrance, J. Lecointre, Eur. Phys. J. D 50 (2008) 265.
[18] D.C. Lis, E. Roueff, M. Gerin, T.G. Phillips, L.H. Coudert, F.F.S. van der Tak, P. Schilke, Astrophys J 571 (1) (2002) L55.
[19] F.F.S. Van der Tak, P. Schilke, H.S.P. Müller, D.C. Lis, T.G. Phillips, M. Gerin, E. Roueff, A&A 388 (2002) L53.
[20] A. Bacmann, et al., A&A 521 (2010) L42.
[21] A. Bacmann, F. Daniel, P. Caselli, C. Ceccarellie, D. Lis, C. Vastel, F. Dumouchel, F. Lique, E. Caux, A&A 587 (2016) A26.
[22] T.G. Ference, S. Burnham, W.F. Clark, T.B. Hook, S.W. Mittl, K.M. Watson, L.-K. Han, IEEE Trans. Electron Devices 46 (4) (1999) 747.
[23] D. Rapp, P. Englander-Golden, J. Chem. Phys. 43 (5) (1965) 1464.
[24] I.R. Cowling, J. Fletcher, J. Phys. B: At. Mol. Phys. 6 (4) (1973) 665.
[25] B.L. Schram, F.J. De Heer, M.J. van der Wiel, J. Kistemaker, Physica 31 (1) (1965) 94.
[26] T.D. Märk, F. Egger, Int. J. Mass Spectrom. Ion Phys. 20 (1) (1976) 89.
[27] V. Tarnovsky, H. Deutsch, K. Becker, J. Chem. Phys. 109 (3) (1998) 932.
[28] (a) H.C. Straub, B.G. Lindsay, K.A. Smith, R.F. Stebbings, J. Chem. Phys. 108 (1) (1998) 109;
(b) N.Lj. Djuric, I.M. Cadez, M.V. Kurepa, Int. J. Mass Spectrom. Ion Processes 83 (1988) R7.
[29] V. Tarnovsky, H. Deutsch, K. Becker, Int. J. Mass Spectrom. Ion Processes 167–168 (1997) 69.
[30] R. Rejoub, B.G. Lindsay, R.F. Stebbings, J. Chem. Phys. 115 (11) (2001) 5053.
[31] V. Tarnovsky, H. Deutsch, K. Becker, J. Chem. Phys. 105 (15) (1996) 6315.
[32] F.J. De Heer, B.L. Schram, M.J. Van Der Wiel, H.R. Moustafa, J. Chem. Phys. 1 (1966).
[33] V. Tarnovsky, A. Levin, H. Deutsch, K. Becker, J. Phys. B: Atomic Mol. Opt. Phys. 29 (1) (1996) 139.
[34] F.A. Baiocchi, R.C. Wetzel, R.S. Freund, Phys. Rev. Lett. 53 (1984) 771.
[35] A. Jain, Phys. Rev. A. 34 (1986) 3707.
[36] A. Jain, K.L. Baluja, Phys. Rev. A. 45 (1) (1992) 202.
[37] N. Thakkar, M. Swadia, M. Vinodkumar, N. Mason, C. Limbachiya, Plasma Sources Sci. Technol. 30 (8) (2021), 085008.
[38] C. Limbachiya, M. Vinodkumar, A. Chaudhary, H. Desai, RSC Adv. 5 (2015), 103964.
[39] C. Limbachiya, M. Vinodkumar, M. Swadia, A. Barot, Mol. Phys. 112 (1) (2014) 101.
[40] K.N. Joshipura, M. Vinodkumar, C.G. Limbachiya, B.K. Antony, Phys. Rev. A. 69 (2004), 022705.
[41] M. Swadia, Y. Thakar, M. Vinodkumar, C. Limbachiya, Eur. Phys. J. D. 71 (4) (2017) 85.
[42] H.L. Cox, R.A. Bonham, J. Chem. Phys. 47 (8) (1967) 2599.
[43] M. Vinodkumar, H. Bhutadia, C. Limbachiya, K.N. Joshipura, Int. J. Mass Spectrom. 308 (2011) 35.
[44] S. Hara, J. Phys. Soc. Jpn. 22 (1967) 710.
[45] Y. Thakar, R. Bhavsar, M. Swadia, M. Vinodkumar, N. Mason, C. Limbachiya, Planet. Space Sci. 168 (2019) 95.
[46] G. Staszewska, D.W. Schwenke, D. Thirumalai, D.G. Truhlar, Phys. Rev. A. 28 (1983) 2740.
[47] K.N. Joshipura, B.G. Vaishnav, C.G. Limbachiya, Pramana J Phys 66 (2006) 403.
[48] www.cccbdb.nist.gov.
[49] http://www.chm.bris.ac.uk/motm/D2O/D2Oh.htm.
[50] M. Melosso, L. Bizzocchi, F. Tamassia, Claudio Degli Esposti, Elisabetta Canè and Luca Dore, Phys. Chem. Chem. Phys. 21 (2019) 3564.
[51] C. Limbachiya, M. Vinodkumar, N.J. Mason, Phys. Rev. A. 83 (2011), 042708.
[52] M. Vinodkumar, K.N. Joshipura, C.G. Limbachiya, B.K. Antony, Nuclear Instru. Methods B 212 (2003) 63.
[53] M. Vinodkumar, C. Limbachiya, A. Barot, Nigel Mason, Phys. Rev. A 87 (2013), 012702.
[54] H. Yadav, M. Vinodkumar, C. Limbachiya, P.C. Vinodkumar, Mol. Phys. 115 (8) (2017) 952.
[55] M. Vinodkumar, C. Limbachiya, H. Desai, P.C. Vinodkumar, Phys. Rev. A 89 (2014), 062715.
[56] J.E. Turner, H.G. Paretzke, R.N. Hamm, H.A. Wright, R.H. Richie, Radiat. Res. 92 (1982) 47.
[57] M.A. Rahman, S. Gangopadhyay, C. Limbachiya, K.N. Joshipura, E. Krishnakumar, Int. J. Mass Spectrom. 319–320 (2012) 48.
[58] J.-S. Yoon, Y.-W. Kim, D.-C. Kwon, M.-Y. Song, W.-S. Chang, C.-G. Kim, V. Kumar, BongJu Lee, Rep. Prog. Phys. 73 (11) (2010), 116401.
[59] P.W. Harland, C. Vallance, Int. J. Mass Spectrom. Ion Process. 171 (1997) 173.
[60] D.G. LeGrand, G.L. Gaines Jr., J. Phys. Chem. 98 (1994) 4842.

Radiation Physics and Chemistry 214 (2024) 111248

Contents lists available at ScienceDirect

Radiation Physics and Chemistry

journal homepage: www.elsevier.com/locate/radphyschem

Scattering of electrons with aqueous biomaterials

Smruti Parikh [a], Dhaval Chauhan [a], Nirav Thakkar [b], Chetan Limbachiya [a,*]

[a] Department of Applied Physics, The Maharaja Sayajirao University of Baroda, Vadodara, 390001, India
[b] Sheth M. N. Science College, Patan, 384265, India

ARTICLE INFO

Handling Editor: Dr. Chris Chantler

Keywords:
Aqueous DNA compounds
Cross-sections
Dielectric constant
Polarisability

ABSTRACT

The aqueous phase of DNA, which is more realistic phase due to the presence of H-bonds is studied in this work for various molecular processes upon electron impact. We report computed probabilities of various interaction processes taking place during the collision of electrons with DNA molecules, viz., Adenine, Guanine, Cytosine, Thymine and Uracil in their aqueous phase. Modified spherical complex potential approach has been employed for the quantification of various (N+1) elastic and inelastic including ionisation interactions through the cross-sections. Since no study for electron scattering with aqueous DNA is available, we compared our results with condensed phase and also a new approach for estimating the elastic and total cross-sections has been proposed in the present work for larger and complex molecules ($55 < Z < 95$) like the DNA compounds and encouraging results are observed. Correlations of molecular ionisation with dielectric constant and polarisability of the compounds have also been investigated.

1. Introduction

The application of ionising radiation in the field of medicine is extremely common. It is frequently utilised in the medical field as a therapeutic agent and in the field of radio diagnostics as a probe. Ballistic impact was traditionally thought to be the mechanism that was responsible for the majority of the damage that high-energy incident radiation caused to living tissue. However, secondary species that result from primary ionisation are responsible for a significant radiation damage (Boudaïffa et al., 2002). The majority of the energy is deposited by the primary ionising particles once they enter the biological medium through several collision processes, including excitations and ionisations. Large amounts of secondary electrons are released as a result of this significant energy transfer, and these electrons can interact with a variety of biological substances causing the radiation damage. Among all the living tissues, DNA molecules are thought to be most sensitive to radiations. Exposure of DNA species to radiations result in multiple types of DNA damage (Nikjoo et al., 2016) through secondary species including electrons.

As primary as well as secondary species induces the radiation damage, it is essential to model their tracks through a biological medium. This makes it possible to anticipate and comprehend the type, location, and severity of cell damage. The route taken by the primary and secondary particles as they move through the medium is depicted by the charged-particle track structures (Goodhead, 1994). The entire range of interaction between the primary and secondary species at the level of each atom or molecule, is modelled in these aleatory (stochastic) simulations using the cross-section values. Hence, accurate cross-sections are crucial to the validity of these types of simulations.

Till now a lot of cross-sectional data has been reported for the DNA constituents upon electron impact in their gaseous phase (Mozejko and Sanche, 2005; Mokrani et al., 2020; Vinodkumar and Limbachiya, 2013; Rahman and Krishnakumar, 2016; Shafranyosh et al., 2015; Champion, 2013; Bull et al., 2014; Aouina and Chaoui, 2018; van der Burgt et al., 2014; Minaev et al., 2014; Zein et al., 2021). Such cross-sections (CSs) are also available for the condensed phase interaction processes but only for the low energy below 20 eV (Toburen, 1998; Bass and Sanche, 1998). But aqueous phase of the DNA rather than gaseous or condensed phase, presents more realistic picture, as they are always found covered with the water molecules through hydrogen bonding (Khesbak et al., 2011; Helmholtz Association of German Research Centres). This has motivated us to take up the work on electron interactions with aqueous DNA constituents. We have computed the ionisation CSs (Q_{ion}), inelastic CSs (Q_{inel}), elastic CSs (Q_{el}), and total CSs (Q_T) for all the five DNA constituents, viz. Adenine, Guanine, Thymine, Cytosine and Uracil upon electron collisions by considering their aqueous phase. This is the maiden attempt to investigate the electron induced processes for the aqueous DNA constituents for the energies from ionisation threshold of the

* Corresponding author.
E-mail address: cglimbachiya-apphy@msubaroda.ac.in (C. Limbachiya).

https://doi.org/10.1016/j.radphyschem.2023.111248
Received 3 May 2023; Received in revised form 22 August 2023; Accepted 27 August 2023
Available online 1 September 2023

molecules to 5000 eV.

Tan et al. (Tan et al., 2004) have reported the Q_{inel} data for the case of DNA in water using dielectric response theory and Penn's approximation for energy range from 20 to 10,000 eV. Recently, Vera et al. (De Vera et al., 2021) and Tan et al. (Tan et al., 2018) have reported the ionisation CSs data for DNA compounds by considering their condensed phase for impact energies from 1 to 10,000 eV and 10–500 eV, respectively. All of these groups (Tan et al., 2004, 2018; De Vera et al., 2021) have used a method that underlines the concept of dielectric response theory.

Since, to the best of our knowledge no work is available for the aqueous phase of DNA molecules; we have developed a new 2-parameter Semi-empirical method (2p-SEM) for computing the Q_T and Q_{el} for these applied biomaterials.

2. Theoretical methodology

The methodologies involved in the present study for the computations of inelastic and elastic interaction events as a result of electron interactions with the aqueous DNA constituents, have been described in this section.

2.1. Spherical complex optical potential approach (SCOP)

The energy-dependent modified complex potential is precisely treated in partial wave decomposition method (Vinodkumar et al., 2013a, 2013b, 2014a; Limbachiya et al., 2011, 2015) with respect to the DNA constituents in their aqueous phase in order to determine the CSs. In essence, a local version of the absorption potential (V_{ab}) (Staszewska et al., 1984) have been modified by keeping $\Delta = IE + E_{gap}$, due to the fact that when dealing with the aqueous or condensed phase, ionisation only occur when the projectile energy exceeds the ionisation energy, IE by an amount equal to the energy-band gap, E_{gap} (Pandya et al., 2012; Joshipura et al., 2007). Table 2 shows the target properties used for the present calculations.

This modified potential is given by,

$$V_{abs}(r, E_i) = -\rho(r)\sqrt{\frac{T_{loc}}{2}}\left(\frac{8\pi}{10{k_F}^3 E_i}\right)\Theta\left(p^2 - {k_F}^2 - 2\Delta\right) \times (A_1 + A_2 + A_3) \tag{1}$$

where, k_F is the appropriate fermi vector, and p is the incident momentum. The A_1, A_2 and A_3 are dynamic parameters, details of which already have been mentioned in our previous articles (Limbachiya et al., 2014, 2015; Vinodkumar et al., 2006, 2011; Joshipura et al., 2006). The local kinetic energy of the incident electron is, $T_{loc} = E_i - (V_s + V_e + V_p)$. Here, V_s is calculated using the Hartree-Fock wave functions (Cox and Bonham, 1967), is used to measure the undeformed molecule charge cloud. The exchange effect that took place between the target electrons and the incoming electrons, is taken into account through V_e (Hara, 1967). The charge cloud of the target system temporarily deforms in the response of the incoming electron. This polarisation effect has been considered through V_p (Zhang et al., 1992).

Since all of these potentials are constructed using the charge density of the molecule under study, it is crucial to represent it. The parameterized charge densities of constituent atomic systems to generate the total $\rho(r)$ of the target molecules have been introduced, which is input to the complex potential (Parikh et al., 2023; Parikh and Limbachiya, 2023).

The inelastic and elastic CSs, are computed by determining the scattering complex phase shifts (δ_l) (Parikh and Limbachiya, 2023). This Q_{inel} totals all the possible ionisations and electronic excitations:

$$Q_{inel} = Q_{ion} + \Sigma Q_{exc} \tag{2}$$

where, Q_{ion} stands for the total ionisation CSs for all permittable ionisations of the molecule and $\sum Q_{exc}$ represents all permitted electronic transitions that are influenced by low-lying states, which is less important than Q_{ion} for the incident energy higher than IE, hence,

$$Q_{inel} \geq Q_{ion} \tag{3}$$

2.2. Complex scattering potential-ionisation contribution (CSP-ic) method

Above inequality (equation (3)) is the cornerstone of this CSP-ic approach (Limbachiya et al., 2015; Vinodkumar et al., 2006; Thakkar et al., 2021) and implies to the ratio,

$$R(E_i) = \frac{Q_{ion}}{Q_{inel}} \tag{4}$$

The boundary conditions of which are as follows,

$$R(E_i) = \begin{cases} 0, for\ E_i \leq \Delta \\ R_P, for\ E_i = E_P \\ \sim 1, for\ E_i \gg \Delta \end{cases} \tag{5}$$

The ionisation events which are dominant part in the inelastic channel, begins to occur at the target's ionisation threshold, which is equal to Δ in this aqueous case. The inelastic CSs attains its peak at energy E_P. However, at high incident energy, ionisation dominates, and excitation CSs drastically drop, as seen by the final condition in equation (5). According to both experimental and theoretical results (Parikh et al., 2023; Swadia et al., 2017; Turner et al., 1982) of the stable targets, the value R_P will be within 0.7–0.8 when the impinging energy reaches E_P. This feature lends uncertainty of 10–15%.

2.3. 2-Parameter semi-empirical method (2p-SEM)

The impact energy dependence of the Q_T for the intermediate energy (Nishimura and Tawara, 1991a; Zecca et al., 1992) and high energy (Joshipura and Vinodkumar, 1996; García and Manero, 1997) have been previously studied and the proposed formula was as follows,

$$Q_T = \frac{A}{E^B} \tag{6}$$

where, parameter A is governed by the molecular characteristics such as molecular size and its polarisability. The value of B for the high energies, above 500 eV will be ~ 0.7, as proposed by Joshipura and Vinodkumar (1996) and García and Manero (1997) only for smaller molecules i.e., for ten electrons ($Z = 10$) and up to $Z = 22$ electrons systems respectively. However, Nishimura and Tawara (1991b) proposed the value of B ~ 0.5 for the intermediate energy range, 50–500 eV. In this work we have derived a single expression from our previous work (Vinodkumar et al., 2014b) and our current results for C_4F_7N, for the wide energy range, 50 $\leq E_i \leq$ 5000 eV and which is applicable for the complex and larger molecules with $55 < Z < 95$.

In Table 3, both the parameters A and B have been tabulated for the larger molecules whose Z ranges from 56 to 94, and it is seen that the

Table 2
Molecular characteristics.

DNA constituents	Aqueous phase IE (eV) (Crespo-Hernández et al., 2004; Fernando et al., 1998)	E_{gap} (eV)
Adenine	5.00	5.25 (Gop et al., 2019)
Cytosine	5.50	5.35 (Baei et al., 2014)
Guanine	4.80	4.80 (Di Felice et al., 2002)
Thymine	5.40	5.20 (MacNaughton et al., 2005)
Uracil	5.55	5.70 (Baei et al., 2014)

Table 3
Parameters vide equation (6).

Parameter	Adenine ($C_5H_5N_5$) (I)	Perfluoroisobutyronitrile (C_4F_7N) (II)	Thymine ($C_5H_6N_2O_2$) (III)	Cytosine ($C_4H_5N_3O$) (IV)	Uracil ($C_4H_4N_2O_2$) (V)
A	43.47	53.64	40.75	31.70	28.33
B	0.61	0.60	0.60	0.59	0.60

value of B (~0.6) is nearly same for all the molecules. However, the value of A is different for each molecule, suggesting its dependency on the number of target electrons (Z) and polarisability (α).

To observe this relation, we plotted the graph of A vs Z as shown in Fig. 1. The linear relationship observed in Fig. 1 is represented through the following equation,

$$A(Z) = 0.6413Z - 4.8016 \text{ (Correlation r = 95\%)} \quad (7)$$

However, for a given Z, the precision can be enhanced by inclusion of polarisability by considering the difference between the actual values of 'A' (from Table 3) and those derived from equation (7) for each molecule. We have observed the dependency of this deviation (A - $A(Z)$) on the molecular size through the polarisability (α). The linear relationship thus obtained from Fig. 2 is,

$$A - A(Z) = 0.1431\alpha - 10.5712 \text{ (Correlation r = 76\%)} \quad (8)$$

Hence, from the equations (6)–(8), a two-parameter expression for Q_T can be formulated for the wider energy range from 50 to 5000 eV for large molecules.

$$Q_T(E_i, Z, \alpha) = \frac{0.6413Z + 0.1431\alpha - 15.3728}{E_i^{0.60}} \quad (9)$$

We note the impact energy dependency as, $E_i^{0.60}$. Equation (9) provides the two-parameter expression for Q_T, which is applicable for the larger molecules with $55 < Z < 95$ and for the wider impact energy 50 eV $\leq E_i \leq$ 5000 eV. This 2p-SEM method provides total cross sections as well as total elastic cross sections for larger and complex molecules and could be very useful where experimental results are difficult to obtain as evident in the present case of aqueous DNA molecules.

3. Results and discussion

In this section, we present the results on Q_{inel}, Q_{ion}, Q_{el} and Q_T for the aqueous DNA compounds, by employing SCOP, CSP-ic and 2p-SEM. Numeric data for the CSs are provided in Appendix vide Tables 6–8 We also report various correlations (section 3.3) of peak ionisation leading to prediction of dipole polarisability (α) and dielectric constant

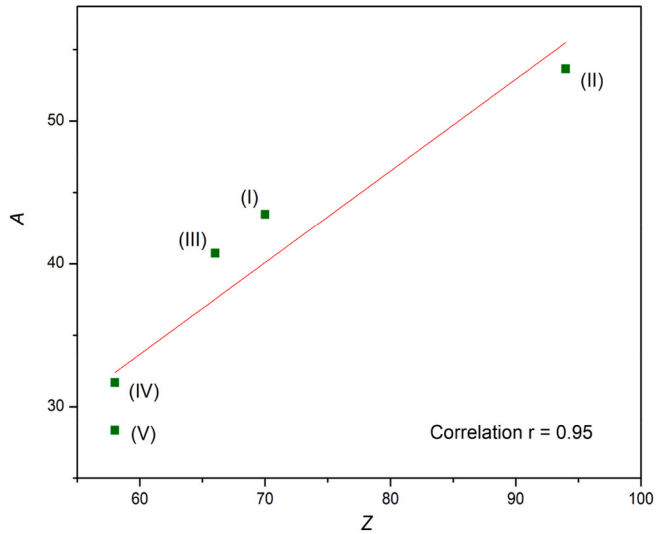

Fig. 1. Parameter A vs Z.

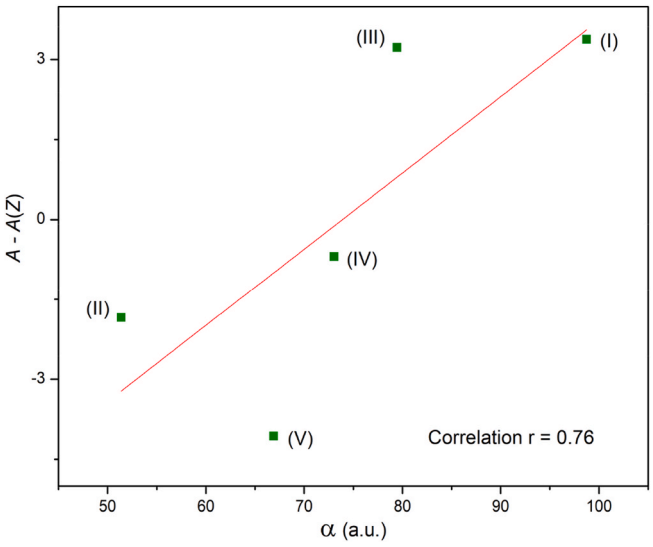

Fig. 2. A - $A(Z)$ vs α

(ε) for all the present aqueous molecules.

3.1. Inelastic contributions

Through Figs. 3–7, Q_{inel} and Q_{ion} are displayed for the investigated aqua-DNA constituents as a function of the electron energy along with the available results for condensed phase molecules (Tan et al., 2004, 2018; De Vera et al., 2021).

Top curves show total inelastic cross sections, Q_{inel}. Tan et al. (Tan et al., 2004) have reported the Q_{inel} data for the case of DNA in water using dielectric response theory and Penn's approximation. They took

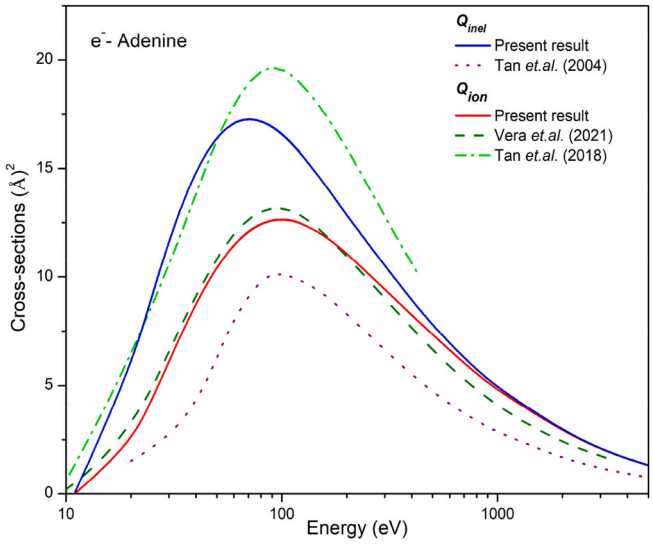

Fig. 3. Inelastic interaction CSs for Adenine
Blue solid: Present Q_{inel}; dot: Tan et al. Q_{inel} (Tan et al., 2004); red solid: Present Q_{ion}; olive green dash dot: Vera et al. Q_{ion} (De Vera et al., 2021); short dash: Tan et al. Q_{ion} (Tan et al., 2018).

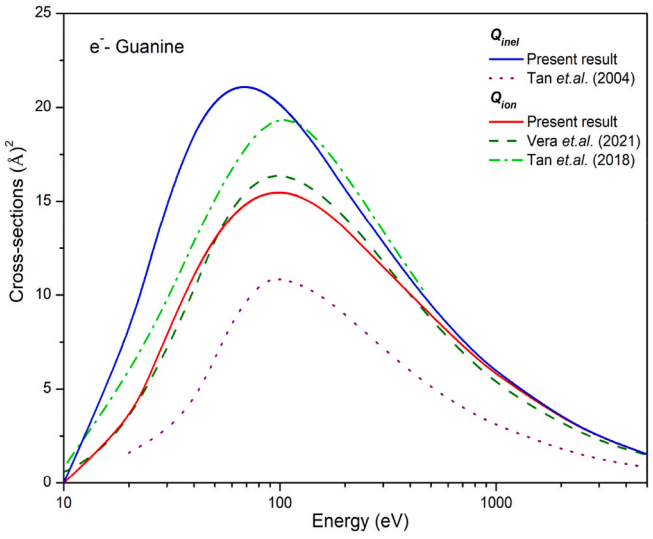

Fig. 4. Inelastic interaction CSs for Guanine
Blue solid: Present Q_{inel}; dot: Tan et al. Q_{inel} (Tan et al., 2004); red solid: Present Q_{ion}; olive green dash dot: Vera et al. Q_{ion} (De Vera et al., 2021); short dash: Tan et al. Q_{ion} (Tan et al., 2018).

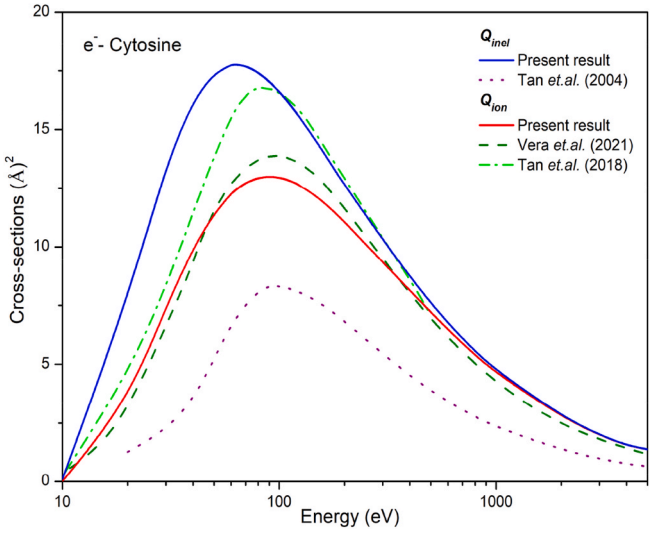

Fig. 5. Inelastic interaction CSs for Cytosine
Blue solid: Present Q_{inel}; dot: Tan et al. Q_{inel} (Tan et al., 2004); red solid: Present Q_{ion}; olive green dash dot: Vera et al. Q_{ion} (De Vera et al., 2021); short dash: Tan et al. Q_{ion} (Tan et al., 2018).

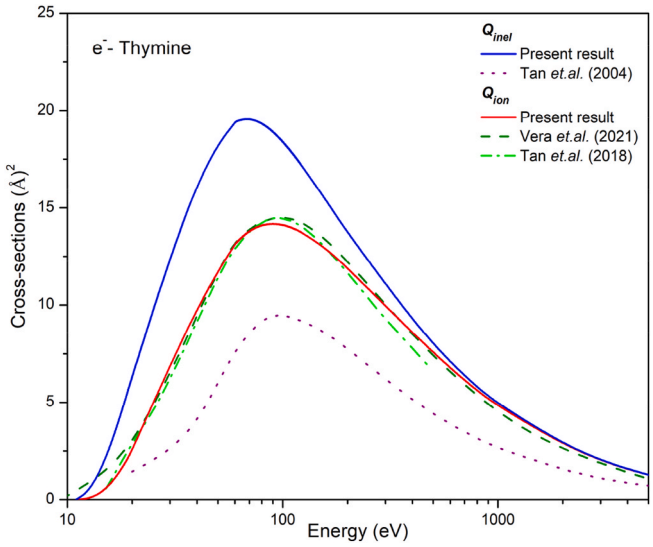

Fig. 6. Inelastic interaction CSs for Thymine
Blue solid: Present Q_{inel}; dot: Tan et al. Q_{inel} (Tan et al., 2004); red solid: Present Q_{ion}; olive green dash dot: Vera et al. Q_{ion} (De Vera et al., 2021); short dash: Tan et al. Q_{ion} (Tan et al., 2018).

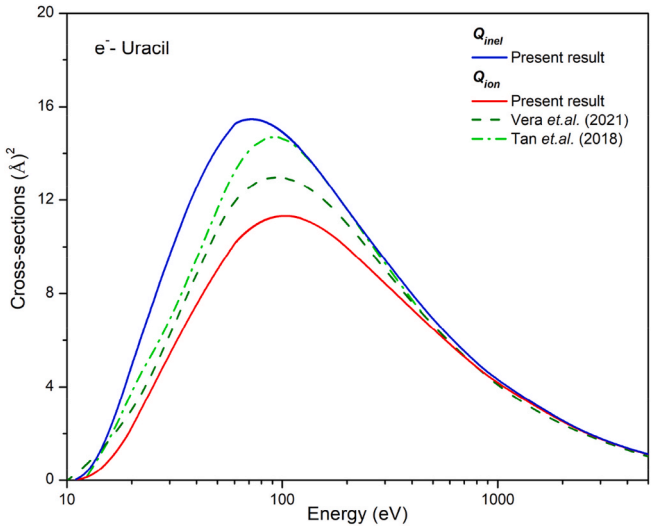

Fig. 7. Inelastic interaction CSs for Uracil Blue solid: Present Q_{inel}; dot: Tan et al. Q_{inel} (Tan et al., 2004); red solid: Present Q_{ion}; dash: Vera et al. Q_{ion} (De Vera et al., 2021); dash dot: Tan et al. Q_{ion} (Tan et al., 2018).

an equivalent unit of DNA molecule in water environment with 50% Guanine-Cytosine and 50% Adenine-Thymine and then separated into 5 constituents of DNA. However, their Q_{inel} underestimate present Q_{inel} and have lower values than even all the reported Q_{ion}.

Tan et al. (Tan et al., 2018) and Vera et al. (De Vera et al., 2021) have reported the Q_{ion} data for condensed DNA bases using the methodologies which underlines the dielectric response theory. The present results of Q_{ion} are observed to be in good accord with those of Vera et al. (De Vera et al., 2021) except in the case of Uracil. The minute deviation at the peak value of Q_{ion} may be because of the consideration of the different phases for the molecules.

As can be seen, the data of Tan et al. (Tan et al., 2018) overestimates both, present data and those of Vera et al. (De Vera et al., 2021) except for Thymine, in which case they show matching.

It is important to compare Q_{ion} for aqua and gas phase (Vinodkumar et al., 2003). Hence, apart from condensed phase results, the present aqueous phase Q_{ion} results are also compared with those of recent gas phase data (Rahman and Krishnakumar, 2015, 2016; Shafranyosh et al., 2015; Champion, 2013; Bull et al., 2014; van der Burgt et al., 2014; Minaev et al., 2014; van der Burgt, 2014, 2015) as shown in Figs. 8–12. As can be observed from the Figs. 8–12, gas phase results overestimate the present aqua phase data. This difference is because of the different threshold values for condensed and gas phase DNA compounds.

3.2. Elastic contributions

We have computed the elastic CSs (Q_{el}) and the total CSs (Q_T) for the electron energies from molecular IE to 5000 eV using the SCOP and 2p-SEM approach.

Figs. 13–17 show the Q_{el} and Q_T plots against the incident electron energies for aqueous Adenine, Cytosine, Guanine, Thymine and Uracil, respectively. We also show recent data of Q_{el} and Q_T in the gas phase.

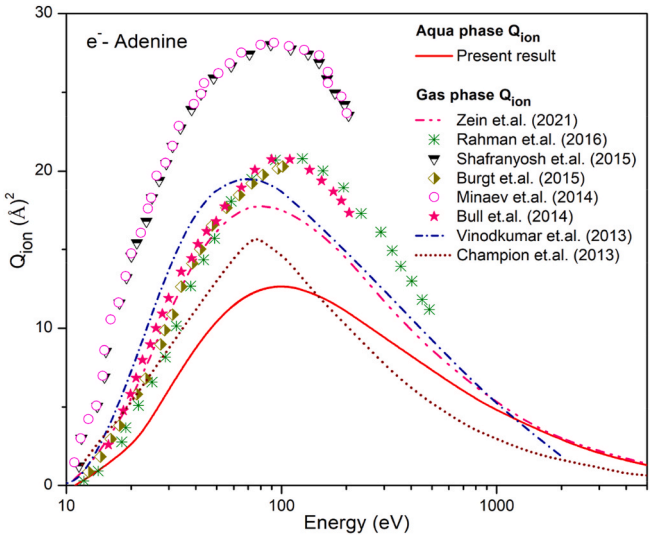

Fig. 8. Q_{ion} for Adenine in aqua and gas phase
Solid: Present Q_{ion} (aqua phase); pink dash dot: Zein et al. (Zein et al., 2021); asterisk: Rahman et al. (Rahman and Krishnakumar, 2016); inverted half-filled triangles: Shafranyosh et al. (Shafranyosh et al., 2015); half-filled diamonds: Burgt et al. (van der Burgt, 2015); open circles: Minaev et al. (Minaev et al., 2014); filled stars: Bull et al. (Bull et al., 2014); short dash dot: Vinodkumar et al. (Vinodkumar and Limbachiya, 2013); short dot: Champion (Champion, 2013).

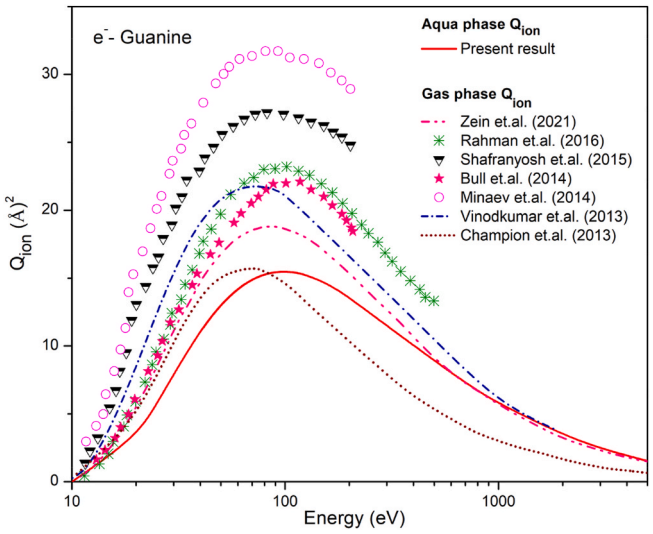

Fig. 9. Q_{ion} for Guanine in aqua and gas phase
Solid: Present aqua phase result; pink dash dot: Zein et al. (Zein et al., 2021); asterisk: Rahman et al. (Rahman and Krishnakumar, 2016); inverted half-filled triangles: Shafranyosh et al. (Shafranyosh et al., 2015); open circles: Minaev et al. (Minaev et al., 2014); filled stars: Bull et al. (Bull et al., 2014); short dash dot: Vinodkumar et al. (Vinodkumar and Limbachiya, 2013); short dot: Champion (Champion, 2013).

The results obtained from 2p-SEM and those from SCOP formalism are seen in good agreement with each other confirming the recently developed 2p-SEM method for larger and complex molecules.

The Q_{el} results from both the methodologies (2p-SEM and SCOP) are observed to be in excellent accord with each other for all the present studied molecules, which validate the newly proposed 2p-SEM formalism even for the aqueous phase molecules.

The gas phase results of Aouina (Aouina and Chaoui, 2018), Vinodkumar et al. (Vinodkumar et al., 2014b), Mokrani et al. (Mokrani et al., 2020) and Gurung (Devi Gurung and Ariyasinghe, 2017) are seen to be deviated at low energy side, which is due to the fact that at lower energies these Q_{el} and Q_T are highly sensitive to threshold values as well as polarisabilities. We observe that Q_{el} data of Zein et al. (Zein et al., 2021) shows significant deviation from the other existing Q_{el} data, mainly at the lower to intermediate energies. This deviation then reduces as we move towards high energy regime.

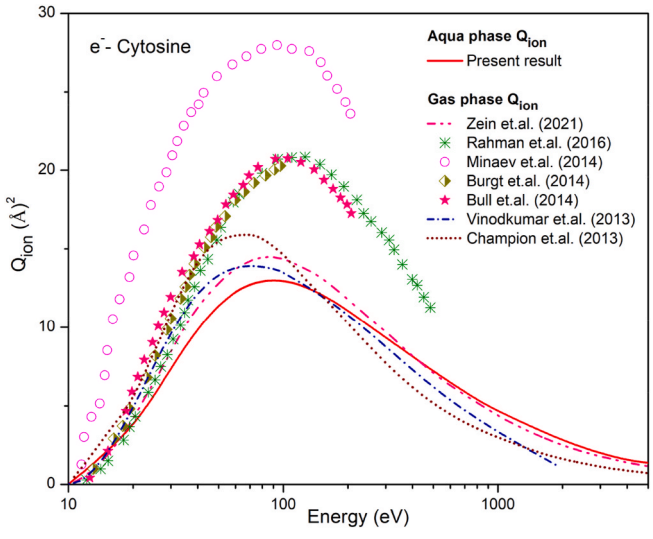

Fig. 10. Q_{ion} for Cytosine in aqua and gas phase
Solid: Present aqua phase result; Solid: Present aqua phase result; pink dash dot: Zein et al. (Zein et al., 2021); asterisk: Rahman et al. (Rahman and Krishnakumar, 2016); open circles: Minaev et al. (Minaev et al., 2014); half-filled diamonds: Burgt (van der Burgt, 2014); filled stars: Bull et al. (Bull et al., 2014); short dash dot: Vinodkumar et al. (Vinodkumar and Limbachiya, 2013); short dot: Champion (Champion, 2013).

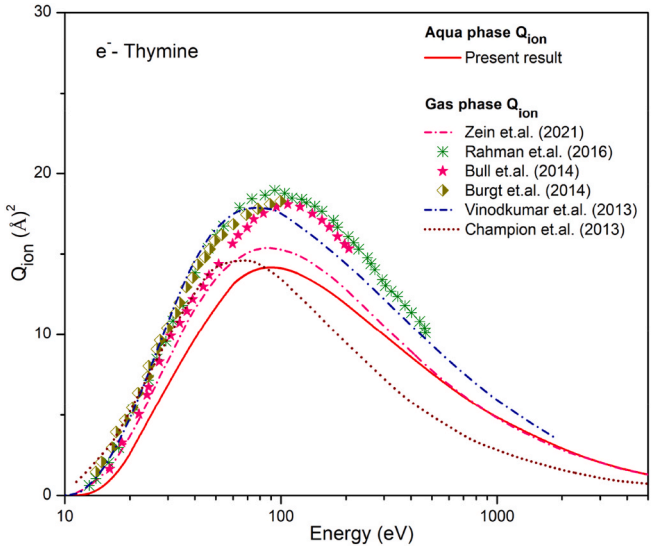

Fig. 11. Q_{ion} for Thymine in aqua and gas phase
Solid: Present aqua phase result; Solid: Present aqua phase result; pink dash dot: Zein et al. (Zein et al., 2021); asterisk: Rahman et al. (Rahman and Krishnakumar, 2016); half-filled diamonds: Burgt et al. (van der Burgt et al., 2014); filled stars: Bull et al. (Bull et al., 2014); short dash dot: Vinodkumar et al. (Vinodkumar and Limbachiya, 2013); short dot: Champion (Champion, 2013).

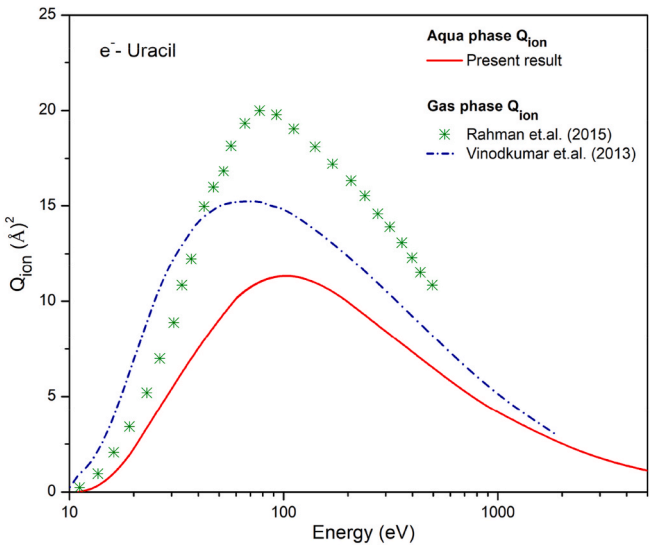

Fig. 12. Q_{ion} for Uracil in aqua and gas phase
Solid: Present aqua phase result; asterisks: Rahman (Rahman and Krishnakumar, 2015); short dash dot: Vinodkumar et al. (Vinodkumar and Limbachiya, 2013).

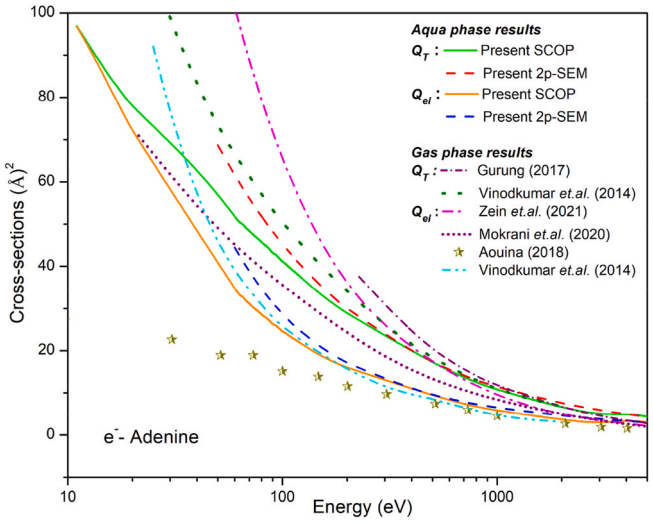

Fig. 13. Elastic and total interaction CSs for Adenine
Aqua phase results
Green solid: Present SCOP Q_T; red dash: Present 2p-SEM Q_T; Present SCOP Q_{el}; blue dash: Present 2p-SEM Q_{el}
Gas phase results
Short dash dot: Gurung Q_T (Devi Gurung and Ariyasinghe, 2017); olive green dot: Vinodkumar et al. Q_T (Vinodkumar et al., 2014b); pink dash dot: Zein et al. Q_{el} (Zein et al., 2021); short dot: Mokrani et al. Q_{el} (Mokrani et al., 2020); half-filled stars: Aouina Q_{el} (Aouina and Chaoui, 2018); dash dot: Vinodkumar et al. (Vinodkumar et al., 2014b).

3.3. Various correlations: prediction of polarisability (α) and dielectric constant (ε)

We have used the calculated total ionisation cross sections to compute useful parameters, polarisability (α) and dielectric constant (ε) for aqua-DNA molecules which are not found in literature.

3.3.1. Polarisability (α)

According to Harland's proposed qualitative dependency nature of the maximum ionisation CSs, ($Q_{ion(m)}$) with its polarisability (α)

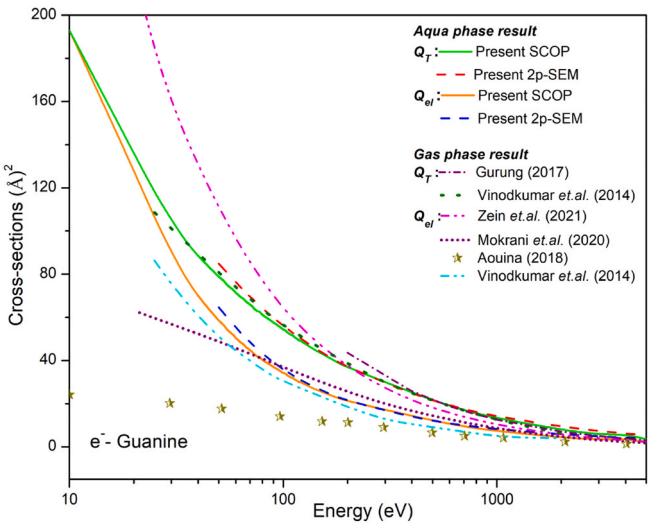

Fig. 14. Elastic and total interaction CSs for Guanine
Aqua phase results
Green solid: Present SCOP Q_T; red dash: Present 2p-SEM Q_T; Present SCOP Q_{el}; blue dash: Present 2p-SEM Q_{el}
Gas phase results
Short dash dot: Gurung Q_T (Devi Gurung and Ariyasinghe, 2017); olive green dot: Vinodkumar et al. Q_T (Vinodkumar et al., 2014b); Pink dash dot: Zein et al. Q_{el} (Zein et al., 2021); short dot: Mokrani et al. Q_{el} (Mokrani et al., 2020); half-filled stars: Aouina Q_{el} (Aouina and Chaoui, 2018); dash dot: Vinodkumar et al. (Vinodkumar et al., 2014b).

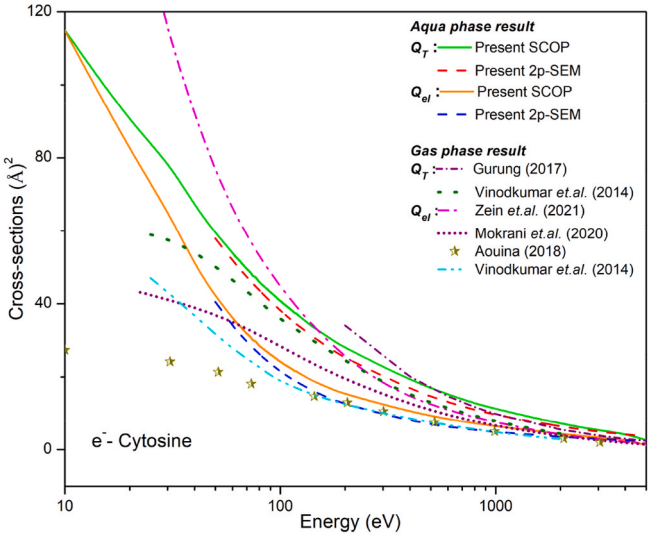

Fig. 15. Elastic and total interaction CSs for Cytosine
Aqua phase results
Green solid: Present SCOP Q_T; red dash: Present 2p-SEM Q_T; orange solid: Present SCOP Q_{el}; blue dash: Present 2p-SEM Q_{el}
Gas phase results
Short dash dot: Gurung Q_T (Devi Gurung and Ariyasinghe, 2017); olive green dot: Vinodkumar et al. Q_T [53]; pink dash dot: Zein et al. Q_{el} (Zein et al., 2021); short dot: Mokrani et al. Q_{el} (Mokrani et al., 2020); half-filled stars: Aouina Q_{el} (Aouina and Chaoui, 2018); dash dot: Vinodkumar et al. (Vinodkumar et al., 2014b).

(Harland and Vallance, 1997),

$$Q_{ion(\mathrm{m})} = \frac{e}{4\varepsilon_o}\sqrt{\frac{\alpha}{\Delta}} \tag{10}$$

Harland proposed the Δ will be equal to *IE* in case of gas phase of the

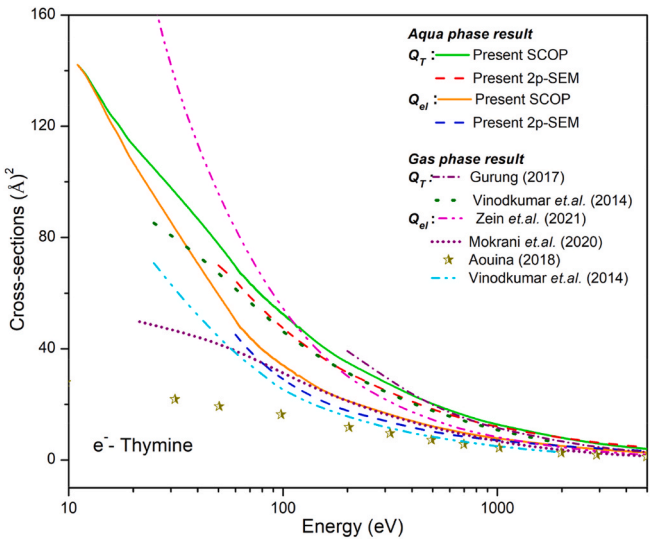

Fig. 16. Elastic and total interaction CSs for Thymine
Aqua phase results
Green solid: Present SCOP Q_T; red dash: Present 2p-SEM Q_T; orange solid: Present SCOP Q_{el}; blue dash: Present 2p-SEM Q_{el}
Gas phase results
Short dash dot: Gurung Q_T (Devi Gurung and Ariyasinghe, 2017); olive green dot: Vinodkumar et al. Q_T (Vinodkumar et al., 2014b); pink dash dot: Zein et al. Q_{el} (Zein et al., 2021); short dot: Mokrani et al. Q_{el} (Mokrani et al., 2020); half-filled stars: Aouina Q_{el} (Aouina and Chaoui, 2018); dash dot: Vinodkumar et al. (Vinodkumar et al., 2014b).

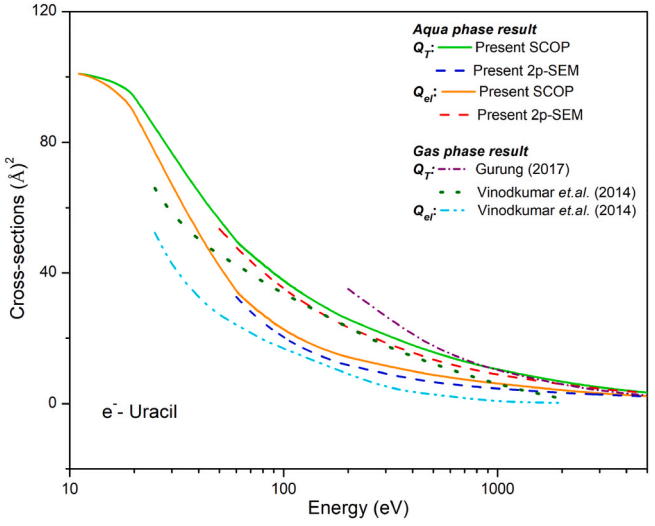

Fig. 17. Elastic and total interaction CSs for Uracil
Aqua phase results
Green solid: Present SCOP Q_T; red dash: Present 2p-SEM Q_T; orange solid: Present SCOP Q_{el}; blue dash: Present 2p-SEM Q_{el}
Gas phase results
Short dash dot: Gurung Q_T (Devi Gurung and Ariyasinghe, 2017); olive green dot: Vinodkumar et al. Q_T (Vinodkumar et al., 2014b); dash dot: Vinodkumar et al. (Vinodkumar et al., 2014b).

target system. While, in the present case of aqueous phase species, the $\Delta = IE + E_{gap}$, and the ionisation of the system actually occurs when the incoming energy is greater than the threshold value, $\Delta = IE + E_{gap}$.

Using this equation (10), we have predicted the α values for the present studied targets as given in the Table 4.

From the table it can be observed that the present predicted α for the aqueous molecules find good agreement with those of Nakagawa (2007), who calculated the α for condensed molecules.

Table 4
Predicted polarisability α (Å^3).

Target	Δ (eV)	$Q_{ion(m)}$ (Å^2)	Predicted α (Å^3)	Reference value of α for condensed phase (Å^3) (Nakagawa, 2007)
Adenine	10.25	12.65	11.54	14.33
Guanine	9.60	15.47	16.17	15.26
Thymine	10.60	14.17	14.99	13.35
Cytosine	10.85	12.99	12.88	11.47
Uracil	11.25	11.32	10.15	10.41

3.3.2. Dielectric constant (ε)

The two expressions for dielectric constant (ε) have been derived in the present work using the dependency of the $Q_{ion(m)}$ on α and ε. The first proposed expression of dielectric constant as a function of $Q_{ion(m)}$, derived using the dependency of $Q_{ion(m)}$ with α (equation (10)) and the Clausius-Mosotti (CM) equation,

$$\frac{\varepsilon-1}{\varepsilon+2} = C\cdot\left(Q_{ion(m)}\right)^2 N\Delta \tag{11}$$

where, C is the constant $= \frac{64\pi}{3}\left(\frac{\varepsilon_0}{e}\right)^2$ and N is the number density of the molecule.

Secondly, the Onsager dielectric equation (Onsager, 1936; Valiskó and Boda, 2005), which works well for the case of liquids is given by,

$$\frac{\varepsilon-1}{\varepsilon+2} = \frac{4\pi}{3}\alpha N + \frac{(\varepsilon-\varepsilon_\infty)(2\varepsilon+\varepsilon_\infty)}{\varepsilon(\varepsilon_\infty+2)^2} \tag{12}$$

This equation is thought to be more applicable in the present aqueous phase study, and again the equation of dielectric constant as a function of $Q_{ion(m)}$ is proposed as,

$$\frac{\varepsilon-1}{\varepsilon+2} = C\cdot\left(Q_{ion(m)}\right)^2 N\Delta + \frac{(\varepsilon-\varepsilon_\infty)(2\varepsilon+\varepsilon_\infty)}{\varepsilon(\varepsilon_\infty+2)^2} \tag{13}$$

where, ε_∞ is the high frequency dielectric constant, which can be obtained from the CM equation. The computed ε values are listed in Table 5.

Form the Table 5 and it can be observed as expected that the ε values computed through equation (13), are in good agreement with those of Szarek (2017).

Conclusion

The aqueous phase of DNA is explored here for several molecular processes upon electron impact, as it is a more realistic phase of DNA due to the presence of H-bonds. Radiation induced damage assessment of DNA due to the single and double strand breaks requires electron interacting with aqueous DNA inelastically. Present study quantifies various interaction processes in response to the impact of electrons on aqueous DNA constituents, viz., Adenine, Guanine, Thymine, Cytosine and Uracil through cross-sections. In order to provide Q_{el} and Q_T results for these biomaterials we have proposed a method 2p-SEM and

Table 5
Computed dielectric constants (ε).

Target	$Q_{ion(m)}$ (Å^2)	Dielectric constant (ε) (vide equation (11))	Dielectric constant (ε) (vide equation (13))	Reference value of ε for condensed phase (Szarek, 2017)
Adenine	12.65	2.22	1.00	1.59
Guanine	15.47	3.23	0.85	1.77
Thymine	14.17	3.39	0.99	1.59
Cytosine	12.99	2.84	1.03	1.71
Uracil	11.32	2.29	0.98	–

encouraging results are observed (Figs. 13–17). The proposed expression for Q_T (equation (9)) is applicable for the larger molecular systems ($55 < Z < 95$) and wider energy range. Numeric data for the CSs are provided in Appendix vide Tables 6–8 Further, from the correlation study of molecular ionisation, we have computed molecular polarisability and dielectric constant. The dielectric constant is obtained from the Q_{ion} using the Clausius-Mosotti (CM) and Onsager approaches (vide equations (11) and (13) respectively). The computed results are compared with previous data. In absence of previous study involving aqueous DNA constituents, this estimation of various cross-sections, computation of polarisability and dielectric constant may prove to be very useful.

CRediT author statement

Smruti Parikh: Data curation, Writing- Original draft preparation, Formal analysis, Conceptualization, Methodology, software. **Dhaval Chauhan:** Data curation, Methodology. **Nirav Thakkar:** Formal analysis. **Chetan Limbachiya:** Reviewing and Editing, Validation, Visualization, Investigation, Supervision.

Declaration of competing interest

The authors declare that they have no known competing financial interests or personal relationships that could have appeared to influence the work reported in this paper.

Data availability

Data will be made available on request.

APPENDIX

Table 6
Numeric data for cross-sections of Aqueous Adenine and Guanine (in Å^2)

E_i (eV)	Adenine					Guanine				
	Q_{ion}	Modified SCOP		2p-SEM		Q_{ion}	Modified SCOP		2p-SEM	
		Q_{el}	Q_T	Q_{el}	Q_T		Q_{el}	Q_T	Q_{el}	Q_T
10	–	–	–	–	–	0.00	192.94	192.95	–	–
11	0.004	96.82	96.88	–	–	0.021	188.95	189.16	–	–
20	2.35	72.02	77.85	–	–	3.27	128.23	136.08	–	–
40	8.76	48.42	63.27	–	–	11.04	70.00	88.51	–	–
60	11.46	34.79	51.86	44.49	61.56	14.17	50.40	71.35	55.34	76.29
70	12.08	31.17	48.43	38.87	56.13	14.87	44.76	65.84	48.47	69.55
80	12.43	28.59	45.76	34.64	51.80	15.25	40.28	61.20	43.28	64.20
100	12.65	24.60	41.18	28.73	45.31	15.47	34.26	54.41	36.00	56.15
400	8.25	11.04	19.91	10.86	19.72	10.04	14.30	25.07	13.67	24.44
800	5.54	6.74	12.47	7.29	13.01	6.71	8.56	15.48	9.20	16.13
1000	4.79	5.81	10.72	6.47	11.38	5.78	7.34	13.27	8.18	14.10
3000	2.07	2.69	4.78	3.80	5.89	2.48	3.17	5.66	4.80	7.30
5000	1.33	3.07	4.40	3.00	4.33	1.53	2.00	3.54	3.84	5.37

Table 7
Numeric data for cross-sections of Aqueous Cytosine and Thymine (in Å^2)

E_i (eV)	Cytosine					Thymine				
	Q_{ion}	Modified SCOP		2p-SEM		Q_{ion}	Modified SCOP		2p-SEM	
		Q_{el}	Q_T	Q_{el}	Q_T		Q_{el}	Q_T	Q_{el}	Q_T
10	0.01	114.81	114.92	–	–	–	–	–	–	–
11	0.08	109.80	110.29	–	–	0.001	142.10	142.12	–	–
20	3.42	82.11	89.88	–	–	2.55	106.87	113.23	–	–
40	9.94	50.70	66.94	–	–	10.01	70.34	87.17	–	–
60	12.26	36.26	54.00	34.14	51.88	13.13	50.41	69.81	45.06	64.46
70	12.71	31.81	49.49	29.62	47.29	13.79	43.97	63.52	39.21	58.76
80	12.93	28.52	45.93	26.25	43.65	14.09	39.72	59.05	34.91	54.24
100	12.95	24.15	40.75	21.58	38.18	14.12	34.05	52.44	29.05	47.44
400	8.13	10.45	19.12	7.95	16.62	8.58	13.73	22.93	11.45	20.65
800	5.40	7.23	12.78	5.41	10.97	5.60	8.88	14.67	7.84	13.62
1000	4.64	6.46	11.21	4.84	9.59	4.81	7.74	12.66	6.99	11.92
3000	1.98	3.35	5.34	2.97	4.96	2.03	3.78	5.82	4.12	6.16
5000	1.37	1.23	2.60	2.27	3.65	1.29	2.69	3.98	3.24	4.54

Table 8
Numeric data for cross-sections of Aqueous Uracil (in Å^2)

E_i (eV)	Uracil				
	Q_{ion}	Modified SCOP		2p-SEM	
		Q_{el}	Q_T	Q_{el}	Q_T
11	0.007	100.96	100.99	–	–
20	2.24	89.44	94.39	–	–
40	7.69	50.97	64.10	–	–
60	10.14	34.53	49.79	32.63	47.88
70	10.73	30.30	45.75	28.20	43.65
80	11.08	27.23	42.62	24.90	40.29
100	11.32	22.71	37.62	20.34	35.24
400	7.33	9.78	17.69	7.43	15.34
800	4.83	6.90	11.91	5.11	10.12
1000	4.15	6.14	10.42	4.58	8.85
3000	1.76	3.20	4.98	2.80	4.58
5000	1.12	2.31	3.43	2.25	3.37

References

Aouina, N.Y., Chaoui, Z.-E.-A., 2018. Simulation *of Positron and electron elastic mean free Path and diffusion Angle on DNA Nucleobases from 10 eV to 100 KeV*. Surf. Interface Anal. 50, 939.

Baei, M.T., Taghartapeh, M.R., Lemeski, E.T., Soltani, A., 2014. A computational study of adenine, Uracil, and cytosine adsorption upon AlN and BN nano-cages. Phys. B Condens. Matter 444, 6.

Bass, A., Sanche, L., 1998. Absolute and effective cross-sections for low-energy electron-scattering processes within condensed matter. Radiat. Environ. Biophys. 37, 243.

Boudaïffa, B., Cloutier, P., Hunting, D., Huels, M.A., Sanche, L., 2002. Cross sections for low-energy (10-50 EV) electron damage to DNA. Radiat. Res. 157, 227.

Bull, J.N., Lee, J.W.L., Vallance, C., 2014. Absolute *electron total ionization cross-sections: molecular Analogues of DNA and RNA Nucleobase and sugar constituents*. Phys. Chem. Chem. Phys. 16, 10743.

Champion, C., 2013. Quantum-mechanical predictions of electron-induced ionization cross sections of DNA components. J. Chem. Phys. 138, 184306.

Cox, H.L., Bonham, R.A., 1967. Elastic electron scattering amplitudes for neutral atoms calculated using the partial wave method at 10, 40, 70, and 100 KV for Z = 1 to Z = 54. J. Chem. Phys. 47, 2599.

Crespo-Hernández, C.E., Arce, R., Ishikawa, Y., Gorb, L., Leszczynski, J., Close, D.M., 2004. Ab initio ionization energy thresholds of DNA and RNA bases in gas phase and in aqueous solution. J. Phys. Chem. A 108, 6373.

De Vera, P., Abril, I., Garcia-Molina, R., 2021. Excitation and ionisation cross-sections in condensed-phase biomaterials by electrons down to very low energy: application to liquid water and genetic building blocks. Phys. Chem. Chem. Phys. 23, 5079.

Devi Gurung, Meera, Ariyasinghe, W.M., 2017. Total electron scattering cross sections of some important biomolecules at 0.2 – 6.0keV energies. Radiat. Phys. Chem. 141, 1.

Di Felice, R., Calzolari, A., Molinari, E., Garbesi, A., 2002. Ab initio study of model guanine assemblies: the role of (formula presented) coupling and band transport. Phys. Rev. B Condens. Matter 65, 1.

Fernando, H., Papadantonakis, G.A., Kim, N.S., Lebreton, P.R., 1998. Conduction-band-edge ionization thresholds of DNA components in aqueous solution. Proc. Natl. Acad. Sci. U. S. A. 95, 5550.

García, G., Manero, F., 1997. Correlation of the total cross section for electron scattering by molecules with 10-22 electrons, and some molecular parameters at intermediate energies. Chem. Phys. Lett. 280, 419.

Goodhead, D.T., 1994. Initial events in the cellular effects of ionizing radiations: clustered damage in DNA. Int. J. Radiat. Biol. 65, 7.

Gop, S., Sutradhar, R., Chakraborty, S., Sinha, T.P., 2019. The study of energetic and electronic properties of metal-adenine complex in solvent phase: a density functional theory approach. In: AIP Conference Proceedings, vol. 2162. American Institute of Physics Inc.

Hara, S., 1967. The scattering of slow electrons by hydrogen molecules. J. Phys. Soc. Jpn. 22, 710.

Harland, P.W., Vallance, C., 1997. Ionization cross-sections and ionization efficiency curves from polarizability volumes and ionization potentials. Int. J. Mass Spectrom. Ion Process. 171, 173.

Helmholtz Association of German Research Centres. Water molecules characterize the structure of DNA genetic material. https://www.sciencedaily.com/releases/2011/04/110426091122.htm#citation_apa.

Joshipura, K.N., Vinodkumar, M., 1996. *Cross Sections and other Parameters of e^- - H_2O scattering (Ei≥50eV)*. Pramana - J. Phys. 47, 57.

Joshipura, K.N., Vaishnav, B.G., Limbachiya, C.G., 2006. Ionization and excitation of some atomic targets and metal oxides by electron impact. Pramana - J. Phys. 66, 403.

Joshipura, K.N., Gangopadhyay, S., Limbachiya, C.G., Vinodkumar, M., 2007. Electron impact ionization of water molecules in ice and liquid phases. J. Phys. Conf. Ser. 80, 012008.

Khesbak, H., Savchuk, O., Tsushima, S., Fahmy, K., 2011. The role of water H-bond imbalances in B-DNA substate transitions and peptide recognition revealed by time-resolved FTIR spectroscopy. J. Am. Chem. Soc. 133, 5834.

Limbachiya, C., Vinodkumar, M., Mason, N., 2011. *Calculation of electron-impact rotationally elastic total cross Sections for NH_3, H_2S, and PH_3 over the energy Range from 0.01 eV to 2 KeV*. Phys. Rev. 83, 042708.

Limbachiya, C., Vinodkumar, M., Swadia, M., Barot, A., 2014. *Electron impact total cross section Calculations for CH_3SH (methanethiol) from Threshold to 5 KeV*. Mol. Phys. 112, 101.

Limbachiya, C., Vinodkumar, M., Swadia, M., Joshipura, K.N., Mason, N., 2015. Electron-impact total cross sections for inelastic processes for furan, tetrahydrofuran and 2,5-dimethylfuran. Mol. Phys. 113, 55.

MacNaughton, J., Moewes, A., Kurmaev, E.Z., 2005. Electronic structure of the nucleobases. J. Phys. Chem. B 109, 7749.

Minaev, B.F., Shafranyosh, M.I., Yu Svida, Yu., Sukhoviya, M.I., Shafranyosh, I.I., Baryshnikov, G.V., Minaev, V.A., 2014. Fragmentation of the adenine and guanine molecules induced by electron collisions. J. Chem. Phys. 140, 175101.

Mokrani, S., Aouchiche, H., Champion, C., 2020. Elastic scattering of electrons by DNA bases. Radiat. Phys. Chem. 172, 108735.

Mozejko, P., Sanche, L., 2005. Cross sections for electron scattering from selected components of DNA and RNA. Radiat. Phys. Chem. 73, 77.

Nakagawa, S., 2007. Polarizable model potential function for nucleic acid bases. J. Comput. Chem. 28, 1538.

Nikjoo, H., Taleei, R., Liamsuwan, T., Liljequist, D., Emfietzoglou, D., 2016. Perspectives in radiation biophysics: from radiation track structure simulation to mechanistic models of DNA damage and repair. Radiat. Phys. Chem. 128, 3.

Nishimura, H., Tawara, H., 1991a. Some aspects of total scattering cross sections of electrons for simple hydrocarbon molecules. J. Physiol. Biochem.: At Mol. Opt. Phys. 24, L363.

Nishimura, H., Tawara, H., 1991b. Some aspects of total scattering cross sections of electrons for simple hydrocarbon molecules. J. Physiol. Biochem.: At Mol. Opt. Phys. 24, L363.

Onsager, L., 1936. Electric moments of molecules in liquids. J. Am. Chem. Soc. 58, 1486.

Pandya, S.H., Vaishnav, B.G., Joshipura, K.N., 2012. Electron inelastic mean free paths in solids: a theoretical approach. Chin. Phys. B 21.

Parikh, S., Limbachiya, C., 2023. Electron driven molecular processes for nucleosides. Radiat. Phys. Chem. 208, 110940.

Parikh, S., Vinodkumar, M., Limbachiya, C., 2023. Electron impact inelastic molecular processes for deuterated compounds. Chem. Phys. 565, 111766.

Rahman, M.A., Krishnakumar, E., 2015. Absolute partial and total electron ionization cross sections of Uracil. Int. J. Mass Spectrom. 392, 145.

Rahman, M.A., Krishnakumar, E., 2016. Communication: electron ionization of DNA bases. J. Chem. Phys. 144, 161102.

Shafranyosh, I.I., Svida, Yu. Yu., Sukhoviya, M.I., Shafranyosh, M.I., Minaev, B.F., Baryshnikov, G.V., Minaev, V.A., 2015. Absolute effective cross sections of ionization of adenine and guanine molecules by electron impact. Tech. Phys. 60, 1430.

Staszewska, G., Schwenke, D.W., Truhlar, D.G., 1984. Investigation of the shape of the imaginary part of the optical-model potential for electron scattering by rare gases. Phys. Rev. 29, 3078.

Swadia, M., Thakar, Y., Vinodkumar, M., Limbachiya, C., 2017. *Theoretical electron impact total cross Sections for tetrahydrofuran (C_4H_8O)*. Eur. Phys. J. D 71, 85.

Szarek, P., 2017. Electric permittivity in individual atomic and molecular systems through direct associations with electric dipole polarizability and chemical hardness. J. Phys. Chem. C 121, 12593.

Tan, Z., Xia, Y., Liu, X., Zhao, M., Ji, Y., Li, F., Huang, B., 2004. Cross sections of electron inelastic interactions in DNA. Radiat. Environ. Biophys. 43, 173.

Tan, H.Q., Mi, Z., Bettiol, A.A., 2018. Simple and universal model for electron-impact ionization of complex biomolecules. Phys. Rev. E 97, 1.

Thakkar, N., Swadia, M., Vinodkumar, M., Mason, N., Limbachiya, C., 2021. Electron induced elastic and inelastic processes for perfluoroketone (PFK) molecules. Plasma Sources Sci. Technol. 30, 085008.
Toburen, L., 1998. Ionization and charge-transfer: basic data for track structure calculations. Radiat. Environ. Biophys. 37, 221.
Turner, J.E., Paretzke, H.G., Hamm, R.N., Wright, H.A., Ritchie, R.H., 1982. Comparative study of electron energy deposition and yields in water in the liquid and vapor phases. Radiat. Res. 92, 47.
Valiskó, M., Boda, D., 2005. Dielectric constant of the polarizable dipolar hard sphere fluid studied by Monte Carlo simulation and theories. Condens. Matter Phys. 8, 357.
van der Burgt, P.J.M., 2014. Electron impact fragmentation of cytosine: partial ionization cross sections for positive fragments. Eur. Phys. J. D 68, 135.
van der Burgt, P.J.M., 2015. Electron impact fragmentation of adenine: partial ionization cross sections for positive fragments. Eur. Phys. J. D 69, 173.
van der Burgt, P.J.M., Mahon, F., Barrett, G., Gradziel, M.L., 2014. Electron impact fragmentation of thymine: partial ionization cross sections for positive fragments. Eur. Phys. J. D 68, 151.
Vinodkumar, M., Limbachiya, C., 2013. Electron impact total and ionization cross-sections for DNA based compounds. Mol. Phys. 111, 215.
Vinodkumar, M., Joshipura, K.N., Limbachiya, C.G., Antony, B.K., 2003. *Electron impact Ionization of H_2O Molecule in crystalline ice*. Nucl. Instrum. Methods Phys. Res. B 212, 63.
Vinodkumar, M., Joshipura, K.N., Limbachiya, C., Mason, N., 2006. Theoretical calculations of the total and ionization cross sections for electron impact on some simple biomolecules. Phys. Rev. 74, 022721.
Vinodkumar, M., Bhutadia, H., Limbachiya, C., Joshipura, K.N., 2011. *Electron impact total ionization cross Sections for H_2S, PH_3, HCHO and HCOOH*. Int. J. Mass Spectrom. 308, 35.
Vinodkumar, M., Limbachiya, C., Barot, M., Swadia, M., Barot, A., 2013a. Electron impact total ionization cross sections for all the components of DNA and RNA molecule. Int. J. Mass Spectrom. 339–340, 16.
Vinodkumar, M., Limbachiya, C., Barot, A., Mason, N., 2013b. Computation of electron-impact rotationally elastic total cross sections for methanol over an extensive range of impact energy (0.1 – 2000 eV). Phys. Rev. 87, 012702.
Vinodkumar, M., Limbachiya, C., Desai, H., Vinodkumar, P.C., 2014a. Electron-impact total cross sections for phosphorous triflouride. Phys. Rev. 89, 062715.
Vinodkumar, M., Limbachiya, C., Barot, M., Barot, A., Swadia, M., 2014b. Electron impact total cross sections for components of DNA and RNA molecules. Int. J. Mass Spectrom. 360, 1.
Antonio Zecca, Grzegorz P. Karwasz, and R. S. Brusa, *Total-Cross-Section Measurements For Electron Scattering by NH_3, SiH_4, and H_2S in the Intermediate-Energy Range*, vol. 45, (1992)..
Zein, S.A., Bordage, M.C., Francis, Z., Macetti, G., Genoni, A., Dal Cappello, C., Shin, W. G., Incerti, S., 2021. Electron transport in DNA bases: an extension of the geant4-DNA Monte Carlo toolkit. Nucl. Instrum. Methods Phys. Res. B 488, 70.
Zhang, X., Sun, J., Liu, Y., 1992. A new approach to the correlation polarization potential-low-energy electron elastic scattering by He atoms. J. Physiol. Biochem.: At Mol. Opt. Phys. 25, 1893.

ChemPhysChem

Research Article
doi.org/10.1002/cphc.202300916

Chemistry Europe
European Chemical Societies Publishing

www.chemphyschem.org

Electron interaction with DNA constituents in aqueous phase

Smruti Parikh[a] and Chetan Limbachiya*[a]

Electron driven chemistry of biomolecules in aqueous phase presents the realistic picture to study molecular processes. In this study we have investigated the interactions of electrons with the DNA constituents in their aqueous phase in order to obtain the quantities useful for DNA damage assessment. We have computed the inelastic mean free path (IMFP), mass stopping power (MSP) and absorbed dose (D) for the DNA constituents (Adenine, Cytosine, Guanine, Thymine and Uracil) in the aqueous medium from ionisation threshold to 5000 eV. We have modified complex optical potential formalism to include band gap of the systems to calculate inelastic cross sections which are used to estimate these entities. This is the maiden attempt to report these important quantities for the aqueous DNA constituents. We have compared our results with available data in gas and other phase and have observed explicable accord for IMFP and MSP. Since these are the first results of absorbed dose (D) for these compounds, we have explored present results vis-a-vis dose absorption in water.

1. Introduction

More than a century of effort has been put into finding a cure for cancer. As a better alternative to conventional photon therapy (radiotherapy), ion beams are becoming widely employed tools for cancer therapy.[1,2] In fact, the phrase "magic bullet" was created to depict Auger electrons' capabilities as a potential solution to the problem of cancer therapy after their discovery in 1925.[3] Electron beams are suitable for intra-operative electron radiation therapy (IOERT), which treats a residual tumour or tumour bed with electron beams in cancer surgery[4] since the dose drops off quickly after the target region depending on the electron energy, sparing healthy tissue.[5]

It is now very well known that ion beams and energetic radiation penetrating a material undergo elastic and inelastic interactions, resulting in a 'shower' of secondary particles, inflicting radiation damage to organisms and cells directly or indirectly.[6] Inside the cells, deoxyribonucleic acid (DNA) is the most sensitive target to the radiations. Radiation exposure causes a range of DNA damage in the nucleus of mammalian cells.[3]

Radiation dosimetry focuses heavily on the knowledge of the energy deposited by electrons in DNA and the damage they produce.[7] The average energy deposited in the inelastic events as a result of ionised particles, can be calculated using two characteristic parameters, Inelastic Mean Free Path (IMFP) and Stopping Power (SP).[8]

Stopping Power (SP), the average energy dissipated by the charged particle,[9] is a critical metric for assessing radiation impact in medical and environmental applications.[10] In addition to being utilised frequently in the simulations of Monte Carlo method for electron transport in biomaterials,[8,11] SP can also be used to estimate dosage or other relevant quantities without relying on complete calculations for electron transport.[12]

The average distance a charged particle travels within a medium between two consecutive inelastic collisions, known as inelastic mean free path, is the fundamental input for track-structure computations in radiation biology.[13–16] In radiation dosimetry and scanning electron spectroscopies, a precise understanding of the inelastic mean free path for electrons having energy below 1000 eV is crucial.[17] Also, it is essential in modelling electron transport through solids and liquids using the Monte Carlo method.[18,19] Fundamental studies in radiation biology as well as biomedical applications, both rely heavily on IMFP and SP.[8]

DNA, a double-stranded helical macromolecule, is responsible for creating the genetic code in all living things. For the cell to remain healthy and to replicate properly, this sequence's integrity must be maintained, and any damage or errors could cause carcinogenesis and cell death.[20] The double helix of DNA never exists alone in the body; rather, water molecules always cover the entire surface of the double helix. The amount of water molecules surrounding the DNA determines its exact structure.[21,22] On the other hand, the accurate damage assessment of the DNA molecules is crucial because they are thought to be the most radiation-sensitive target within cells. And hence, considering aqueous phase, rather than gaseous phase or condensed phase of the DNA elements leads us to the more realistic way. Thus, in the present work we have reported three quantities, IMFP, mass SP and absorbed dose for the electron inelastic interactions with the DNA components in their aqueous phase.

The term "absorbed dose (D)" refers to a measurement that expresses how much energy is absorbed by a substance per unit mass. It is a general term, defined for any kind of radiation or substance, used in radiobiology because it is a great way to predict the harm a particular kind of radiation will do to an organ.[23] In the present study absorbed dose is also reported for all the five components of DNA. This is the maiden attempt

[a] S. Parikh, C. Limbachiya
The Maharaja Sayajirao University of Baroda, Vadodara-390 001
E-mail: cglimbachiya-apphy@msubaroda.ac.in

to report the absorbed dose data for the present investigated molecules.

The calculation of IMFP and SP done by Tan *et. al.*,[8,24,25] Tanuma *et. al.*,[26] Akkerman and Akkerman,[27] and Jablonski *et. al.*[28] based on the dielectric response theory, followed by the evaluation of optical energy loss function (OELF) through different methods. Theoretical methods like generalized oscillator strength (GOS) model by Akar and Gümüş,[29–31] Quantitative structure–property relationship (QSPR) scheme by Cumpson *et. al.*,[32] SP calculation from Modified Rohrlich and Carlson formula by Gümüş and Bentabet,[33] Rudd model calculation by Francis *et. al.*,[34] Predictive S-lamda expression by Jablonski *et. al.*,[28] the expressions of Joy and Luo[35] and that of of Fernandez-Varea *et. al.*[36] are employed for such study. Most of these theoretical and semi-empirical approaches are not suitable for low energy calculations, but they are good at higher energy regime.[8,24–29,31,32] The present theory employs partial wave calculations which provide reliable results even at low energy side.

The present research work focuses on the inelastic collisions of electrons with the DNA constituents (Adenine, Cytosine, Guanine, Thymine and Uracil) in aqueous phase and quantify them through IMFP, MSP and absorbed dose for the incident energy range from ionization threshold to 5000 eV. This is the first report to quantify these three inelastic metrics for all of the five DNA components in their very realistic form by considering them in aqueous phase. We briefly outline the method to compute the Inelastic Mean Free Path, Mass stopping power and absorbed dose for the electron interactions with DNA constituents in their aqueous phase. We display target properties in table 1.

2. Theoretical Methodology

The inelastic mean free path, λ_{inel} is given in terms of the inelastic scattering cross-sections, (Q_{inel}) as,[37,38]

$$\lambda_{inel} = \frac{1}{NQ_{inel}} \tag{1}$$

where, $N = \frac{N_a \rho}{M}$, represents the number density of the target molecule. N_a is the Avogadro's number ($=6.023\times10^{23}$), ρ is the molecular density and M is the molar mass of the molecule.

Table 1. Target properties.

Target	Aqueous phase ***IE*** (eV)	Band gap E_{gap} (eV)	Target density, ρ (gm/cm^3)	Molar mass, ***M*** (gm/mol)	Mean excitation energy, $\bar{E}$ (eV)
Adenine	5.00[53,54]	5.25[55]	1.35[25]	135.14[25]	69.06[56]
Cytosine	5.50[53,54]	5.35[57]	1.30[25]	111.11[25]	69.60[56]
Guanine	4.80[53,54]	4.80[58]	1.58[25]	151.14[25]	71.58[56]
Thymine	5.40[53,54]	5.20[59]	1.48[25]	126.12[25]	70.00[56]
Uracil	5.55[53]	5.70[57]	1.32[25]	112.09[25]	73.13[56]

We define an energy dependent complex optical potential of the following form that describes the electron-molecule interaction in order to achieve Q_{inel} using the spherical complex optical potential (SCOP) approach,[39–42]

$$V_{opt}(r, E_i) = V_R + iV_I \tag{2}$$

The real terms, V_R covers the elastic events. It involves the static, exchange, and polarisation effects through various model potentials. It involves static potential, V_{st},[43] exchange potential, V_{exc}[44] and polarization potential, V_p,[45] respectively. The imaginary term, V_I in equation (2) is the absorption potential[46] to take into consideration all the allowed inelastic channels.

$$V_I(r, E_i) = -\rho(r)\sqrt{\frac{T_{loc}}{2}}\left(\frac{8\pi}{10k_F^3 E_i}\right)\Theta\left(p^2 - k_F^2 - 2\Delta\right) (A_1 + A_2 + A_3) \tag{3}$$

Here, $\Theta(x)$ is the Heaviside unit step-function, T_{loc} is the local kinetic energy of impacted electrons and k_F is the Fermi wavevector. The dynamic functions A_1, A_2, and A_3 are influenced by the energy parameter Δ, which sets a threshold below which inelastic processes are forbidden. In the free phase of the molecule a valance electron is ejected when the incident electron energy is equal to the molecule's first ionisation energy (I). However, the issue is challenging in an aqueous or condensed medium. Only when the impact energy, E_i of the projectile exceeds the ionisation energy, I by an amount equal to the energy-band gap, E_{gap} does the ionisation actually occur.[37,38] In other words,

$$\Delta = I + E_{gap} \tag{4}$$

By computing the complex scattering phase shifts, the inelastic cross section (Q_{inel}) are calculated.[47] In our earlier articles, we have covered the details of the present scattering model.[38,47–49] This Q_{inel} sums up all the permitted ionisations and electronic excitations,

$$Q_{inel} = Q_{ion} + \Sigma Q_{exc} \tag{5}$$

where the ΣQ_{exc} includes collectively all allowed electronic transitions that are influenced by low-lying states, and the Q_{ion} symbolizes the total ionisation cross sections for all possible ionizations of the target by electron collisions.

The electron stopping power or energy loss per unit path length of electron in the target medium $\left(\frac{dE}{dx}\right)$ is given in terms of mass stopping power $\frac{1}{\rho}\left(\frac{dE}{dx}\right)$, which takes into account the density of the medium from the following equation,[50]

$$-\frac{1}{\rho}\left(\frac{dE}{dx}\right) = \frac{N_a}{M}\bar{E}Q_{inel} \tag{6}$$

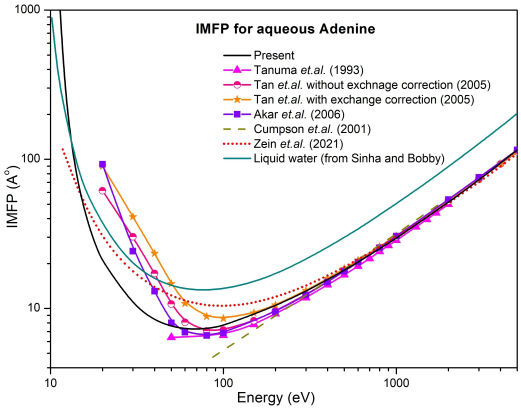

Figure 1. IMFP for aqueous Adenine. Line: Present; Filled triangles: Tanuma *et. al.*[26]; half-filled circles: Tan *et. al.* without exchange;[25] filled stars: Tan *et. al.* with Born-Ochkur;[25] filled squares: Akar *et. al.*;[31] dash line: Cumpson *et. al.*;[32] short dot line: Zein *et. al.*[20]

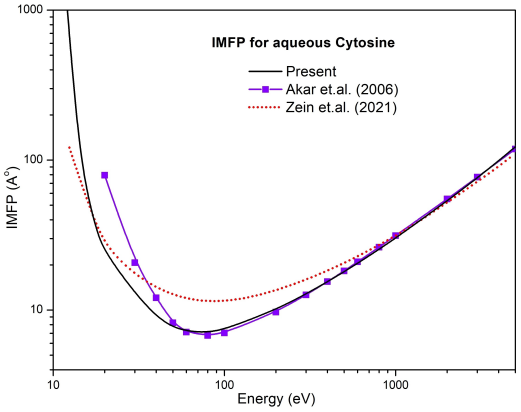

Figure 2. IMFP for aqueous Cytosine. Line: Present; filled squares: Akar et. al.;[31] short dot line: Zein et. al.[20]

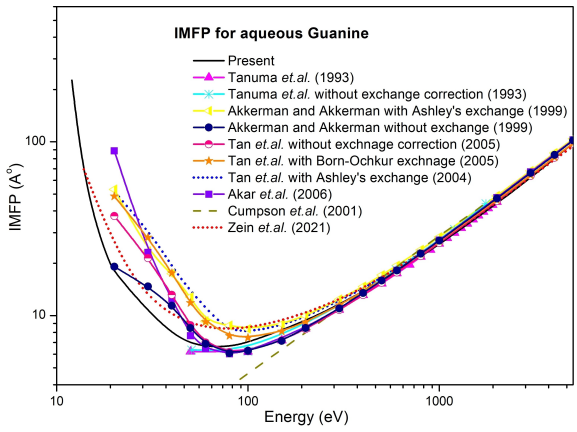

Figure 3. IMFP for aqueous Guanine. Line: Present; filled triangles: Tanuma et. al.;[26] asterisk: Tanuma et. al. without exchange;[26] half-filled triangles: Akkerman and Akkerman with Ashley exchange;[27] solid circles: Akkerman and Akkerman without exchange;[27] half-filled circles: Tan et. al. without exchange;[25] filled stars: Tan et. al. with Born-Ochkur exchange;[25] short blue dot: Tan et. al. with Ashley exchange;[24] filled squares: Akar et. al.;[31] dark yellow dash line: Cumpson et. al.;[32] short red dot: Zein et. al.[20]

where, $\bar{E}$ is the average excitation energy of the target molecule.

When the particle penetrates the distance r that the particle travelled in the medium, the absorbed dose, D is obtained from the following equation at the distance,[51,52]

$$D = \frac{-\left(\frac{dE}{dx}\right)}{4\pi\rho r^2} \tag{7}$$

For the present target molecules all the required parameters are listed in Table 2.

3. Results and Discussions

In the present section we report the IMFP, mass SP and absorbed dose (D) values for the DNA constituent molecules, viz., Adenine, Cytosine, Guanine, Thymine and Uracil in their aqueous phase in figures 1–17 along with comparisons wherever available from literature.

3.1. Inelastic mean free path (IMFP)

We have displayed IMFP for Adenine and Cytosine in figure 1 and 2, respectively. The nature of the IMFP curve is explained through inelastic cross-sections. At the ionisation threshold, the mean distance travelled by the electron between the consecutive collisions within the medium is maximum. As the energy increases, collisions increase and IMFP decreases. Further at the energy 80–90 eV, the peak of the Q_{inel} is reached, which indicates the minima of the mean distance travelled in this energy region. With energies beyond 100 eV, the electrons have less time to collide with the molecules, resulting in the reduction in the Q_{inel}, which further implies increasing in the IMFP values from its valley region.

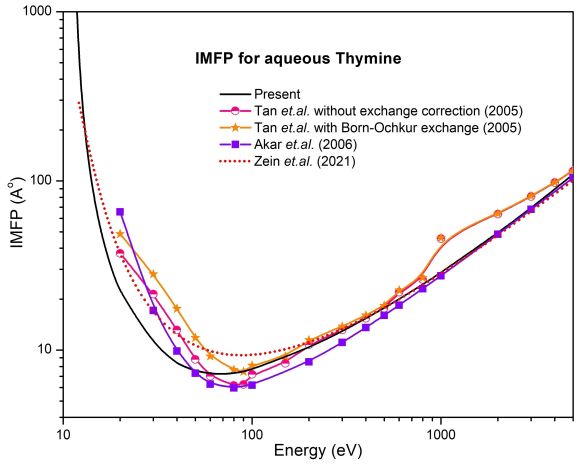

Figure 4. IMFP for aqueous Thymine. Line: Present; half-filled circles: Tan et. al. without exchange;[25] filled stars: Tan et. al. with Born-Ochkur exchange;[25] filled squares: Akar et. al.;[31] short red dot: Zein et. al.[20]

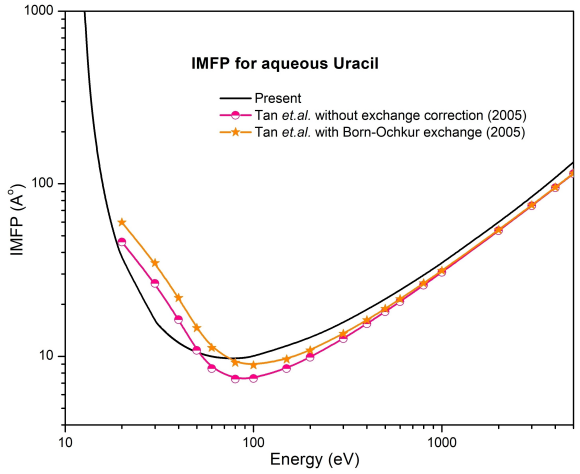

Figure 5. IMFP for aqueous Uracil. Line: Present; half-filled circles: Tan et. al. without exchange;[25] filled stars: Tan et. al. with Born-Ochkur exchange.[25]

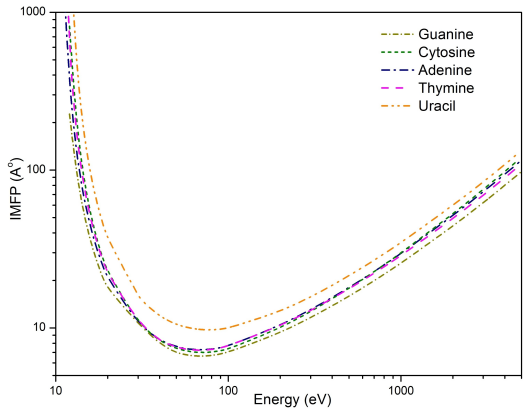

Figure 6. IMFP for DNA constituents.

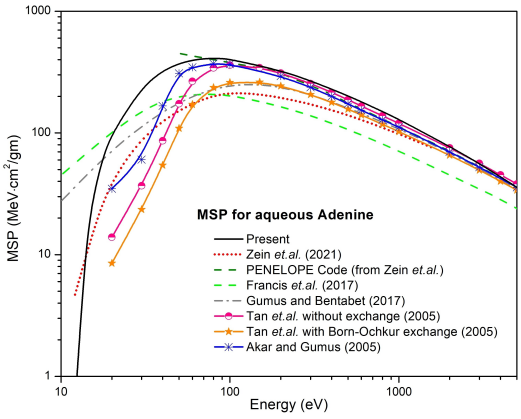

Figure 7. MSP for aqueous Adenine. Line: Present; short red dot: Zein et. al.[20]; pink dash line: Zein et. al.,[20] green dash line: Francis et. al.,[34] gray dash dot: Gümüş and Bentabet;[33] half-filled circles: Tan et. al. without exchange;[25] filled stars: Tan et. al. with Born-Ochkur exchange;[25] asterisk: Akar and Gümüş.[29]

The present results as shown in figure 1 are in good agreement with the results obtained using optical energy loss function (OELF) followed by Penn's algorithm by Tanuma

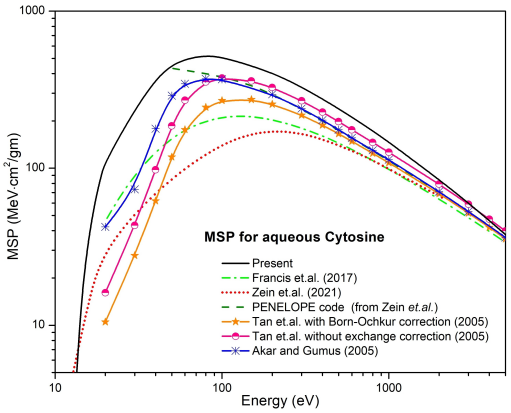

Figure 8. MSP for aqueous Cytosine. Line: Present; dash line: Francis et. al.,[34] short dot line: Zein et. al.,[20] pink dash: PENELOPE code;[20] half-filled circles + line: Tan et. al. without exchange;[25] filled stars + line: Tan et. al. with Born-Ochkur;[25] asterisk: Akar and Gümüş.[29]

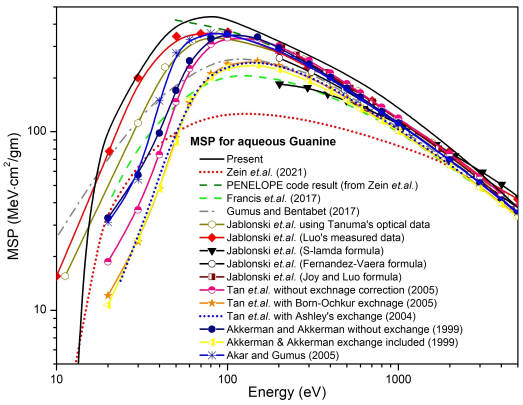

Figure 9. MSP for aqueous Guanine. Line: Present; short dot line: Zein et. al.,[20] pink dash: PENELOPE code;[20] dash line: Francis et. al.,[34] grey dash dot: Gümüş and Bentabet;[33] open hexagons: Jablonski et. al. using optical data;[28] diamonds: measured by Luo taken from Joy's database;[28] inverted triangles: S-lamda approach;[28] open circles: Fernández-Varea formula;[28] half-filled squares: Joy and Luo formula;[28] blue dot line: Tan et. al. with Ashley exchange;[24] half-filled circles: Tan et. al. without exchange;[25] filled stars: Tan et. al. with Born-Ochkur exchange;[25] half-filled triangles: Akkerman and Akkerman with Ashley exchange;[27] solid circles: Akkerman and Akkerman without exchange;[27] asterisk: Akar and Gümüş.[29]

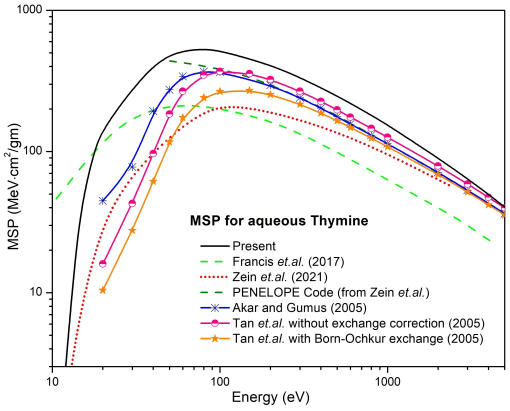

Figure 10. MSP for aqueous Thymine. Line: Present; green dash: Francis et. al.,[34] red dot line: Zein et. al.,[20] pink dash line: PENELOPE code;[20] asterisk: Akar and Gümüş;[29] half-filled circles: Tan et. al. without exchange;[25] filled stars: Tan et. al. with Born-Ochkur exchange.[25]

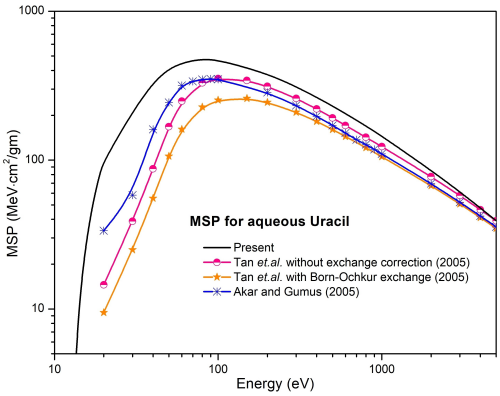

Figure 11. MSP for aqueous Uracil. Line: Present; half-filled circles: Tan et. al. without exchange;[25] filled stars: Tan et. al. with Born-Ochkur exchange;[25] asterisk: Akar and Gümüş.[29]

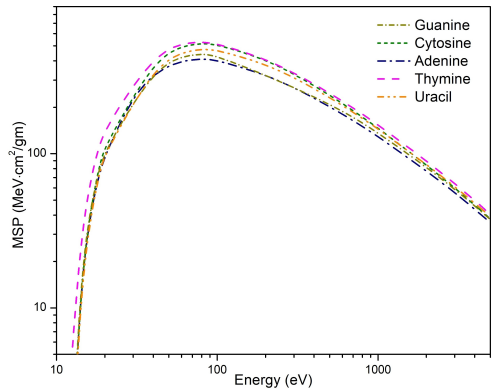

Figure 12. MSP for DNA constituents.

et. al.[26] and Tan *et. al.*,[25] with those data of Cumpson *et. al.*[32] through Quantitative Structure-Property relationships (QSPR) and results of Akar *et. al.*[31] using Generalized Oscillator strength (GOS) model for the electron energy above 70 eV. As energy increases the present curve starts merging with all the existing data. For the energy below 50 eV, the deviation between the present values and the results of Tanuma *et. al.*[26] and Tan *et. al.*[25] is observed, as they have used Penn's statistical approximation in their calculations, which is more appropriate for the energy higher than 50 eV.[60] Moreover, IMFP values obtained using optical data are less reliable for energy below 200 eV.[26,32] Tan *et. al.*[25] used Linhard dielectric function in OELF calculation and also involved the exchange correction of Born-Ochkur in their methodology, which deals with the approximation of free electron gas assuming that the energy-momentum relation for a non-relativistic electron in solid is similar to that of a free electron in vacuum. The present data obtained considering the molecules in their aqueous phase are thus more realistic. Akar *et. al.*[31] results calculated from the GOS model calculation involve the first-Born approximation, which is more accurate at higher energies. Hence, at lower energy region their data is also believed to be less reliable than the present ones. Cumpson *et. al.*[32] reported the IMFP values using QSPR relationships and the data of Tanuma *et. al.*[26] were used for fitting the IMFP equation reliable for the energy 200–2000 eV. The present data overestimates the results of Cumpson *et. al.*[32] for energy below 300 eV and for higher energies, it starts merging. The results of the simulations of Geant4-DNA code by Zein *et. al.*[20] are of the higher values at the valley region but shows the similar trend as the present one.

In figure 2, we have plotted the IMFP results of Cytosine molecule. Only Akar *et. al.*[31] and Zein *et. al.*[20] reported the IMFP data for this target. The deviation of the data of Akar *et. al.*[31] from the present values is observed here again for energy $E < 50$ eV due to the mentioned reasons in the case of Adenine, while for the rest of the energy range ($E > 50$ eV) the present data overlaps with that of Akar *et. al.*[31] Present values show good agreement with the data of Zein *et. al.*[20] obtained by Geant4-DNA code except at the valley region, where they underestimate.

Figure 3 shows the IMFP plot for the most studied target, Guanine molecule. Similar behaviour of the present IMFP curve with respect to that of Tanuma *et. al.*,[26] Tan *et. al.*,[25] Akar

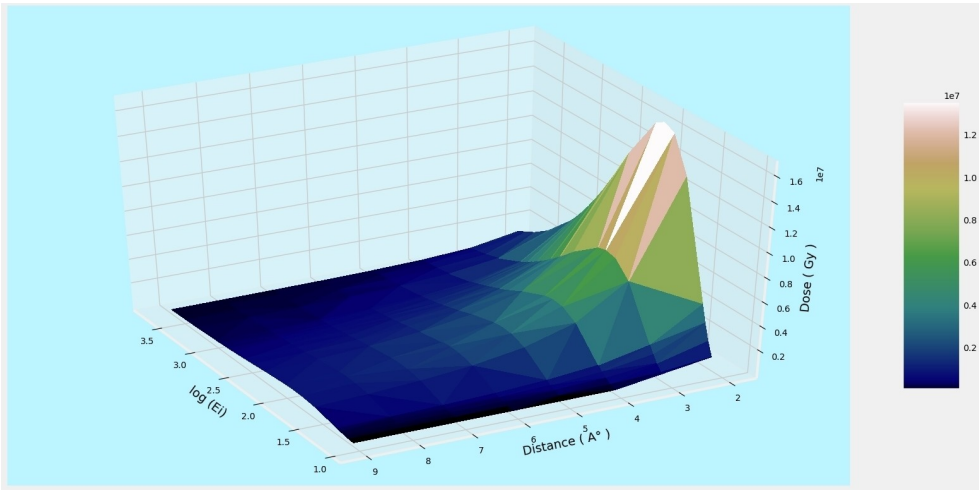

Figure 13. 3D plot of absorbed dose for Thymine. X-axis: $\log_{10}(E_i)$; Y-axis: Distance (Å); Z-axis: Absorbed Dose ($\times 10^7$ Gy).

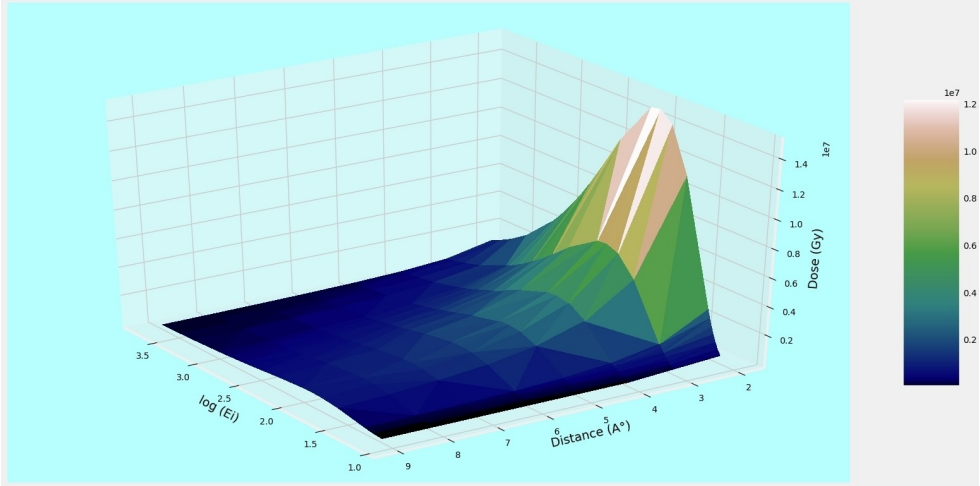

Figure 14. 3D plot of absorbed dose for Uracil. X-axis: $\log_{10}(E_i)$; Y-axis: Distance (Å); Z-axis: Absorbed Dose ($\times 10^7$ Gy).

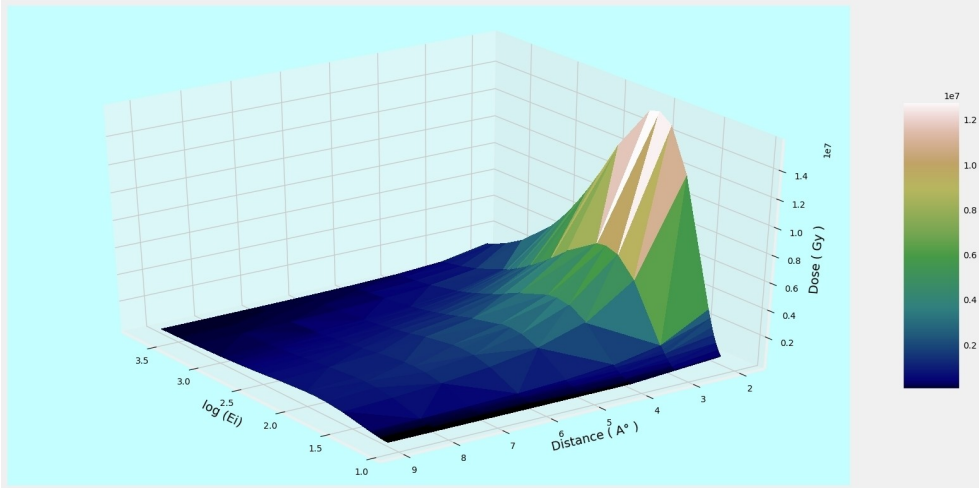

Figure 15. 3D plot of absorbed dose for Cytosine. X-axis: $\log_{10}(E_i)$; Y-axis: Distance (Å); Z-axis: Absorbed Dose ($\times 10^7$ Gy).

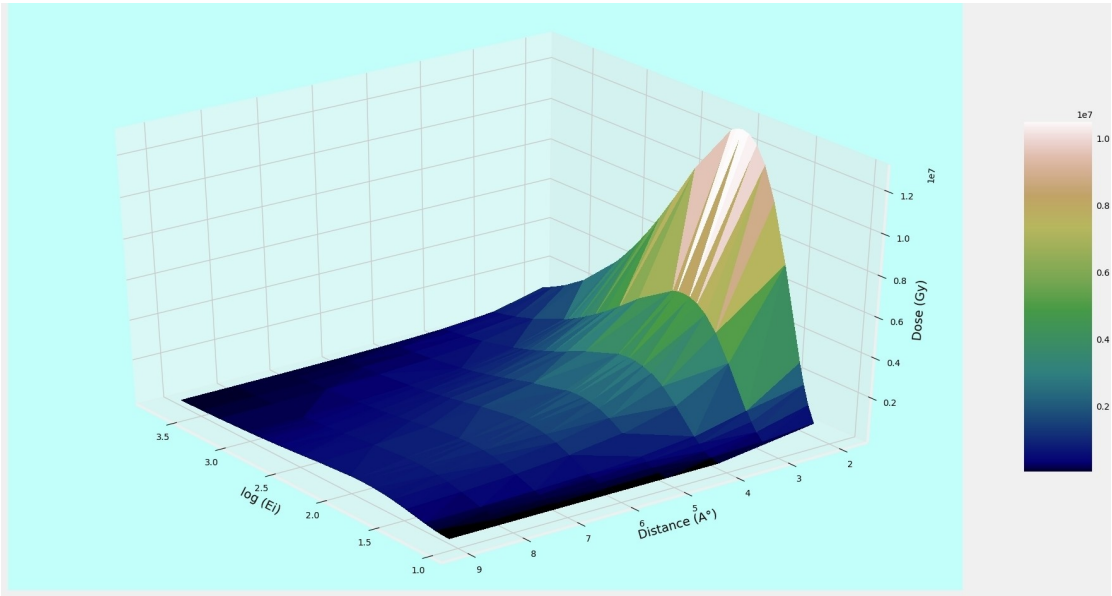

Figure 16. 3D plot of absorbed dose for Adenine. X-axis: $\log_{10}(E_i)$; Y-axis: Distance (Å); Z-axis: Absorbed Dose ($\times 10^7$ Gy).

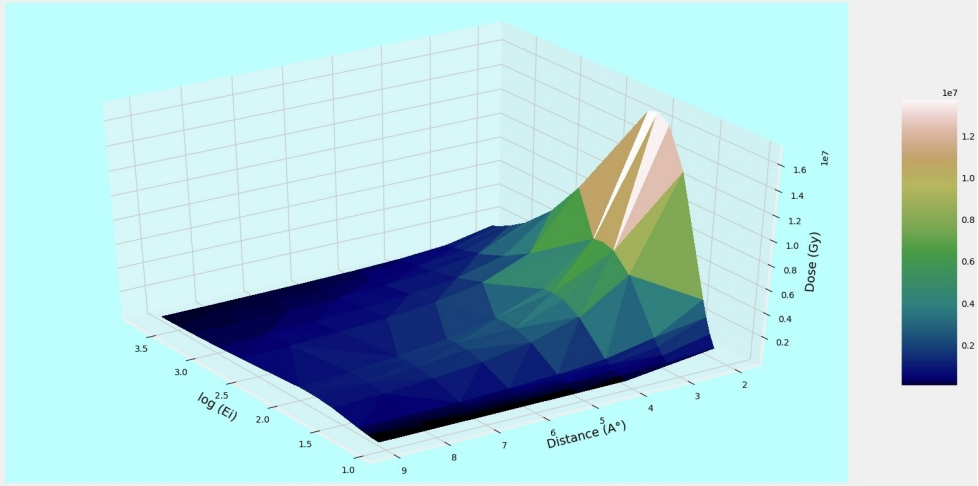

Figure 17. 3D plot of absorbed dose for Guanine. X-axis: $\log_{10}(E_i)$; Y-axis: Distance (Å); Z-axis: Absorbed Dose ($\times 10^7$ Gy).

et. al.,[31] Cumpson *et. al.*[32] and Zein *et. al.*[20] is observed because of the reasons discussed earlier. For energy E > 70 eV, a good matching of the present data with the data of Tan *et. al.* without exchange correction[25] and those of Tanuma *et. al.*[26] and Akar *et. al.*[31] is observed. The results of Akkerman and Akkerman[27] without including exchange correction is seen in good accord with the present data beyond 70 eV. They have fitted the experimental energy loss function (ELF) by a sum of Drude-type function to calculate the IMFP and SP values for the Guanine molecule. At energy below 50 eV, the discrepancy of their[27] data with respect to the present one is seen. The reason behind this mentioned by them is that the accuracy of their data is lower as the approximated treatment of exchange effect might increase the possible errors in the calculations of IMFP and SP up to 100%.[27] Here also, the present curve underestimates the Zein *et. al.*[20] data specifically in the valley region and then starts merging at the higher energy region.

The electron IMFP for Thymine, is shown in figure 4. A good agreement between the present values of IMFP and the results of Tan *et. al.*[25] is observed. They start overlapping at energy above 150 eV. The data of Akar *et. al.*[31] is observed to be lower than the present ones at the valley region and at higher energy they match well. Similar trend of Zein *et. al.*[20] as seen in earlier cases is observed here too.

Figure 5 depicts the case of Uracil molecule. Only Tan *et. al.*[25] reported the IMFP values for this target without exchange correction and with Born-Ochkur exchange correction. The present results show good agreement with their data.[25]

Figure 6 displays the present IMFP results for the five DNA base species. The IMFP values depend on the size of the target species (through number of target electrons) and the threshold value of the opening of inelastic channels, since the ionizing probability of the target species is directly proportional to the number of electrons contained by that target.[61]

3.2. Mass stopping power (MSP)

In this subsection, we display vide., figures 7–11, our results on MSP for the DNA constituents in aqueous medium along with available comparisons. Stopping power is the energy loss per unit length due to the successive inelastic collisions between electron and molecules. However, we have reported the MSP through equation 6 for the present studied molecules, as it is more important quantity because it involves the density of the medium through which the electron energy loss takes place. For the low energy, due to less probabilities of the inelastic collisions, the energy loss is low. At the peak value of inelastic cross-sections (Q_{inel}), the energy loss is highest, resulting into maximum value of MSP. With increasing energies of the incident particle, the interaction time decreases causing reduction in energy loss leading to receding MSP.

Figure 7 depicts the present MSP data for aqueous Adenine with the available comparison. As the figure depicts, in the lower energy regime, discrepancies are seen among all existing data. The present values can be seen in excellent matching with the Tan *et. al.* data without exchange,[25] results of Akar and Gümüş[29] and those of PENELOPE code simulation[20] for energy beyond 50 eV. Tan *et. al.*[25] have reported data with Born-Ochkur exchange correction as well. Tan *et. al.*[25] and Francis *et. al.*[34] has reported the SP values (in eV/A°), which then converted into MSP (MeV·cm^2/gm) by author using the present reported density values for the particular target. The Born-Ochkur formalism-based DCSs produce collision stopping powers of somewhat lower values, about a few hundred eV, resulting in the dispersion of electron tracks in all directions.[62] Therefore, Tan *et. al.*[25] data with Born-Ochkur correction underestimates the present results. Francis *et. al.*[34] used the Rudd model for the calculation of differential cross-section, which gives the values within ±10–20% uncertainty and then those DCS fed into the Geant4-DNA class to calculate the SP. Their results underestimate all the available data including present ones for the energy above 70 eV. Gümüş and Bentabet[33] reported the MSP values for the energy 10–10^7 eV by extending

the semi-empirical model[63,64] to give MSP data for gaseous bioorganic compounds, whereas the present data deals with the aqueous phase of the target molecule. Thus, the deviation of their data with the present values can be understood. The present curve overestimates the data of Zein *et. al.*[20]

The case for electron MSP of aqueous Cytosine is shown in figure 8. We observe discrepancies among all the results below 600 eV.[20,25,29,34] The present results tend to overestimate the available data.[20,25,29,34] As discussed earlier, the Tan *et. al.*[25] data carried through Born-Ochkur exchange effect yield lower SP values and the data of Francis *et. al.* are uncertained by ±10–20%.[34] As electron energy increases, the deviation of the present values of the MSP with the others goes on reducing. However, the present curve shows the similar trend as the others.

The plot of MSP vs incident electron energy for aqueous Guanine is shown in figure 9. Akkerman and Akkerman,[27] Jablonski *et. al.*,[28] Tan *et. al.*[25] reported the SP values, which are converted to MSP by us using the density mentioned in Table 2. Jablonski *et. al.*[28] reported the SP values using the three different expressions for energy E > 200 eV, viz. S-lamda approach,[28] Joy and Luo formula[35] and Fernández-Varea formula.[36] They also reported the measured SP values by Luo taken from Joy's database[65] and calculated SP using the optical data of Tanuma *et. al.* in dielectric response theory-based calculation. All of these SP values were roughly calculated by weighted sum of the SP of the solid's atomic constituents with weights determined by mass fractions. It is mentioned that the calculated SP between 10–100 eV energy range is being less accurate than those for higher energies.[28] Thus, the deviation of their data at lower energy regime from the present data expected. The results of the PENELOPE code simulation[20] and Jablonski *et. al.*[28] data obtained using optical data of Tanuma *et. al.* are seen as less deviated from the present curve. Though the discrepancy has been observed among the reported data and the present data, same trend is observed.

In figure 10, the plot of MSP data for aqueous Thymine molecule is shown with the available comparisons.[20,25,29,34] As discussed earlier, the results of Tan *et. al.*[25] with Born-Ochkur correction show lower values of MSP. While the behaviour of present curve with the reported data of Akar and Gümüş,[29] Zein *et. al.*,[20] and Francis *et. al.*[34] shows similar trend. The mutual deviation is seen as specially at lower energy range.

In figure 11, the present data of MSP for aqueous Uracil molecule is shown. Tan *et. al.*[25] have reported the data with Born-Ochkur exchange and without exchange effect. Akar and Gümüş [29] have reported the SP data using generalized oscillator strength (GOS) model.

Figure 12 displays the MSP results for present DNA target molecules. As in the case of IMFP, MSP values also influenced by the threshold value, number of target electrons[61] and density of the material.

The collisional SP data of Akar and Gümüş[29] for all reported DNA constituent molecules, were converted into MSP through consideration of density of the medium (Table 2) as discussed earlier. Here, we note that the total SP consists of collisional SP and bremsstrahlung SP.[30] However, bremsstrahlung SP is relevant only beyond the 300 keV. Therefore, for the present study, that range is threshold energy to 5000 eV, collisional SP data have been used for comparison for all studied molecules.

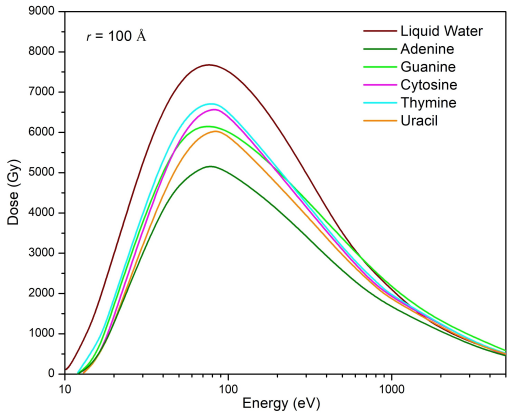

Figure 18. Dose vs Energy plot for DNA molecules and water at distance $r = 100$ A°.

3.3. Absorbed dose (D)

Along with IMFP and MSP, we have also computed absorbed dose (D) viz., equation 7 for all the molecules under study. Three dimensional plots of the absorbed dose (D) against incident energy (E_i) and distance (r) are shown in figures 13–17 for these molecules. The energy values shown are in log scale. (e.g., for energy = 100 eV, the value on the scale will be $\log_{10}(100) = 2$).

Figures 13–15 display the absorbed dose computation results for pyrimidine bases viz., Thymine, Uracil and Cytosine.

The peak values of the dose for these bases, (T, U and C) occurs at around 80–90 eV incident energy. This is because as the incident energy of the incoming electrons surpasses the Δ value (equation 4), the absorption of the energy in the target medium begins and attains its maximum value shown by peak of Q_{inel} at about 80–90 eV. At this energy, maximum energy transfers and hence peak of dose absorption occurs.

In figures 16 and 17, the D values against the distance and incident energy have been plotted for purine bases, viz., Adenine and Guanine, respectively.

The dose values are found to be continuously decreasing with the distance increasing for both the pyrimidine and purine bases. This decreasing nature of the absorbed dose with the distance is understood from its inverse dependence to with it.

In figure 18, the dose vs energy curve is plotted for the present DNA molecules for the particular distance, $r = 100$ A°. Since, we have investigated these DNA constituents in aqueous phase, we have computed the absorbed dose of water for comparison to get better insight. In figure 16, the absorbed dose for these molecules is shown along with that for water for a particular distance, $r = 100$ A°.

From the figure, it can be seen that the liquid water shows the maximum dose value, which means the maximum amount

of the energy is absorbed by the liquid water in comparison to the DNA constituents. Elahe Alizadeh and Leon Sanche[66] also bring up the fact that the water molecules absorb about ~66% of the radiation energy. Present calculation for the dose values of the liquid water is carried out using the IMFP values of Nidhi Sinha and Bobby Antony.[67]

Conclusions

Present study deals with the realistic picture for the electron induced DNA damage assessment by considering the DNA compounds in their aqueous phase, since the DNA is always covered with the water molecules through hydrogen bonding[21,22] in human body. We have reported our results on the major tools for the modelling of DNA damage assessment, the inelastic mean free path (IMFP), MSP (mass stopping power) and absorbed dose (D), for aqueous DNA bases, viz. Adenine, Guanine, Cytosine, Thymine and Uracil from ionisation energy to 5000 eV. The route adopted in the present work to calculate these applied quantities is the maiden attempt. This study is the first report on IMFP, MSP and absorbed dose (D) calculation for aqueous DNA compounds. Since these are the first results of absorbed dose (D) for these compounds, we have explored present results vis-a-vis dose absorption in water.

Conflict of Interests

The authors declare no conflict of interest.

Data Availability Statement

The data that support the findings of this study are available from the corresponding author upon reasonable request.

Keywords: Inelastic mean free path · mass stopping power · absorbed dose · aqueous DNA compounds

[1] H. Tsujii et al, *New J. Phys.* **2008**, *10*, 075009.
[2] U. Amaldi, G. Kraft, *Reports on Progress in Physics* **2005**, *68*, 1861.
[3] H. Nikjoo, R. Taleei, T. Liamsuwan, D. Liljequist, D. Emfietzoglou, *Radiat. Phys.Chem.* **2016**, *128*, 3.
[4] F. A. Calvo, *Oncology* **2004**, *27*, 345.
[5] Wikipedia, https://en.wikipedia.org/wiki/Intraoperative electron radiation therapy#cite note-1.
[6] Francesc. Salvat Gavaldà, J. M. Fernández Varea, Josep. Sempau Roma, and Organització de Cooperació i Desenvolupament Econòmic., *PENELOPE 2008: A Code System for Monte Carlo Simulation of Electron and Photon Transport: Workshop Proceedings, Barcelona*,OECD, **2009** *Spain, 30 June-3 July 2008.*
[7] J. A. Laverne, S. M. Pimblott, *Radiat. Res.* **1995**, *141*, 208..
[8] Z. Tan, Y. Xia, M. Zhao, X. Liu, *Radiat Environ Biophys* **2006**, *45*, 135.
[9] *ICRU Report*-37, **1984**.
[10] A. Muñoz, J. C. Oller, F. Blanco, J. D. Gorfinkiel, P. Limão-Vieira, G. García, *Phys Rev A* **2007** *76*, 052707.
[11] F. Salvat, J. M. Fernández-Varea, J. Sempau, J. Mazurier, *Radiat Environ Biophys* **1999**, *38*, 15.
[12] J. Sempau, P. Andreo, J. Aldana, J. Mazurier, F. Salvat, *Phys Med Biol* **2004**, *49*, 4427.
[13] D. Emfietzoglou, K. Karava, G. Papamichael, M. Moscovitch, *Phys Med Biol* **2003**, *48*, 2355.
[14] H. Nikjoo, S. Uehara, I. Khvostunov, F. A. Cucinotta, W. E. Wilson, D. T. Goodhead, *Phys. Medica* **2001**, *17*, 38.
[15] W. Friedland, P. Jacob, H. G. Paretzke, T. Stork, *Radiat. Res.* **1998**, *150*, 170.
[16] H. Nikjoo, S. Uehara, W. E. Wilson, M. Hoshi, D. T. Goodhead, *Int. J. Radiat. Biol.* **1998**, *73*, 355.
[17] M. A. Flores-Mancera, J. S. Villarrubia, G. Massillon-Jl, *ACS Omega* **2020**, *5*, 4139.
[18] Maurizio Dapor, *Transport of Energetic Electrons in Solids: Computer Simulation with Applications to Materials Analysis and Characterization,* 4th ed, Springer Nature, Switzerland **2023**.
[19] R. Garcia-Molina, I. Abril, I. Kyriakou, D. Emfietzoglou, *Surf Interface Anal* **2017**, *49*, 11.
[20] S. A. Zein, M. C. Bordage, Z. Francis, G. Macetti, A. Genoni, C. Dal Cappello, W. G. Shin, S. Incerti, *Nucl. Instrum. Methods. Phys. Res. B* **2021**, *488*, 70.
[21] H. Khesbak, O. Savchuk, S. Tsushima, K. Fahmy, *J. Am. Chem. Soc.* **2011**, *133*, 5834.
[22] Helmholtz Association of German Research Centres, *Water Molecules Characterize the Structure of DNA Genetic Material.*, https://www.sciencedaily.com/releases/2011/04/110426091122.htm#citation apa.
[23] A. E. Andisco, D. Blanco, S. Buzzi, *Rev. Argent Radiol* **2014** *78*, 114.
[24] Z. Tan, Y. Xia, M. Zhao, X. Liu, F. Li, B. Huang, Y. Ji, *Nucl. Instrum. Methods. Phys. Res. B* **2004**, *222*, 27.
[25] Z. Tan, Y. Xia, X. Liu, M. Zhao, Y. Ji, F. Li, B. Huang, *Appl. Phys. A Mater. Sci. Process.* **2005**, *81*, 779.
[26] S. Tanuma, C. J. Powell, D. R. Penn, *Surf Interface Anal* **1994**, *21*, 165.
[27] A. Akkerman, E. Akkerman, *J. Appl. Phys.* **1999**, *86*, 5809.
[28] A. Jablonski, S. Tanuma, C. J. Powell, *Journal of Surface Analysis* **2006**, *13*, 170.
[29] A. Akar, H. Gümüş, *Radiat Phys. Chem.* **2005**, *73*, 196.
[30] A. Akar, H. Gümüş, N. T. Okumuşoğlu, *Advances in Quantum Chemistry* **2007**, *52*, 277.
[31] A. Akar, H. Gümüş, N. T. Okumuşoğlu, *Appl. Radiat Isot* **2006**, *64*, 543.
[32] P. J. Cumpson, *Surf Interface Anal* **2001**, *31*, 23.
[33] H. Gümüş, A. Bentabet, *Appl. Phys. A Mater. Sci. Process.* **2017**, *123:334*, 333.
[34] Z. Francis, Z. el Bitar, S. Incerti, M. A. Bernal, M. Karamitros, H. N. Tran, *J. Appl. Phys.* **2017**, *122*, 014701.
[35] D. C. Joy, S. Luo, *Scanning* **1989**, *11*, 176.
[36] J. M. Fernandez-Varea, R. Mayol, D. Liljequist, F. Salvat, *J.Phys.: Condens. Matter* **1993**, *5*, 3593.
[37] S. H. Pandya, B. G. Vaishnav, K. N. Joshipura *Chinese Phys. B* **2012**, *21(9)*, 093402.
[38] K. N. Joshipura, S. Gangopadhyay, C. G. Limbachiya, M. Vinodkumar, *J. Phys. Conf. Ser.* **2007**, *80*, 012008.
[39] C. Limbachiya, M. Vinodkumar, M. Swadia, K. N. Joshipura, N. Mason, *Mol. Phys.* **2015**, *113*, 55.
[40] M. Vinodkumar, C. Limbachiya, H. Desai, P. C. Vinodkumar, *Phys. Rev. A* **2014**, *89*, 062715.
[41] C. Limbachiya, M. Vinodkumar, N. Mason, *Phys. Rev. A* **2011**, *83*, 042708.
[42] Hitesh Yadav, Minaxi Vinodkumar, Chetan Limbachiya, P. C. Vinodkumar, *Mol. Phys.* **2017**, *115*, 952.
[43] H. L. Cox, R. A. Bonham, *J. Chem. Phys.* **1967**, *47*, 2599.
[44] S. Hara, *J. Phys. Soc. Jpn* **1967**, *22*, 710.
[45] X. Zhang, J. Sun, Y. Liu, *J.Phys. B: At. Mol. Opt. Phys.* **1992**, *25*, 1893.
[46] G. Staszewska, D. W. Schwenke, D. G. Truhlar, *Phys. Rev. A* **1984**, *29*, 3078.
[47] S. Parikh, D. Chauhan, N. Thakkar, C. Limbachiya, *Radiat. Phys. Chem.* **2024**, *214*, 111248.
[48] M. Vinodkumar, K. N. Joshipura, C. G. Limbachiya, B. K. Antony, *Nucl. Instrum. Methods. Phys. Res. B* **2003**, *212*, 63.
[49] B. G. Vaishnav, K. N. Joshipura, S. Pandya, *J. Phys. Conf. Ser.* **2012**, *388*, 052076.
[50] A. Muñoz, J. C. Oller, F. Blanco, J. D. Gorfinkiel, G. García, *Chem. Phys. Lett.* **2007**, *433*, 253.
[51] William V. Prestwich, Josane Nunes, Cheuk S. Kwok, *The Journal of Nuclear Medicine* **1989**, *30*, 1036.
[52] S. Mohammed, A. Trabelsi, K. Manai, *Indian J. Sci. Technol.* **2018**, *11*, 1.
[53] C. E. Crespo-Hernández, R. Arce, Y. Ishikawa, L. Gorb, J. Leszczynski, D. M. Close, *J. Phys.Chem. A* **2004**, *108*, 6373.
[54] H. Fernando, G. A. Papadantonakis, N. S. Kim, P. R. Lebreton, *.PNAS* **1998**, *95*, 5550.

[55] S. Gop, R. Sutradhar, S. Chakraborty, T. P. Sinha, *AIP Conf. Proc.* **2019**, *2162*, 020041.
[56] S. P. A. Sauer, J. Oddershede, J. R. Sabin, *Advances in Quantum Chemistry*, vol. 62 (Academic Press Inc., 2011), **2011**, pp. 215-242.
[57] M. T. Baei, M. R. Taghartapeh, E. T. Lemeski, A. Soltani, *Physica B Condens. Matter* **2014**, *444*, 6.
[58] R. Di Felice, A. Calzolari, E. Molinari, A. Garbesi, *Phys. Rev. B* **2002**, *65*, 1.
[59] J. MacNaughton, A. Moewes, E. Z. Kurmaev, *J. Phys* Chem. B **2005**, *109*, 7749.
[60] D. R. Penn, *Phys. Rev. B* **1987**, *35*, 482.
[61] W. A. Bernhard, Radical and Radical Ion Reactivity in Nucleic Acid Chemistry, edited by M. C. Greenberg (John Wiley & Sons, Inc., 2009), **2009**, pp. 41–68.
[62] K. Wiklund, J. M. Fernández-Varea, B. K. Lind, *Phys. Med. Biol.* **2011**, *56*, 1985.
[63] H. Gümüş, F. Köksal, *Radiation Effects and Defects in Solids* **2002**, *157*, 445.
[64] H. Gümüş, *Radiat.Phys. Chem.* **2005**, *72*, 7.
[65] D. C. Joy, *A Database of Electron-Solid Interactions*, Metrology and Lithography Group of the University of Tennessee2004, **2004**.
[66] E. Alizadeh, L. Sanche, *Chem. Rev.* **2012**, *112*, 5578.
[67] N. Sinha, B. Antony, *J. Phys. Chem. B* **2021**, *125*, 5479.

Manuscript received: December 2, 2023
Revised manuscript received: January 20, 2024
Accepted manuscript online: January 23, 2024
Version of record online: ■■, ■■

RESEARCH ARTICLE

The front cover picture illustrates electron interaction with DNA/RNA constituents, adenine, cytosine, guanine, thymine and uracil in aqueous phase. Biomolecules in aqueous phase present a realistic condition. The computed quantities, inelastic mean free path, mass stopping power and absorbed dose are useful to assess/model the radiation damage to DNA/RNA.

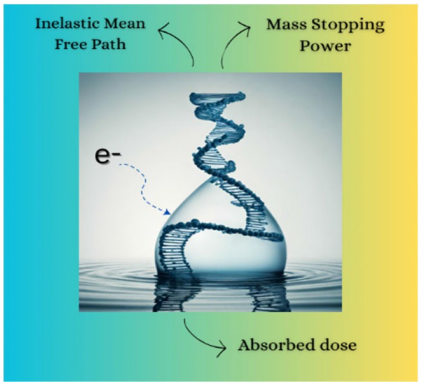

*S. Parikh, C. Limbachiya**

Radiation Physics and Chemistry 208 (2023) 110940

Contents lists available at ScienceDirect

Radiation Physics and Chemistry

journal homepage: www.elsevier.com/locate/radphyschem

Electron driven molecular processes for nucleosides

Smruti Parikh, Chetan Limbachiya *

Department of Applied Physics, The Maharaja Sayajirao University of Baroda, Vadodara, 390 001, India

ARTICLE INFO

Keywords:
Electron interactions
Nucleosides
Cross-sections

ABSTRACT

In the present study we investigate electron interactions with important cell molecules, nucleosides viz. Adenosine, Guanosine, Cytidine, Thymidine and Uridine from ionisation energy to 5000 eV. While nucleobases are studied extensively, these nucleosides have not been investigated enough. We focus to quantify various molecular processes induced by electrons through inelastic (Q_{inel}), ionisation (Q_{ion}), electronic excitations (Q_{exc}), elastic (Q_{el}) and total (Q_{total}) cross-sections. We used the complex optical potential approach to compute inelastic and elastic probabilities and employed complex scattering potential-ionisation contribution method to perform the calculations to bifurcate inelastic processes in to discrete and continuum contribution. This work is the first report of all these quantities, except Q_{ion}, to investigate the electron induced local chemistry of these important DNA/RNA compounds.

1. Introduction

The primary role of electrons in radiation induced damage is explored through investigating how they interact with biological target molecules. The majority of the consequences of ionising radiation are caused by DNA damage that develops as a result of the radiation's exposure to cell nuclei, which is well-known in radiation biology (Ward, 1988; Iliakis, 1991; Cox, 1994; Goodhead, 1994; Olive, 1998). Cell death, immediate or delayed inability to reproduce, chromosomal abnormalities, mutations, and neoplastic transformation are a few examples of these impacts (Iyer and Lehnert 2000). At the cellular level, frequent and lethal lesions that shut down or alter cellular function are thought to have an impact on the human DNA. These include DNA-protein or DNA-DNA cross-linkages, single-strand breaks (SSB) and double-strand breaks (DSB), base release and other chemical changes, and many DNA damage sites (Sonntag, 1987; Alizadeh et al. 2015). Either direct radiation interaction with any one DNA moiety (Uehara et al. 1999; Michael and William, 2008) or indirect reactive species interaction mediated by molecules around the DNA are responsible for this damage (O'Neill, 2001; Wishart and Rao, 2010). The by-products of water radiolysis (solvated electron, hydroxyl radicals, and hydrogen atoms), which react with DNA/RNA, are primarily responsible for the indirect effect (Alizadeh et al. 2015). The energy delivered to the biological media in both indirect and direct effects, primarily comes from ionisation (Mark et al. 1995), producing a lot of secondary particles along radiation trail, including secondary electrons, radicals and ions (Sonntag, 2006). The majority of secondary species are nonthermal secondary electrons (SEs), which are generated at a rate of about 50,000 per 1 MeV of deposited energy (Alizadeh et al. 2015). These SEs undergo inelastic collisions with the media molecules through ionisation and excitations, which cause them to lose energy. Therefore, SEs can cause significant chemical and structural changes prior to thermalization (Sonntag, 2006).

The electron collision effects on nucleobases have been studied extensively (Vries et al. 2002; Sanche, 2005; Vinodkumar et al. 2013a,b; Gao et al. 2021; Ashouri et al. 2022; Rehman and Krishnakumar 2022), but recent work (Deng et al. 2005) on base-sugar complex nucleosides has revealed that sugar damage predominates in nucleoside damage pathways (Deng et al. 2005; Penhoat et al. 2014; Ma et al. 2019). Wintstead and McKoy (Winstead and McKoy, 2006, 2007, 2008) have also studied the low energy electron effects to the nucleosides. Hence, in the present contribution we investigated electron impact with Nucleosides (Adenosine, Guanosine, Cytidine, Thymidine and Uridine). It belongs to the class of nucleosides known as glycosylamines, which are essentially nucleotides devoid of phosphate groups. Nucleosides, nucleic acid structural units, are essential to all biological systems (Voet and Voet, 1995; Nucleosides- https://en.wikipedia.org/wiki/Nucleoside#cite_note-2). They treat tumours and viruses by selectively inhibiting enzymes necessary for cancer or viral replication (Gumina et al. 2002) or by stopping cancer cell or virus reproduction with nucleic acid chain terminators (Orr et al. 1992). Nucleosides and their analogues are of interest in many areas of chemistry and biology, and their

* Corresponding author.
E-mail address: cglimbachiya-apphy@msubaroda.ac.in (C. Limbachiya).

https://doi.org/10.1016/j.radphyschem.2023.110940
Received 28 January 2023; Received in revised form 1 March 2023; Accepted 21 March 2023
Available online 23 March 2023

characterization or structural determination is particularly useful in the synthesis of nucleoside analogues for the study of their anticoagulant properties and the detection of the structure and sequence of altered nucleosides in ribonucleic acid (RNA) (Turner et al. 2000; Anderson, 2002; Maga and Spadari, 2002).

The fundamental interaction between the electrons and biomolecules has thus been the subject of research in recent years (Nikjoo et al. 2016). A critical first step in such modelling is determining the cross-sections of various molecular processes due to the collisions between electrons and biomolecules. Therefore, to comprehend and model the cell damage accurately, it is required to calculate the cross-sections for electron interaction with biomolecules (Nikjoo et al. 2006; Alloni, 2007; Dingfelder, 2012).

The total ionisation cross sections for nucleosides from target's ionisation threshold to 5000 eV are reported in the current work. Inelastic cross-sections were calculated using the well-known complex optical potential method (Jain, 1986; Jain and Baluja, 1992) and ionisation cross-sections were retrieved using our own complex scattering potential-ionisation contribution (CSP-ic) approach (Vinodkumar et al. 2003; Joshipura et al. 2004; Limbachiya et al. 2014). We also point out the lack of prior research on the inelastic cross sections. Only (Możejko, 2020) has reported the ionisation cross sections using Binary Encounter Bethe (BEB) model for these molecules up to 200 eV. This inspired us to start investigation of electron colliding with these molecules from ionisation energy (IE) to 5000 eV. To report these interactions comprehensively, we have also calculated the elastic Q_{el} and total Q_{total} cross section for these biomolecules. In Fig. 1 the complete geometrical structure of nucleosides has been shown (Chemspider).

2. Theoretical methodology

We employ Complex Optical Potential (COP) approach with a multi-center group additivity method (Vinodkumar et al. 2011; Vinodkumar et al. 2013a,b) to calculate the cross-sections from the ionisation energy to 5000 eV. Various additivity rules can be used for electron scattering studies (Blanco and Garcia, 2009). A fact that the large sized molecules require the small groups of constituent atoms to serve as separate scattering centres lends support to the hypothesis of multi-centre group formation. For the large molecules such as the ones investigated in this work, the group additivity approach is more appropriate, because the target system appears as multiple scattering centres when the wavelength of the electron reduces with the energy. Hence, to observe the

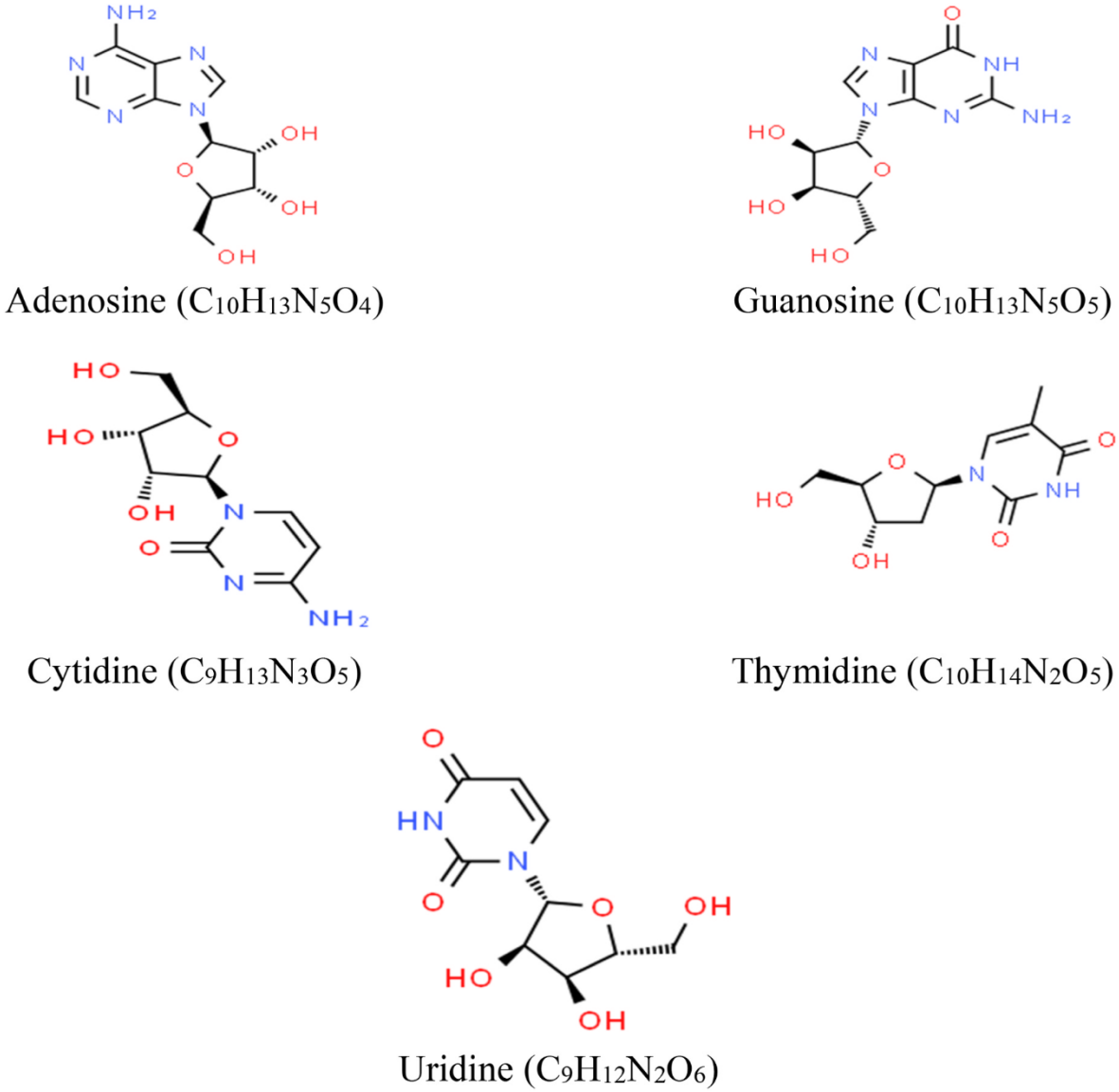

Fig. 1. Geometrical structure of nucleosides (Chemspider) (http://www.chemspider.com/Default.aspx).

effects of various groups on the cross-section, we utilized this approach. Furthermore, the COP approach uses spherical potential, which we may describe by superimposing the atomic charge density of smaller atoms on larger atoms within the groups. Also, molecular geometry is taken into account in the multi-centre group additivity method to identify various scattering centres of the target molecule.

In our previous articles, we have provided a thorough discussion of this formalism (Vinodkumar et al. 2003; Joshipura et al. 2004; Limbachiya et al. 2015). The complex potential is given as,

$$V_{optical} = V_{real} + iV_{Ima} \tag{1}$$

Here,

V_{real} = real part of $V_{optical} = V_{ex} + V_s + V_{pol}$

V_{Ima} = imaginary part of $V_{optical}$

Exchange potential (V_{ex}), static potential (V_s), and polarisation potential (V_{pol}) are incorporated in V_{real}. V_s measures the distortion-free molecular charge cloud and is computed with the use of Hartree-Fock wave functions (Cox and Bonham, 1967). To determine the V_{ex} contribution, we have used the exchange model proposed by (Hara, 1967) as follows,

$$V_{ex}(r) = \frac{-2}{\pi} k_f \left(\frac{1}{2} + \frac{1-\eta^2}{4\eta} \ln \left| \frac{1+\eta}{1-\eta} \right| \right) \tag{2}$$

where, $\eta = \frac{\sqrt{k^2 + k_f^2 + 2(IE)}}{k_f}$.

Here, k is the momentum and k_f is the fermi wave-vector. The contortion of the scattering centre's charge cloud caused by incident electron's electric field is represented by the polarisation potential. This potential is taken into consideration by employing (Zhang et al. 1992) polarisation potential model,

$$V_{pol}(r) = \begin{cases} V_c(r), r \le r_c \\ \dfrac{-\alpha}{2r^4}, r > r_c \end{cases} \tag{3}$$

where $V_c(r)$ is the short-range correlation potential proposed by (Perdew and Zunger, 1981), and the first crossing point of the long-range dipole component $-\alpha/2r^4$ and the short-range correlation potential $V_c(r)$ is denoted by r_c.

The V_{Ima} addresses the absorption or loss of the incoming flux through the inelastic processes, viz., ionisation and excitations. To account for this absorption effect, we have used the modified quasi-free potential model (Staszewska et al. 1983),

$$V_{Ima}(r, E_i) = -\rho(r) \sqrt{\frac{T_{loc}}{2}} \left(\frac{8\pi}{10 k_F^3 E_i} \right) \Theta\left(p^2 - k_F^2 - 2\Delta\right) (A_1 + A_2 + A_3) \tag{4}$$

where, T_{loc} represents the local kinetic energy of incident electrons, and $\Theta(x)$ is the Heaviside unit step-function. A_1, A_2 and A_3, the dynamic functions depend upon the molecular ionisation energy and energy parameter Δ that decides a threshold below which $V_{Ima} = 0$ (i.e. ionisation and excitations are forbidden). By considering Δ as a slowly varying function of E_i around IE, we have modified the original model such that $\Delta(E_i) = 0.8I + \beta(E_i - I)$, allowing excitations to take place below ionisation threshold of the target. Now, this final resultant $V_{optical}$ (equations (1)–(4)) is then utilized to solve the Schrodinger equation numerically employing the partial wave approximation. Then by obtaining the phase shifts (δ_l), the electron scattering inelastic (Q_{inel}) and elastic (Q_{el}) cross-sections are computed and hence $Q_{total} = Q_{el} + Q_{inel}$, is obtained through,

$$Q_{el}(k) = \frac{\pi}{k^2} \sum_{l=0}^{\infty} (2l+1) \left(\eta_l e^{2i\mathrm{Re}\delta_l} - 1 \right)^2 \tag{5}$$

$$Q_{inel}(k) = \frac{\pi}{k^2} \sum_{l=0}^{\infty} (2l+1) \left(1 - \eta_l^2 \right) \tag{6}$$

Here, η_l is the inelasticity factor given by $\eta_l = e^{-2Ima(\delta_l)}$. There are two main components that add up to the total Q_{inel},

$$Q_{inel}(E_i) = \sum Q_{exc}(E_i) + Q_{ion}(E_i) \tag{7}$$

Here, the total cross section of all permitted ionisation processes is incorporated through the first term Q_{Ion}. The second term $\sum Q_{Exc}$ is caused by all the allowed electronic excitations, for which the cross-sections fall fast as energy increases. As energy is increased above the ionisation energy, the Q_{Exc} becomes less relevant in comparison to the Q_{Ion}. We have,

$$Q_{inel} \ge Q_{ion} \tag{8}$$

which is the foundation for the complex scattering potential-ionisation contribution (CSP-ic) approach (Vinodkumar et al. 2003; Joshipura et al. 2006; Rahman et al. 2012; Limbachiya et al. 2014) and implies to a ratio

$$R(E_i) = Q_{inel}/Q_{ion} \tag{9}$$

such that,

$$R(E_i) = \begin{cases} 0, for\ E_i \le IE \\ R_P, for\ E_i = E_P \\ \sim 1, for\ E_i \gg E_P \end{cases} \tag{10}$$

Since no ionisation is allowed when the incoming energy is less than or equal to IE, the first condition is precise. The third criterion results from the fact that excitations greatly falls and only ionisation is dominant in the inelastic processes when incident energy is much higher than E_P, which is the peak energy value for which Q_{inel} has its maxima. As a result, the ratio $R(E_i)$ gets closer to 1. The second criterion is empirical. The value of $R(E_i)$ at the peak energy is around 0.7–0.8, as revealed by the experimental and theoretical results of many stable molecules (Turner et al. 1982; Vinodkumar et al. 2011; Vinodkumar et al. 2012; Vinodkumar et al. 2014; Yadav et al. 2017). We report molecular properties in Table 1.

3. Results & discussion

For lower energy electron interactions studies are carried out by various authors (Winstead and McKoy, 2006, 2007, 2008). The various cross-sections for all the present biomolecules are displayed as a function of input energy from the ionisation threshold to 5000 eV.

A. Total inelastic cross-sections:

The Q_{inel}, cover the ionisation and discrete inelastic effects for electron interaction with Nucleosides (adenosine, cytidine, guanosine, uridine, and thymidine) and is shown in Figs. 2–6, respectively. The topmost curves in all these figures show Q_{inel}, whereas the lowermost curves reflect the total electronic excitations cross-sections, $\sum Q_{exc}$. We

Table 1
Molecular properties.

Molecule	[a]IE (eV)	[b]Polarizability (α) in Å^3
Adenosine	8.4	23.8
Guanosine	8.0	24.1
Cytidine	8.6	20.9
Thymidine	8.7	22.1
Uridine	9.0	20.9

[a] (Yu et al. 1981).
[b] (http://www.chemspider.com/Default.aspx).

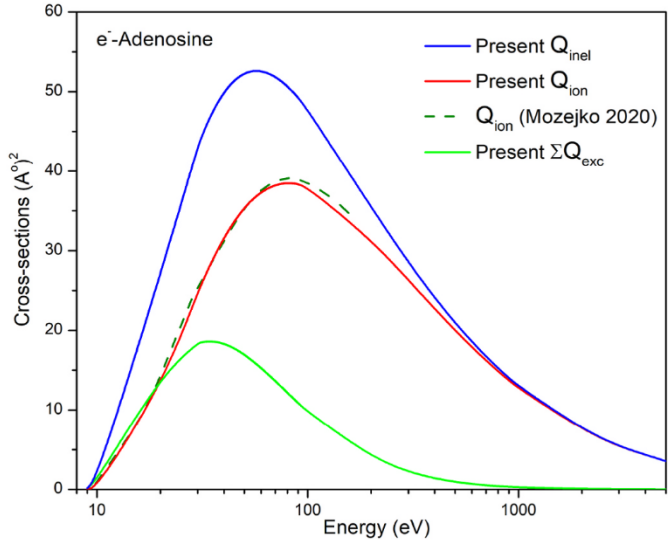

Fig. 2. Q_{inel}, Q_{ion} and $\sum Q_{exc}$ for Adenosine. Blue line: Present Q_{inel}; Red line: Present Q_{ion}; Dash line: Mozejko Q_{ion} [38]; Green line: Present $\sum Q_{exc}$.

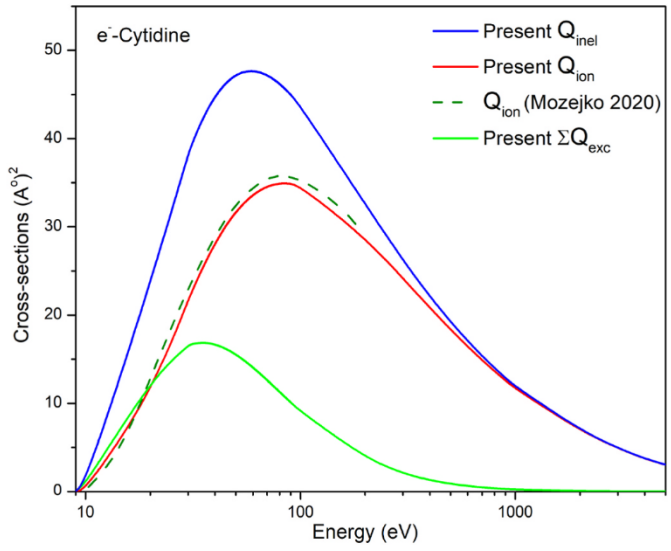

Fig. 3. Q_{inel}, Q_{ion} and $\sum Q_{exc}$ for Cytidine. Blue line: Present Q_{inel}; Red line: Present Q_{ion}; Dash line: Mozejko Q_{ion} [38]; Green line: Present $\sum Q_{exc}$.

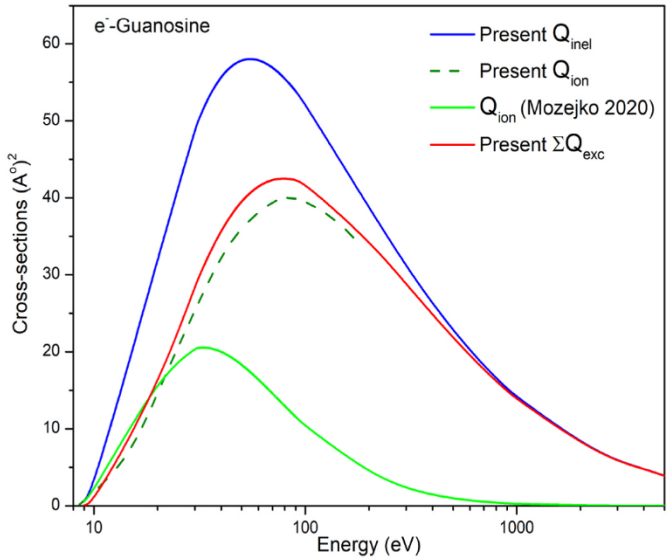

Fig. 4. Q_{inel}, Q_{ion} and $\sum Q_{exc}$ for Guanosine. Blue line: Present Q_{inel}; Red line: Present Q_{ion}; Dash line: Mozejko Q_{ion} [38]; Green line: Present $\sum Q_{exc}$.

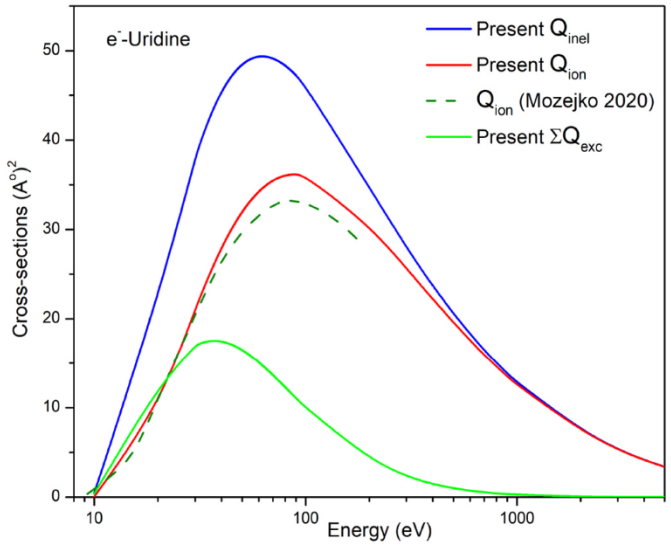

Fig. 5. Q_{inel}, Q_{ion} and $\sum Q_{exc}$ for Uridine. Blue line: Present Q_{inel}; Red line: Present Q_{ion}; Dash line: Mozejko Q_{ion} [38]; Green line: Present $\sum Q_{exc}$.

point that this work is the first attempt to report these cross-sections of all the present biomolecules. The centre curves are total ionisation cross-sections from Q_{ion} data. Till now, neither theoretical nor experimental studies have been carried out on the electron interaction cross-sections for these Nucleosides, except by (Możejko, 2020). Moreover, they only calculated the Q_{ion} for four of the nucleosides, i.e., adenosine, guanosine, cytidine and uridine from ionisation threshold to 200 eV using BEB formalism.

In Figs. 2–5, present Q_{ion} are compared with the Q_{ion} of (Możejko, 2020) calculated through BEB. Present curves for Adenosine and Cytidine (Figs. 2 and 3) show excellent agreement with the Binary Encounter Bethe (BEB) data (Możejko, 2020), while present Q_{ion} values of Guanosine and Uridine (Figs. 4 and 5) are minutely higher within the mentioned uncertainty ±15% of BEB data (Możejko, 2020). The cross sections are quite sensitive to ionisation potential used. We observe that the cross-sections tend to merge beyond the peak and that the BEB results (Możejko, 2020) are up to 200 eV.

There are no cross-section data available for thymidine molecule for comparison (Fig. 6). We are the first to report the cross-section data for thymidine upon electron interaction. The inelastic cross sections rise with the incident energies as the energetic electrons transfer the kinetic energy to the molecular systems. However, at higher energies these probabilities fall as $\frac{1}{E_i}$ beyond a peak energy value. The peak value is determined through the two competing quantities, electron energy and the time of interaction between incident electrons and molecular target.

Figs. 7 and 8 show the elastic cross-sections, Q_{el} and total cross-sections Q_{total}, respectively, where N represents the size of molecule in terms of number of molecular electrons. The later involves all the inelastic and elastic processes induced by incoming electron. There are no data available for the comparison, but present data follow the general trend. Q_{total} is used in a number of modelling methodologies (Vinodkumar et al. 2013a,b; Vinodkumar et al. 2014) and represents the probabilities that all electron-induced molecular processes will occur. As can be observed, Q_{total} follows the Born-Bethe trend at higher energies and falls as $\frac{\ln E_i}{E_i}$ (Thakkar et al. 2021). Further we can note from Figs. 7 and 8,

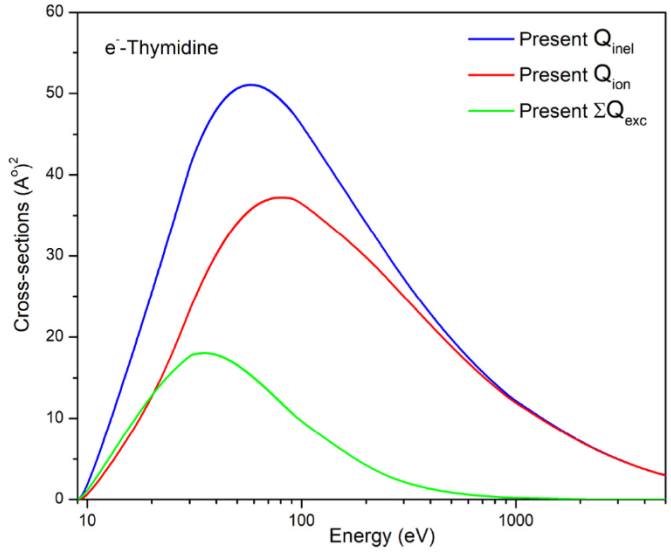

Fig. 6. Q_{inel}, Q_{ion} and $\sum Q_{exc}$ for Thymidine. Blue line: Present Q_{inel}; Red line: Present Q_{ion}; Dash line: Mozejko Q_{ion} [38]; Green line: Present $\sum Q_{exc}$.

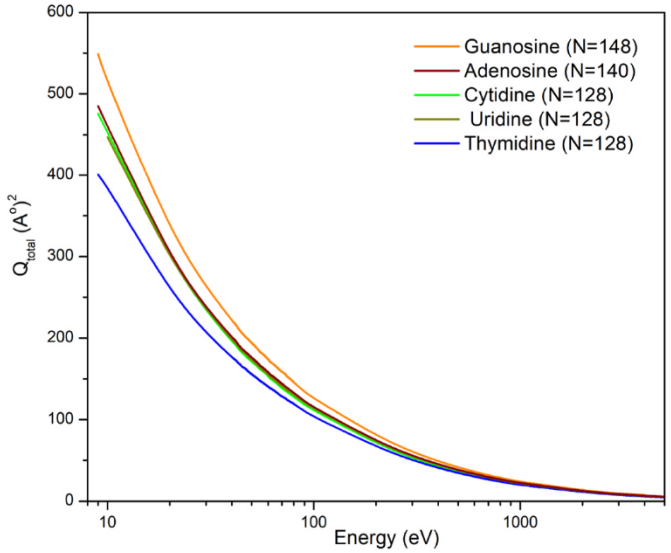

Fig. 8. Q_{total} **for all Nucleosides.** Red line: Adenosine; Blue line: Guanosine; Black line: Cytidine; Green line: Thymidine; Dark yellow line: Uridine.

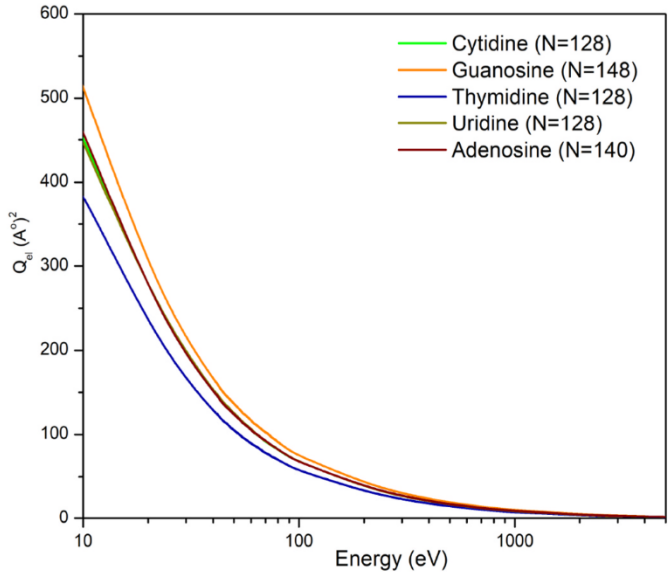

Fig. 7. Q_{el} for all Nucleosides. Green Line: Cytidine; Orange line: Guanosine; Blue line: Thymidine; Dark yellow line: Uridine; Wine line: Adenosine.

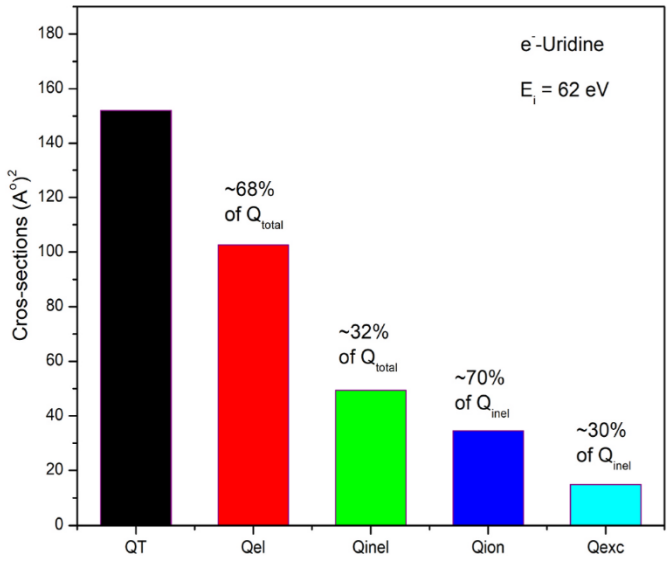

Fig. 9. Relative estimation of various quantified molecular processes.

B. Elastic cross-sections:

the size dependency of Q_{el} and Q_{total}.

For e^--Uridine at $E_p = 62$ eV, we present relative estimation of various quantified molecular processes in Fig. 9. While Q_{total} is the top bound for the events induced by electrons, Q_{el} and Q_{inel} is of 68% and 32%, respectively, of Q_{total}. As anticipated, Q_{exc} makes up 30% of Q_{inel} while Q_{ion} contributes 70%.

With the help of our semi-empirical CSP-ic theoretical methodology discussed earlier, we could report various types of electrons induced scattering cross-sections data. However, the current theory involves approximation due to the need to construct spherical potential and modelling of charge density using group additivity rule. These approximations incorporate 10–15% of uncertainty in the final data which is at par with most experimental data. Therefore, the data reported here are reliable enough for the applications in applied fields such as biomedical field, radiology etc.

4. Conclusions

We have investigated a detailed theoretical analysis of the electron interactions with nucleosides, Adenosine, Guanosine, Cytidine, Thymidine and Uridine for a broad energy range, from the molecular IE to 5000 eV. These are important DNA/RNA compounds which are scantly studied. Total (Q_{total}), total inelastic (Q_{inel}), and total elastic (Q_{el}) cross sections were evaluated using the complex optical potential method, and total ionisation (Q_{ion}) and summed electronic excitation cross sections ($\sum Q_{exc}$) were determined using the CSP-ic approach (Vinodkumar et al. 2003; Joshipura et al. 2006; Rahman et al. 2012; Limbachiya et al. 2014). All these quantities are reported for the first time, except Q_{ion}. A lone calculation of (Możejko, 2020) is available using BEB method for Adenosine, Guanosine, Cytidine and Uridine for the ionisation cross-sections from IE to 200 eV only. We have compared the present ionisation cross-sections with the data of (Możejko, 2020) and observed good agreement within the mentioned uncertainty ±15% of BEB results (Możejko, 2020). This study is aimed to enable the understanding of various molecular processes including ionisation caused by secondary

charges generated by impinging energetic radiation. These results would help in modelling various tracks of radiation damage to the DNA/RNA compounds.

CRediT authorship contribution statement

Smruti Parikh: Data curation, Writing – original draft, Formal analysis, Conceptualization, Methodology, Software. **Chetan Limbachiya:** Writing – review & editing, Validation, Visualization, Investigation, Supervision.

Declaration of competing interest

The authors declare that they have no known competing financial interests or personal relationships that could have appeared to influence the work reported in this paper

Data availability

Data will be made available on request.

Appendix

Table 2
Various cross-sections (A^{o2}) for Adenosine

Energy (eV)	Q_{inel}	Q_{ion}	Q_{exc}	Q_{el}	Q_{total}
9	0.18	0.01	0.16	484.93	485.11
10	1.31	0.19	1.12	459.47	460.78
20	27.04	12.74	14.30	272.05	299.09
30	43.00	24.65	18.35	193.97	236.97
40	49.84	31.55	18.29	151.83	201.68
70	51.83	38.19	13.64	92.26	144.09
100	47.71	37.95	9.76	67.42	115.13
300	28.51	26.31	2.19	27.16	55.66
500	20.94	20.01	0.94	17.33	38.27
700	16.75	16.24	0.51	12.75	29.49
1000	12.99	12.74	0.26	9.24	22.24
3000	5.40	5.37	0.03	3.17	8.57
5000	3.54	3.53	0.01	1.97	5.51

Table 3
Various cross-sections (A^{o2}) for Guanosine

Energy (eV)	Q_{inel}	Q_{ion}	Q_{exc}	Q_{el}	Q_{total}
9	0.62	0.06	0.56	548.21	548.84
10	2.40	0.43	1.97	511.08	513.50
20	32.05	15.49	16.56	299.41	331.53
30	48.84	28.41	20.43	213.74	262.49
40	55.65	35.65	20.00	166.62	222.00
70	56.88	42.31	14.58	102.54	158.77
100	52.18	41.83	10.35	74.71	125.97
300	31.11	28.82	2.29	30.19	60.35
500	22.84	21.87	0.97	19.28	41.31
700	18.25	17.72	0.53	14.21	31.75
1000	14.14	13.87	0.27	10.31	23.85
3000	5.82	5.79	0.03	3.54	9.07
5000	3.54	3.53	0.01	2.11	6.02

Table 4
Various cross-sections (A^{o2}) for Cytidine

Energy (eV)	Q_{inel}	Q_{ion}	Q_{exc}	Q_{el}	Q_{total}
9	0.07	0	0.07	475.67	475.74
10	0.89	0.12	0.78	452.99	453.88
20	23.54	10.89	12.65	273.20	296.74
30	38.18	21.63	16.55	195.42	233.60
40	44.69	28.03	16.66	151.76	196.45
70	47.15	34.53	12.62	91.64	138.79
100	43.69	34.60	9.10	67.56	111.26
300	26.21	24.16	2.05	26.75	52.96
500	19.24	18.37	0.87	17.19	36.43
700	15.38	14.91	0.47	12.59	27.97
1000	11.93	11.69	0.24	9.04	20.97
3000	4.94	4.91	0.03	3.11	8.05
5000	3.05	3.04	0.01	1.94	4.98

Table 5
Various cross-sections (A^{o2}) for Thymidine

Energy (eV)	Q_{inel}	Q_{ion}	Q_{exc}	Q_{el}	Q_{total}
9	0.03	0	0.03	400.49	400.53
10	0.83	0.10	0.73	384.92	387.75
20	25.13	11.63	13.50	231.93	257.06
30	40.99	23.28	17.71	165.26	206.26
40	48.00	30.18	17.82	129.00	177.00
70	50.39	36.97	13.4	78.13	128.52
100	46.27	36.68	9.59	57.14	103.41
300	27.14	25.03	2.11	23.10	50.24
500	19.75	18.86	0.89	14.79	34.53
700	15.70	15.22	0.48	10.89	26.59
1000	12.11	11.87	0.24	7.85	19.96
3000	4.97	4.94	0.02	2.71	7.68
5000	3.01	3.00	0.01	1.69	4.70

Table 6
Various cross-sections (A^{o2}) for Uridine

Energy (eV)	Q_{inel}	Q_{ion}	Q_{exc}	Q_{el}	Q_{total}
10	0.43	0.04	0.39	446.69	447.12
20	22.33	9.96	12.37	273.84	296.16
30	37.96	21.01	16.95	197.25	235.21
40	45.36	27.91	17.45	153.02	198.38
70	49.13	35.47	13.66	150.14	141.39
100	46.01	36.01	10.00	67.64	113.65
300	27.99	25.67	2.32	26.78	54.77
500	20.61	19.61	1.00	17.05	37.66
700	16.51	15.96	0.55	12.57	29.08
1000	12.83	12.55	0.28	9.01	21.84
3000	5.36	5.33	0.03	3.11	8.47
5000	3.40	3.39	0.01	1.94	5.34

References

Alizadeh, E., Orlando Thomas, M., Sanche, L., 2015. Annu. Rev. Phys. Chem. 66, 379–398.
Alloni, D., 2007. Sci. Acta 1, 164.
Anderson, K.S., 2002. Biochim. Biophys. Acta 1587, 296–299.
Ashouri, M., Hajivaliei, M., Gholami, N., 2022. Phys. Scripta 97, 035402.
Blanco, Garcia, 2009. J. Physiol. Biochem. Mol. Opt. Phys. 42, 145203.
Chemspider. Royal Society of Chemistry. [accessed 2021 Feb 14] http://www.chemspider.com/Default.aspx.
Cox, R., 1994. Int. J. Radiat. Biol. 65, 57–64.
Cox, H.L., Bonham, R.A., 1967. J. Chem. Phys. 47, 2599–2608.
de Vries, J., Hoekstra, R., Morgenstern, R., Schlatholter, T., 2002. J. Physiol. Biochem. 35, 4373–4382.
Deng, Z., Bald, I., Illenberger, E., Huels, M.A., 2005. Phys. Rev. Lett. 95, 153201–153204.
Dingfelder, M., 2012. Health Phys. 103, 590.
Gao, Y., Zheng, Y., Sanche, L., 2021. Int. J. Mol. Sci. 22, 7879.
Goodhead, D.T., 1994. Int. J. Radiat. Biol. 65, 7–17.
Gumina, G., Chong, Y., Choo, H., Song, G., Chu, C.K., 2002. Curr. Top. Med. Chem. 2, 1065–1086.
Hara, S., 1967. J. Phys. Soc. Japan 22, 710.
Herve du Penhoat, M.A., Lopez-Tarifa, P., Ghose, K.K., Jeanvoine, Y., Gaigeot, M.P., Vuilleumier, R., Politis, M.F., Bacchus-Montabonel, M.C., 2014. J. Mol. Model. 20, 2221.
Iliakis, G., 1991. Bioessays 13, 641–648.
Jain, A., 1986. Phys. Rev. 34, 3707.
Jain, Baluja, K.L., 1992. Phys. Rev. 45, 202.
Joshipura, K.N., Vinodkumar, M., Limbachiya, C.G., Antony, B., 2004. Phys. Rev. 69, 022705.
Joshipura, K.N., Vaishnav, B.G., Limbachiya, C.G., 2006. Pramana 66 (2), 403–414.
Limbachiya, C., Vinodkumar, M., Swadia, M., Barot, A., 2014. Mol. Phys. 112 (1), 101–106.
Limbachiya, C., Vinodkumar, M., Swadia, M., Joshipura, K.N., Mason, N., 2015. Mol. Phys. 113 (1).
Ma, Jun, Kumar, A., Muroya, Y., Yamashita, S., Sakurai, T., Denisov, S.A., Sevilla, M.D., Adhikary, A., Seki, S., Mostafavi, M., 2019. Nat. Commun. 10, 102.
Maga, G., Spadari, S., 2002. Curr. Drug Metabol. 3, 73–96.
Mark, T.D., Hatano, Y., Linder, F., 1995. Atomic and Molecular Data for Radiotherapy and Radiation Research: Electron Collision Cross Sections. Int. At. Energy Agency, Vienna, pp. 163–275. IAEA-TECDOC-799.
Michael, Sevilla, William, Bernhar, 2008. Radiation Chemistry: from Basics to Applications in Material and Life Sciences. Les Ulis: EDP Sciences, pp. 191–202. Chapter 13, Mechanisms of direct radiation damage to DNA.
Mozejko, P., 2020. J. Phys. Conf. 1412, 152002.
Nikjoo, H., Uehara, S., Emfietzoglou, D., Cucinotta, F.A., 2006. Radiat. Meas. 41, 1052.
Nikjoo, H., Emfietzoglou, D., Liamsuwan, T., Taleei, R., Liljequist, D., Uehara, S., 2016. Rep. Prog. Phys. 79, 116601.
Nucleosides [accessed 2022 Jan 14]. https://en.wikipedia.org/wiki/Nucleoside#cite_note-2.
Olive, P.L., 1998. Radiat. Res. 150, S42–S51.
Orr, D.C., Figueiredo, H.T., Mo, C.L., Penn, C.R., Cameron, J.M., 1992. J. Biol. Chem. 267, 4177–4182.
O'Neill, P., 2001. Radiation-induced damage in DNA. In: Radiation Chemistry: Present Status and Future Trends. Elsevier Sci., Amsterdam, pp. 585–622.
Perdew, J.P., Zunger, A., 1981. Phys. Rev. B Condens. Matter 23, 5048–5079.
Rahman, M.A., Gangopadhyay, S., Limbachiya, C., Joshipura, K.N., Krishnakumar, E., 2012. Int. J. Mass Spectrom. 319–320, 48–54.
Rashi, Iyer, Lehnert Bruce, E., 2000. Arch. Biochem. Biophys. 376 (No. 1), 14–25.
Rehman, M.A., Krishnakumar, E., 2022. Atoms 10 (4), 100.
Sanche, L., 2005. Eur. Phys. J. D 35, 367–390.
Sonntag, C., 1987. The Chemical Basis of Radiation Biology. Taylor & Francis, London.
Sonntag, C., 2006. Free-Radical-Induced DNA Damage and its Repair: A Chemical Perspective. Springer-Verlag, Berlin.
Staszewska, G., Schwenke, D.W., Thirumalai, D., Truhlar, D.G., 1983. Phys. Rev. 28, 2740.
Thakkar, N., Swadia, M., Vinodkumar, M., Mason, N., Limbachiya, C., 2021. Plasma Sources Sci. Technol. 30, 085008.
Turner, J., Paretzke, H., Hamm, R., Wright, H., Richie, R., 1982. Radiat. Res. 92, 47.
Turner, M.A., Yang, X., Yin, D., Kuczera, K., Borchardt, R.T., Howell, P.L., 2000. Cell Biochem. Biophys. 33, 101–125.
Uehara, S., Nikjoo, H., Goodhead, D.T., 1999. Radiat. Res. 152 (2), 202–213.
Vinodkumar, M., Joshipura, K.N., Limbachiya, C.G., Antony, B.K., 2003. Nucl. Inst. Methods Phys. Res. Sec. B Beam Interact. Mater. Atoms 212, 63–66.
Vinodkumar, M., Bhutadia, H., Limbachiya, C., Joshipura, K.N., 2011. Int. J. Mass Spectrom. 308 (1), 35–40.
Vinodkumar, M., Limbachiya, C., Barot, A., Mason, N., 2012. Phys. Rev. 86 (1), 012706.
Vinodkumar, M., Limbachiya, C., Barot, A., Mason, N., 2013a. Phys. Rev. 87, 012702.
Vinodkumar, M., Limbachiya, C., Barot, M., Swadia, M., Barot, A., 2013b. Int. J. Mass Spectrom. 339–340, 16–23.

Vinodkumar, M., Limbachiya, C., Desai, H., Vinodkumar, P.C., 2014. Phys. Rev. 89, 062715.
Voet, D., Voet, J.G., 1995. Biochemistry, second ed. John Wiley & Sons, New York.
Ward, J.F., 1988. Prog. Nucleic Acid Res. Mol. Biol. 95–125.
Winstead, C., McKoy, V., 2006. J. Chem. Phys. 125, 244302.
Winstead, C., McKoy, V., 2007. J. Chem. Phys. 127, 085105.
Winstead, C., McKoy, V., 2008. Radiat. Phys. Chem. 77, 1258.
Wishart, J.F., Rao, B.M.S., 2010. Recent Trends in Radiation Chemistry. World Sci, Singapore.
Yadav, H., Vinodkumar, M., Limbachiya, C., Vinodkumar, P.C., 2017. Mol. Phys. 115 (8), 952–961.
Yu, C., O'Donnell, T.J., LeBreton, P.R., 1981. J. Phys. Chem. 85, 3851–3855.

Chapter 49
Calculations of Total Ionization Cross-Sections for Electron Impact on H_2SO_4

Smruti Parikh, Chetan Limbachiya, and K. N. Joshipura

Abstract The present study investigates the total ionization cross-section, Q_{ion} for the electron collisions with Sulfuric acid (H_2SO_4), which has been identified as key component in aerosol formation over energy range from ionization potential (IP) to 5000 eV. For the calculation of total inelastic cross-section, Q_{inel} Spherical Complex Optical Potential (SCOP) method is used. The Q_{ion}, is then calculated using a semi-empirical approach, called the Complex Spherical Potential-ionization contribution (CSP-ic). We have studied Q_{ion} using various models employed for molecular charge density.

49.1 Introduction

The main human-caused sulfur-containing compound, sulfur dioxide (SO_2) is directly emitted into the Earth's atmosphere and by the atmospheric oxidation of SO_2, sulfuric acid (H_2SO_4) is produced [1]. Isotopic and geological evidence indicates that the water in liquid form was earlier present on all the planets of our solar system. Moreover, the clouds made up of H_2SO_4 and H_2O solution are present in the atmosphere of Venus [2]. Furthermore, geological study suggests that Mercury, Venus, Earth and Mars were volcanically active in their earlier time period. The typical component of volcanic degassing is sulfur dioxide, which is soluble in water and by oxidizing it can form sulfuric acid (H_2SO_4) [2]. In the atmospheric nucleation, this H_2SO_4 has been identified as the key component [3, 4]. The major source of atmospheric aerosol particles are atmospheric nucleation and successive growth of newly formed particles. These aerosol particles are part of the climate of our Earth [5]. The aerosol particles scatter the sunlight and lowers the temperature. Also, aerosols present in the troposphere can alter the dimensions of the cloud particles, and hence modify the characteristics of clouds of absorbing and reflecting the sunlight,

S. Parikh (✉) · C. Limbachiya
The Maharaja Sayajirao University of Baroda, Vadodara 390001, India

K. N. Joshipura
(Retd) Sardar Patel University, Vallabh Vidyanagar 388120, India

V. Singh et al. (eds.), *Proceedings of the International Conference on Atomic, Molecular, Optical & Nano Physics with Applications*, Springer Proceedings in Physics 271,
https://doi.org/10.1007/978-981-16-7691-8_49

Table 49.1 Ionization potentials [8]

Target	IP (eV)	Target	IP (eV)	Target	IP (eV)
H	13.60	S	10.36	O	13.62
P	10.48	H_2SO_4	12.40	H_3PO_4	11.72

which in turn affects the Earth's energy budget. The most remarkable impact of these aerosols is damaging of stratospheric ozone layer [6].

The molecules present in the atmosphere are impacted by the secondary electrons generated by the cosmic ray particles and radiations from the sun. Hence, electron-interactions with atmospheric molecules is the dominant natural phenomenon in the atmosphere. Ionization is the most basic channel in all the inelastic processes which opens for the energy above the ionization potential of the molecules and ionization cross-sections of electron collisions with atmospheric compounds are very important in many applied fields of sciences, like plasma sciences, astrophysics, biomedical researchs, radio sciences, industrial fields, etc. [7].

For the present study, the target we choose here is H_2SO_4, because of its importance in atmosphere of Earth as well as other planets. Lack of theoretical and experimental investigations for this molecule encouraged us to carry out this study. In this present work, the data of the ionization cross-section, Q_{ion} for electron collision with H_2SO_4 has been reported for the energy from the molecular IP to 5 keV. For this calculation, we have used CSP-ic (Complex Scattering Potential-ionization contribution) method. Since this is the first attempt to study the electron interactions with H_2SO_4, we have computed the Q_{ion} using various models. These models include Independent Atom Model (IAM) using atomic as well as molecular properties. Moreover, we have carried a study to understand the dependence of Q_{ion} on the molecular IP and the molecular size through number of target electrons (N) by evaluating Q_{ion} for H_3PO_4 which is having same number of electrons (N = 50) as H_2SO_4 and comparing with cross sections of H_2SO_4. In Table 49.1 we show ionization potential of the target atom/molecules [8].

49.2 Theoretical Methodology

Total ionization cross-section, Q_{ion}, for the electron interaction with H_2SO_4 molecule is calculated using SCOP method as mentioned in our earlier publications [9, 10]. The e-molecule scattering potential is defined as,

$$V\ (r, E_i) = V_R(r, E_i) + V_I(r, E_i) \tag{49.1}$$

Here the real term V_R consists of potentials to describe static, electron exchange and polarization effects caused by electron impact on the molecule. The imaginary term V_I corresponds to absorption potential which takes care of the lost flux of

electrons leading to inelastic effects. Various model potentials have been used to represent these effects and to construct the complex potential which is then used as input for solving the Schrödinger equation and the total inelastic cross-sections are then computed using the partial wave analysis [9, 10] such that,

$$Q_{inel}(E_i) = Q_{ion}(E_i) + \sum Q_{exc}(E_i) \tag{49.2}$$

Here, ΣQ_{exc} represent all allowed electronic excitation cross-sections, which gradually reduce at higher energies above the IP [11, 12]. Thus, we can have

$$Q_{inel} \geq Q_{ion} \tag{49.3}$$

The Complex Scattering Potential-ionization contribution (CSP-ic) method [13] is developed on the basis of (3) and is applied to derive the total ionization cross-section from Q_{inel} by defining a ratio $R(E_i)$ which depends on energy,

$$R(E_i) = \frac{Q_{ion}(E_i)}{Q_{inel}(E_i)} \tag{49.4}$$

such that,

$$R(E_i) = \begin{cases} 0, E_i < I \\ R_P, E_i = E_P \\ 1, E_i \gg I \end{cases} \tag{49.5}$$

where, E_P is the energy at which calculated Q_{inel} gains its maximum value. The particular form of the ratio as a continuous function of energy is developed by us,

$$R(E_i) = 1 - C_1\left[\frac{C_2}{U+a} + \frac{\ln U}{U}\right] \tag{49.6}$$

where, C_1, C_2 and a are target specific parameters. The detailed CSP-ic method can be found in our earlier publications [13–15].

49.3 Results and Discussion

In the present section, the results of total ionization cross-sections (Q_{ion}) for the gaseous H_2SO_4 molecule on collision with electrons for energy ranging from circa ionization threshold to 5000 eV have been reported along with Q_{inel} and $\sum Q_{exc}$. There are no previous results available for this molecule for comparison. Hence, we have adopted various models to study the e^-- H_2SO_4 scattering and the results are shown in Fig. 49.1. The Q_{ion} of H_2SO_4 are evaluated using different approximate

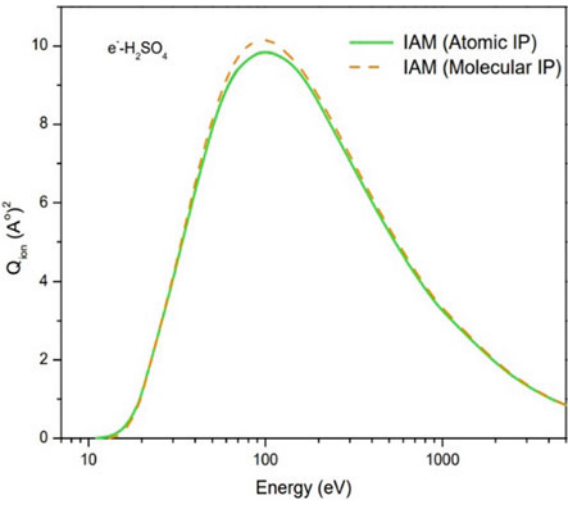

Fig. 49.1 Present Q_{ion} for e^-- H_2SO_4 collision. Red line: IAM with atomic IP, Green line: IAM with molecular IP

models, viz, Independent Atom model (IAM) with atomic ionization potential (IP) and molecular IP for constituent atoms are shown.

An interesting feature observed in Fig. 49.1 is that the cross-sections for IAM with atomic IP's and with molecular IP's are close to each other. One of the reasons may be due to the fact that IP's of the constituent atoms i.e. H (IP = 13.60 eV), S (IP = 10.36 eV), O (IP = 13.62 eV) and H_2SO_4 molecule (IP = 12.40 eV) do not differ much except for S. Particularly the IP of Oxygen and Hydrogen have values close to IP of H_2SO_4. IP of S is lower to IP of H_2SO4. When we add the cross-section of constituent atoms, the contribution of O is significantly more than that of S. For ready perusal we provide cross section data for e-H_2SO_4 collision using the IAM using the molecular properties in Table 49.2.

In Fig. 49.2 we show our result of e-H_2SO_4 for Q_{inel}, Q_{ion} and $\sum Q_{exc}$. We have compared our target molecule with other molecule, H_3PO_4 whose number of electrons is same as that of H_2SO_4 (N = 50). We have plotted the Q_{ion} for H_2SO_4 and H_3PO_4 molecules as shown in Fig. 49.2. The Q_{ion} are very sensitive to ionization potential of the target molecule. It can be seen that our calculated data and the data of Mozejko et al. [16] for H_3PO_4 show good matching with each other. The cross-sections for both the molecules seem to follow the same path. One of the reasons is their IP's are comparable to each other (11.72 eV for H_3PO_4 and 12.40 eV for H_2SO_4) and the number of electrons are also same.

Hence, it can be now noted that our Q_{ion} depends not only on ionization potential of the target molecule, but also the size of the target molecule that is number of electrons since the molecular charge cloud serves as the scatterer.

Table 49.2 Q_{inel}, Q_{ion} and ΣQ_{exc} in $(A^o)^2$ for e^--H_2SO_4 collision

Energy (eV)	Q_{inel}	Q_{ion}	ΣQ_{exc}
12.4 (IP)	0	0	0
20	3.07	1.07	2.00
40	11.26	6.48	4.78
60	13.88	9.12	4.76
80	14.12	10.00	4.11
100	13.61	10.14	3.46
150	11.92	9.63	2.28
200	10.30	8.73	1.57
500	5.70	5.34	0.36
1000	3.41	3.31	0.10
2000	1.94	1.91	0.02
3000	1.36	1.35	0.01
4000	1.04	1.03	0.00
5000	0.85	0.84	0.00

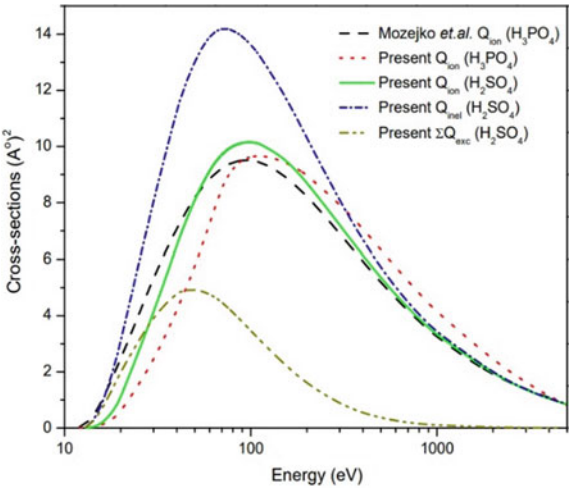

Fig. 49.2 Total cross-sections of H_2SO_4 and H_3PO_4. Solid line: present Q_{ion} of H_2SO_4; dash line: Mozejko et al. Q_{ion} for H_3PO_4; dot line: present Q_{ion} of H_3PO_4; short dash dot line: present Q_{inel} of H_2SO_4 and dash dot dot line: present ΣQ_{exc} of H_2SO_4

49.4 Conclusion

In this work results on computation of ionization probability through Q_{ion} is reported for electron interactions with H_2SO_4, which is a key element in atmospheric nucleation. We used the quantum mechanical approach, SCOP to compute Q_{inel} and obtained Q_{ion} using the (CSP-ic) formalism. We have studied the Q_{ion} using various models employed for molecular charge density viz., Independent Atom Model (IAM) with atomic and molecular IP's. We have shown Q_{ion} for H_2SO_4 and H_3PO_4 molecules

and it can be seen that our calculated data for H_3PO_4 is in good matching with available data of Mozejko et al. [16]. The Q_{ion} are very sensitive to ionization potential of target molecule and its size in terms of number of electrons (N = 50). As the IP of the target molecule increases, the peak value of Q_{ion} shifts towards high energy regime. Also, as the size of target decreases, the peak value of Q_{ion} also decreases. This observation can be seen in most of the targets.

References

1. J.H.Seinfeld et.al., Int. J. Mass Spect. **231**, 17–30 (2004)
2. K. McGouldrick, O.B.Toon, D.H.Grinspoon, Planet. Space Sci. **59**, 934–941 (2011)
3. Yao et al., Science **361**, 278–281 (2018)
4. M. Sipilä et al., Science **327**, 1243–1246 (2010)
5. U. Lohmannn, J. Frichter, Atmos. Chem. Phys. **5**, 715–737 (2005)
6. https://www.nasa.gov/centers/langley/news/factsheets/Aerosols.html
7. M. Swadia, Y. Thakar, M. Vinodkumar, C. Limbachiya, Eur. J. D **71**(4), 85 (2017)
8. D.R. Lide, *CRC Handbook of Chemistry and Physics* (CRC Press, Boca Raton FL2005, 1993–1994)
9. M. Vinodkumar, C. Limbachiya, A. Barot, N. Mason, Phys. Rev. A **87(1)**, 012702 (2013)
10. Y. Thakkar et al., Planet. Space Sci. **168**, 95–103 (2019)
11. A. Zecca, G.P. Karwasz, R.S. Brusa, Cz.Szmytkowski, J. Phys. B **24**, 2747 (1991)
12. A. Zecca, G.P. Karwasz, R.S. Brusa, Cz. Szmytkowski, J. Phys. Rev. A **45**, 2777 (1992)
13. K.N. Joshipura, B.G. Vaishnav, C.G. Limachiya, Pramana **66**(2), 403 (2006)
14. K.N. Joshipura, M.Vinodkumar, C.G.Limbachiya, B.K. Antony, Phys. Rev. A **69**, 022705 (2004)
15. K.N. Joshipura, N.J. Mason, *Atomic Molecular Ionization by Electron Scattering* (Cambridge University Press, 2019)
16. P. Mozejko, L. Sanche, Radiat. Phys. Chem. **73**, 77 (2005)

Total cross-sections for Adenine in aqua phase, by electron collision

Dhaval Chauhan[1], Smruti Parikh[1] and Chetan Limbachiya[1]
[1] *Department of Applied Physics, Faculty of Technology & Engineering, The Maharaja Sayajirao University of Baroda, India – 390002;*
Email: dschauhan-apphy@msubaroda.ac.in
Email: sparikh-apphyphd@msubaroda.ac.in
Email: *cglimbachiya-apphy@msubaroda.ac.in*

Abstract

In the present study we report, the total cross section (Q_T) for electron interaction with aqua adenine. To compute Q_T, we have used two different theoretical formalism: (1) Spherical Complex Optical potential (SCOP) at energy range threshold to 5 keV and (2) Two parameter semi empirical formalism (2p-SEM) at energy range 50 to 10 keV. The semi-empirical formula for electron scattering total cross-sections (Q_T) by analyzing its dependence on the impact energy and the target parameters, viz., number of molecular electrons (n_e) and the polarizability (α) of the molecule. This study is the first attempt to deduce the formula of Q_T for the large molecules ($55<n_e<95$) and for wide energy range from 50 eV to 10 keV. To validate the proposed formalism, the Q_T for aqua adenine molecule, who has 70 molecular electrons (i.e., $n_e=70$) has been computed and reliable data are obtained. This is the maiden attempt to compute Q_T for aqua Adenine.

Keywords: Total cross-sections, molecular polarizability, SCOP, DNA base

1. Introduction

The study of electron interaction with bio molecules and its constituents is strongly related to the importance of secondary electrons in the ionizing radiation damage to the living tissues(Bouchiha et al., 2006; Boudaiffa et al., 2000). The interaction of high energy ionizing radiation (i.e. β-rays, ϒ-rays, X-rays and others) with living tissue can produces different type of damages in DNA such as SSB (single strands breaks), DSB (double strand breaks), mutagenesis, lethality(Blanco et al., 2013; Sanche, 2003). Furthermore, it has capacity to induced cell death and produced carcinogenic effect. The low-energy electrons interact with biological media by inelastic effect such as ionization, vibrational, electronic excitation, rotational etc. To study and complete understanding of biological effect, Monte Carlo simulation(Rogers, 2006) is widely used. In MC simulation various parameters are needed include cross sections i.e. total cross section, ionization cross section, excitation cross section, elastic and inelastic cross section, etc.

In this paper, we report total cross section of electron collision with adenine ($C_5H_5N_5$) in aqua phase. To compute total cross section (Q_T), we have used two different formalisms: (1) SCOP formalism(Joshipura et al., 2004; Vinodkumar et al., 2011), energy range from threshold-5000 eV (2) 2p-SEM formalism, energy range from 50 eV to 10000 eV. The targets properties are shown in Table 1.

Table 1 Target Properties

Target	Aqueous phase *IE* (eV)	Energy band gap (E_{gap}) in eV	Polarizability α $(A^o)^3$
Adenine	5.00 (Crespo-Hernández et al., 2004; Fernando et al., 1998)	5.25 (Gop et al., 2019)	11.54

2. Theoretical Methodology

2.1 SCOP formalism

To calculate Q_{inel} and Q_{el}, we have employed spherical complex optical potential formalism with group additivity rule(Vinodkumar et al., 2011, 2013) since present molecules have larger physical size. This approach has been thoroughly discussed in our previous articles (Joshipura et al., 2004; Vinodkumar et al., 2013). The complex potential is given as,

$$V_{optical} = V_{real} + iV_{Ima} \quad (1)$$

The effect of static potential (V_s), exchange potential (V_{ex}), and polarization potential (V_{pol}) are included through the real part of the complex potential (V_{real}) and inelastic effects are incorporated through imaginary potential (V_{Ima}). To construct these potentials the primary input is charge density of the target(H.L.Cox ; R.A.Bonham, 1967). For exchange effects,(S. Hara, 1967) proposed model has been employed and for polarization, Zhang *et.al.* model potential is used.

$$V_{opt}(E_i, r) = V_{st}(r) + V_{ex}(E_i, r) + V_{pol}(E_i, r) + iV_{abs}(E_i, r) \quad (2)$$

To account inelastic effect the quasi-free modified model potential(Staszewska et al., 1983) is used. The final $V_{optical}$ is then fed into the Schrodinger equation, which is then solved numerically employing the partial wave approximation to compute the Q_{inel}, Q_{el}, and finally Q_T.

$$Q_T(E_i) = Q_{inel}(E_i) + Q_{el}(E_i) \quad (3)$$

The total cross section (Q_T) is the summed of all the inelastic and elastic processes(Chauhan &

Limbachiya, 2023; Limbachiya et al., 2014; Vinodkumar et al., 2003, 2005, 2011).

2.2 Two-parameter semi-empirical method (2p-SEM)

The impact energy dependence of the Q_T for the intermediate energy (Nishimura and Tawara, 1991; Zecca *et.al.*, 1991) and high energy (Joshipura and Vinodkumar, 1996; García and Manero, 1997) have been previously studied and the proposed formula was as follows,

$$Q_T = \frac{A}{E^B} \tag{1}$$

where, parameter A is governed by the molecular characteristics such as size of the molecule and its polarizability. The value of B for the high energies, above 500 eV will be ~ 0.7, which is proposed by (Joshipura and Vinodkumar, 1996; García and Manero, 1997) for smaller molecules i.e. for ten electrons (n_e=10) and up to n_e=22 electrons systems respectively. In the present work this formula has been derived for large molecules with $55 < n_e < 95$. Also, the dependence of Q_T on E_i is different for diverse energy regimes. In this work we have derived two different expressions for the intermediate ($50 < E_i < 500$ eV) and high energy regions ($E_i >$ 500 eV) for the complex and larger molecular systems with $55 < n_e < 95$.

Table 2 Parameter for 50 - 500 eV

Target	*Adenine*	*Guanine*	*Thymine*	*Cytosine*	*Uracil*
A	*46.53*	*54.79*	*43.66*	*34.68*	*34.56*
B	*0.58*	*0.56*	*0.57*	*0.56*	*0.53*

In table I, both the parameters A and B have been tabulated for the DNA bases and it is seen that the value of B is nearly same for all the molecules and is ~ 0.5. Our calculations reveal that the Q_T depends on energy (Vinodkumar *et.al.*, 2014) and the dependence on incident energy is similar as that of (Nishimura and Tawara, 1991) for 50-500 eV as,

$$Q_T = \frac{A}{\sqrt{E}} \tag{2}$$

However, the value of A is different for each molecule, suggesting its dependency on the number of target electrons (n_e).

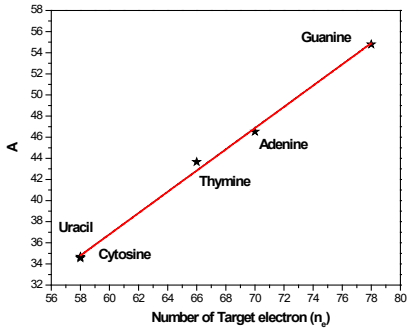

Figure 1 Parameter A vs. n_e (50<E_i<500)

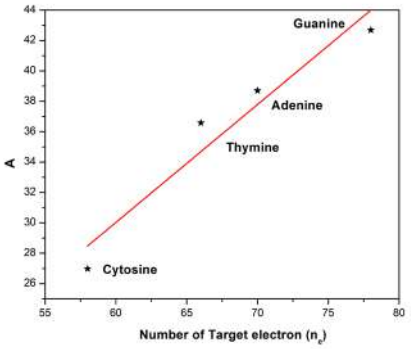

Figure 2 Parameter A vs. n_e (E_i > 500 eV)

To observe this relation, we plotted the graph of A vs n_e as shown in figure 1 and 2 for 50<E_i<500 eV and E_i > 500 eV respectively. The linear relationship observed in figure 1 is represented through the following equation,

$$A(n_e) = n_e - 23.54 \tag{3}$$

However, for a given n_e, the precision of this approximation can be enhanced by considering the difference between the actual values of 'A' (from table I) and those derived from equation (9) for each molecule. We have observed the dependency of this deviation (A - A(n_e)) on the molecular size through the polarizability (α). The linear relationship between them is,

$$A - A(n_e) = -0.003\alpha + 0.63 \tag{4}$$

Hence, from the equations (2), (3) and (4), a two-parameter expression for Q_T can be formulated for the energy range from 50-500 eV,

$$Q_T(n_e, \alpha) = \frac{n_e - 0.003\alpha - 22.91}{E^{0.56}} \tag{5}$$

Similar method has been followed to derive the two-parameter expression of Q_T as a function of α and n_e for the energies above 500 eV.

$$Q_T(n_e, \alpha) = \frac{0.016\alpha + 0.776n_e - 17.88}{E^{0.77}} \tag{6}$$

We note the power of energy E is $E^{0.56}$ for lower side and $E^{0.77}$ for higher side of the incident energy.

The two equations (5) and (6) provide the two parameter expressions for Q_T for impact energy 50 eV < E_i < 500 eV and E_i >500 eV respectively allowing the estimation of Q_T for the entire energy range of current study.

3. Results and Discussions

Total cross section (Q_T) is the sum of inelastic cross section (Q_{inel}) and inelastic cross section (Q_{el}). Figure 3, illustrate total cross-section for electron interaction with adenine in aqua phase using SCOP and 2p-SEM formalism for impact energy range from 11 to 10 keV.

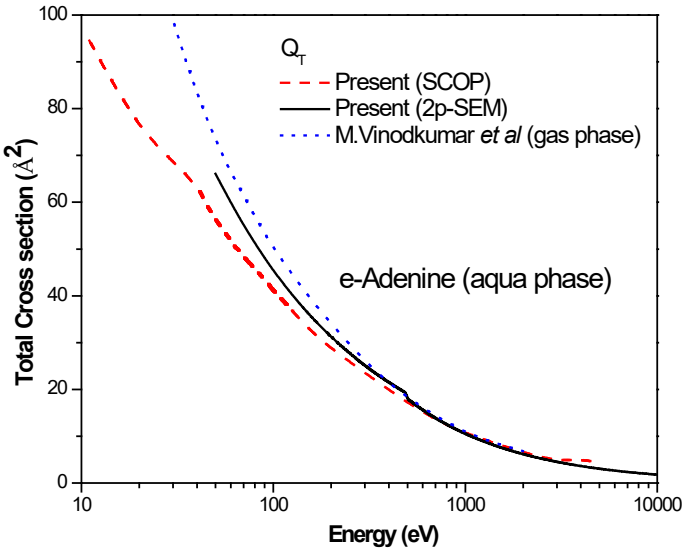

Figure 3 Total cross-sections for e^--Adenine.

In figure 3, Dash line denotes present SCOP result and Solid line denotes present 2p-SEM results. The total cross section (Q_T) data, of present SCOP result is excellent matching with present 2p-SEM result. There is no other comparison is available for aqua Adenine. So we compare our present Q_T (aqua phase) data with available total cross section of adenine in gas phase(Vinodkumar et al., 2014). Total cross section of gaseous phase is comparatively higher than the aqueous phase.

4. Conclusions

In the present work we have used SCOP method and 2p-SEM method to compute total cross section (Q_T) for the electron scattering with aqua Adenine. Also, we have proposed the two-parameter semi-empirical formula for the electron scattering total cross-sections (Q_T). This is the maiden attempt to derive the semi-empirical formula for Q_T for such molecules who has large number of electrons ($55<n_e<95$) and for the energy range from 50-10 keV. The proposed formula of Q_T shows the dependency of it on the two main target characteristics, i.e., number of electrons (n_e) and electric dipole polarizability (α). We computed the Q_T for aqua Adenine, who has 70 molecular electrons (i.e., $n_e=70$) by employing the proposed formulas and reliable

results were obtained.

References

Blanco, F., Muñoz, A., Almeida, D., Da Silva, F. F., Limão-Vieira, P., Fuss, M. C., Sanz, A. G., & García, G. (2013). Modelling low energy electron and positron tracks in biologically relevant media. *The European Physical Journal D 2013 67:9*, *67*(9), 1–18. https://doi.org/10.1140/EPJD/E2013-40276-1

Bouchiha, D., Gorfinkiel, J. D., Caron, L. G., & Sanche, L. (2006). Low-energy electron collisions with tetrahydrofuran. *Journal of Physics B: Atomic, Molecular and Optical Physics*, *39*(4), 975. https://doi.org/10.1088/0953-4075/39/4/021

Boudaiffa, B., Cloutier, P., Hunting, D., Huels, M. A., & Sanche, L. (2000). Resonant Formation of DNA Strand Breaks by Low-Energy (3 to 20 eV) Electrons. *Science*, *287*, 1658–1660.

Chauhan, D., & Limbachiya, C. (2023). Electron interactions with analogous of DNA/RNA nucleobases: 3-hydroxytetrahydroFuran and α-Tetrahydrofurfuryl alcohol. *Radiation Physics and Chemistry*, *207*. https://doi.org/10.1016/j.radphyschem.2023.110802

Crespo-Hernández, C. E., Arce, R., Ishikawa, Y., Gorb, L., Leszczynski, J., & Close, D. M. (2004). Ab initio ionization energy thresholds of DNA and RNA bases in gas phase and in aqueous solution. *Journal of Physical Chemistry A*, *108*(30), 6373–6377. https://doi.org/10.1021/jp049270k

Fernando, H., Papadantonakis, G. A., Kim, N. S., & Lebreton, P. R. (1998). Conduction-band-edge ionization thresholds of DNA components in aqueous solution. *Proceedings of the National Academy of Sciences of the United States of America*, *95*(10), 5550–5555. https://doi.org/10.1073/PNAS.95.10.5550/ASSET/DE08AE91-0885-4333-8540-6B4706FC83FB/ASSETS/GRAPHIC/PQ0980730006.JPEG

Gop, S., Sutradhar, R., Chakraborty, S., & Sinha, T. P. (2019). The study of energetic and electronic properties of metal-adenine complex in solvent phase: A density functional theory approach. *AIP Conference Proceedings*, *2162*. https://doi.org/10.1063/1.5130251

H.L.Cox ; R.A.Bonham. (1967). Cox_-_B. *The Journal of Chemical Physics*, *47*, 8.

Joshipura, K. N., Vinodkumar, M., Limbachiya, C. G., & Antony, B. K. (2004). Calculated total cross sections of electron-impact ionization and excitations in tetrahedral(XY4) and SF6 molecules. *Physical Review A* , *69*(2), 022705. https://doi.org/10.1103/PhysRevA.69.022705

Limbachiya, C., Vinodkumar, M., Swadia, M., & Barot, A. (2014). Electron impact total cross section calculations for CH3SH (methanethiol) from threshold to 5 keV. *Molecular Physics*, *112*(1), 101–106. https://doi.org/10.1080/00268976.2013.802038

Rogers, D. W. O. (2006). Fifty years of Monte Carlo simulations for medical physics. In *Physics in Medicine and Biology* (Vol. 51, Issue 13, p. 287). Institute of Physics Publishing. https://doi.org/10.1088/0031-9155/51/13/R17

S. Hara. (1967). hara1967. *JOURNAL OF THE PHYSICAL SOCIETY OF JAPAN*, *22*, 3.

Sanche, L. (2003). *NANOSCOPIC ASPECTS OF RADIOBIOLOGICAL DAMAGE : FRAGMENTATION INDUCED BY SECONDARY LOW-ENERGY ELECTRONS*. 349–369. https://doi.org/10.1002/mas.10034

Staszewska, G., Schwenke, D. W., Thirumalai, D., & Truhlar, D. G. (1983). Quasifree-

scattering model for the imaginary part of the optical potential for electron scattering. *Physical Review A*, *28*(5), 2740. https://doi.org/10.1103/PhysRevA.28.2740

Vinodkumar, M., Bhutadia, H., Limbachiya, C., & Joshipura, K. N. (2011). Electron impact total ionization cross sections for H2S, PH3, HCHO and HCOOH. *International Journal of Mass Spectrometry*, *308*(1), 35–40. https://doi.org/10.1016/j.ijms.2011.07.017

Vinodkumar, M., Joshipura, K. N., Limbachiya, C. G., & Antony, B. K. (2003). Electron impact ionization of H2O molecule in crystalline ice. *Nucl. Instr. and Meth. in Phys. Res. B 212*, *212*(1–4), 63–66. https://doi.org/10.1016/S0168-583X(03)01480-0

Vinodkumar, M., Joshipura, K. N., Limbachiya, C. G., & Antony, B. K. (2005). Electron impact total and ionization cross-sections for some hydrocarbon molecules and radicals. *The European Physical Journal D - Atomic, Molecular, Optical and Plasma Physics 2005 37:1*, *37*(1), 67–74. https://doi.org/10.1140/EPJD/E2005-00257-7

Vinodkumar, M., Limbachiya, C., Barot, A., & Mason, N. (2013). Computation of electron-impact rotationally elastic total cross sections for methanol over an extensive range of impact energy (0.1 - 2000 eV). *Physical Review A - Atomic, Molecular, and Optical Physics*, *87*, 012702. https://doi.org/10.1103/PhysRevA.87.012702

Vinodkumar, M., Limbachiya, C., Barot, M., Barot, A., & Swadia, M. (2014). Electron impact total cross sections for components of DNA and RNA molecules. *International Journal of Mass Spectrometry*, *360*(1), 1–7. https://doi.org/10.1016/j.ijms.2013.12.027

Correlation study of electron scattering total cross-sections, impact energy and target parameters

Smruti Parikh[1], Dhaval Chauhan[1] and Chetan Limbachiya[1]
[1]*Department of Applied Physics, Faculty of Technology & Engineering, The Maharaja Sayajirao University of Baroda, India – 390002*
Email: sparikh-apphyphd@msubaroda.ac.in
Email: dschauhan-apphy@msubaroda.ac.in
Email: *cglimbachiya-apphy@msubaroda.ac.in*

Abstract

Present study aims to derive the semi-empirical formula for electron scattering total cross-sections (Q_T) by analysing its dependence on the impact energy and the target parameters, viz., number of molecular electrons (n_e) and the polarisabilty (α) of the molecule. This study is the first attempt to deduce the formula of Q_T for the large molecules ($55<n_e<95$) and for wide energy range from 50 eV to 10 keV. To validate the proposed formalism, the Q_T for α-tetrahydrofurfuryl alcohol (THFA) molecule, who has 56 molecular electrons (i.e., $n_e=56$) has been computed and reliable data are obtained.

Keywords: Total cross-sections, molecular polarizability, number of molecular electrons

1. Introduction

The total cross-sections (Q_T) for electron interactions with atom and molecules were first measured in the early 20th century (Lennard, 1903; Ramsauer, 1921; Brüche, 1927). Many scientific and technological applications, such as astrophysics, atmospheric physics, nuclear fusion, etc., require the total cross section values for electron-molecule interactions. As a result, there has been an upsurge in the number of relevant works (Joshipura *et.al.*, 1997; 2004; Itikawa, 2009; Limbachiya *et.al.*, 2014; 2015; Swadia *et.al.*, 2017) done since more than 100 years.

Ever since the first rigorous measurements of electron interaction cross sections, efforts to study the relationships between these cross sections and the physico-chemical characteristics of the target systems have been made. When such correlations discovered, they may reveal the role of specific microscopic target features in the scattering process, while the semiempirical equations defining these correlations should aid in estimating Q_T of molecules for which experimental data or computations are not available.

In order to determine how the cross sections differ amongst target families, Q_T at intermediate energies have been studied since the early of 20th century (Brüche, 1927). For a series of simple hydrocarbons, (Floeder *et.al.*, 1985) measured Q_T for positron and electron collisions and discovered that, for the intermediate energies 100-400 eV, the Q_T for these species is linearly

correlated with the number of constituent electrons (n_e). (Nishimura and Tawara, 1991) also found the relationship between the geometrical size of the compounds and the Q_T in the intermediate energy range. (Szmytkowski, 1989) found that the total cross section is strongly correlated with the dipole polarizability (α) of the molecule for a group of different atoms and molecules, for the energy range from 50 to 400 eV. The association between the Q_T and n_e has been also validated by (Jain and Baluja, 1992), but failed to support the molecular polarizability correlation with Q_T. The energy dependence of the Q_T has been studied by (Joshipura and Vinodkumar, 1996) and (García and Manero, 1997) for the high energies (beyond 500 eV) for the small molecules (n_e=10 to 22).

The aim of the reported work is to come up with a 2-parameters semi-empirical formula of Q_T, which includes the dependency of the target parameters (n_e and α) for the energies from 50 eV-10 keV for larger molecules, whose number of electrons (n_e) ranges between 55-95.

2. Theoretical Methodology

2.1 Two-parameter semi-empirical method (2p-SEM)

The impact energy dependence of the Q_T for the intermediate energy (Nishimura and Tawara, 1991; Zecca *et.al.*, 1991) and high energy (Joshipura and Vinodkumar, 1996; García and Manero, 1997) have been previously studied and the proposed formula was as follows,

$$Q_T = \frac{A}{E^B} \tag{1}$$

where, parameter A is governed by the molecular characteristics such as size of the molecule and its polarizability. The value of B for the high energies, above 500 eV will be ~ 0.7, which is proposed by (Joshipura and Vinodkumar, 1996; García and Manero, 1997) for smaller molecules i.e., for ten electrons (n_e=10) and up to n_e=22 electrons systems respectively. In the present work this formula has been derived for large molecules with $55 < n_e < 95$. Also, the dependence of Q_T on E_i is different for diverse energy regimes. In this work we have derived two different expressions for the intermediate ($50 < E_i < 500$ eV) and high energy regions ($E_i >$ 500 eV) for the complex and larger molecular systems with $55 < n_e < 95$.

Table 1 Parameter for 50 - 500 eV

Target	*Adenine*	*Guanine*	*Thymine*	*Cytosine*	*Uracil*
A	*46.53*	*54.79*	*43.66*	*34.68*	*34.56*
B	*0.58*	*0.56*	*0.57*	*0.56*	*0.53*

In table I, both the parameters A and B have been tabulated for the DNA bases and it is seen that the value of B is nearly same for all the molecules and is ~ 0.5. Our calculations reveal that the Q_T depends on energy (Vinodkumar *et.al.*, 2014) and the dependence on incident energy is similar as that of (Nishimura and Tawara, 1991) for 50-500 eV as,

$$Q_T = \frac{A}{\sqrt{E}} \tag{2}$$

However, the value of A is different for each molecule, suggesting its dependency on the number of target electrons (n_e).

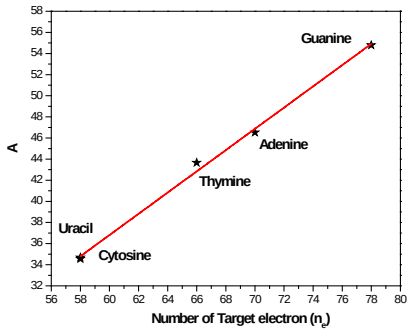

Figure 1 Parameter A vs. n_e ($50<E_i<500$)

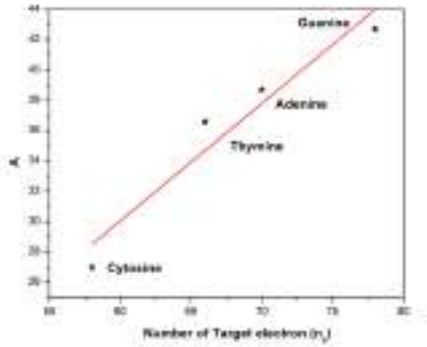

Figure 2 Parameter A vs. n_e ($E_i > 500$ eV)

To observe this relation, we plotted the graph of A vs n_e as shown in figure 1 and 2 for $50<E_i<500$ eV and $E_i > 500$ eV respectively. The linear relationship observed in figure 1 is represented through the following equation,

$$A(n_e) = n_e - 23.54 \tag{3}$$

However, for a given n_e, the precision of this approximation can be enhanced by considering the difference between the actual values of 'A' (from table I) and those derived from equation (9) for each molecule. We have observed the dependency of this deviation ($A - A(n_e)$) on the molecular size through the polarizability (α). The linear relationship between them is,

$$A - A(n_e) = -0.003\alpha + 0.63 \tag{4}$$

Hence, from the equations (2), (3) and (4), a two-parameter expression for Q_T can be formulated for the energy range from 50-500 eV,

$$Q_T(n_e, \alpha) = \frac{n_e - 0.003\alpha - 22.91}{{E_i}^{0.56}} \tag{5}$$

Similar method has been followed to derive the two-parameter expression of Q_T as a function of α and n_e for the energies above 500 eV.

$$Q_T(n_e, \alpha) = \frac{0.016\alpha + 0.776 n_e - 17.88}{{E_i}^{0.77}} \tag{6}$$

We note the power of energy E_i is ${E_i}^{0.56}$ for lower side and ${E_i}^{0.77}$ for higher side of the incident energy.

The two equations (5) and (6) provide the two parameter expressions for Q_T for impact energy 50 eV < E_i < 500 eV and E_i >500 eV respectively allowing the estimation of Q_T for the entire energy range of current study.

3. Results and Discussions

To validate our 2p-SEM formalism, we choose the case of α-tetrahydrofurfuryl alcohol (THFA), who has a total of 56 molecular electrons (i.e., n_e=56) and its polarisability (α) is 10.4 $Å^3$. The computed Q_T of THFA molecule has been displayed in figure 3 for impact energies from 50-10000 eV.

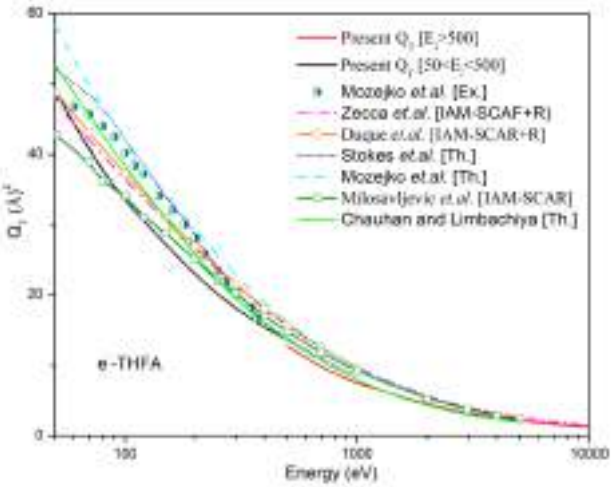

Figure 3 Total cross-sections for e^--THFA.

The connection between the present Q_T data for energies 50-500 eV and that of for 500-10000 eV can be observed from figure 3, which validates our proposed 2p-SEM formalism. We have compared the present Q_T results with the existing theoretical and experimental data. From the figure it can be seen that the present data can be seen in good agreement with the results of (Milosavljevic *et.al.*, 2006). However, the present curve shows minute deviation at low energy side from the existing results of (Zecca *et.al.*, 2011; Duque *et.al.*, 2014; Chauhan and Limbachiya, 2023). The Q_T data of (Mozejko *et.al.*, 2005;2006; Stokes *et.al.*, 2021) shows the higher values than the existing ones. However, at the energies above 300 eV, all the existing results tend to merge with each other.

4. Conclusions

In the present work we have proposed the two-parameter semi-empirical formula for the electron scattering total cross-sections (Q_T). This is the maiden attempt to derive the semi-empirical formula for Q_T for such molecules who has large number of electrons (55<n_e<95)

and for the energy range from 50-10 keV. The proposed formula of Q_T shows the dependency of it on the two main target characteristics, i.e., number of electrons (n_e) and electric dipole polarizability (α). We computed the Q_T for α-tetrahydrofurfuryl alcohol (THFA) molecule, who has 56 molecular electrons (i.e., n_e=56) by employing the proposed formulas and reliable results were obtained.

References

Brüche, E. (1927). Ann. Phys. 83, 70.
Chauhan, D., and Limbachiya, C. (2023). Radiat. Phys. Chem. 207, 110802.
Duque, H. V., Chiari, L., Jones, D. B., Thorn, P. A., Pettifer, Z., da Silva, G. B., Limao-Vieira, P., Duflot, D., Hubin-Franskin, M. J., Delwiche, J., Blanco, F., Garcia, G., Lopes, M. C. A., Ratnavelu, K., White, R. D., Brunger, M. J., (2014). Chem. Phys. Lett. 608, 161–166.
Floeder, K., Fromme, D., Raith, W., Schwab, A., and Sinapius, G. (1985). J. Phys. B: At. Mol. Phys. 18, 3347.
García, G., and Manero, F. (1997). Chem. Phys. Lett. 280, 419.
Itikawa, Y. (2009). Journal of Physical and Chemical Reference Data 38, 1.
Jain, A., and Baluja, K. L. (1992). Phys. Rev. A 45, 202.
Joshipura, K., and Vinodkumar, M. (1996). Pramana-Journal of Physics 47, 57-63.
Joshipura, K. N., and Vinodkumar, M. (1997). Phys. Lett. A 224, 361-366.
Joshipura, K. N., Vinodkumar, M., Limbachiya, C., and Antony, B. K. (2004). Phys. Rev. A 69, 22705.
Lennard, P. (1903). Ann. Phys. 12, 714.
Limbachiya, C., Vinodkumar, M., Swadia, M., and Barot, A. (2014). Molecular Physics 112, 101-106.
Limbachiya, C., Chaudhary, A., Desai, H., and Vinodkumar, M. (2015). RSC Advances 5, 103964-103976.
Milosavljević, A. R., Blanco, F., Šević, D., Garcia, G., and Marinković, B. P. (2006). European Physical Journal D 40, 107–114.
Mozejko, P., Sanche, L., (2005). Radiat. Phys. Chem. 73, 77–84.
Mozejko, P., Domaracka, A., Ptasińska-Denga, E., Szmytkowski, C., (2006). Chem. Phys. Lett. 429, 378–381.
Nishimura, H., and Tawara, H., (1991). J. Phys. B: At. Mol. Opt. Phys. 24, L363.
Ramsauer, C. (1921). Ann. Phys. 64, 513.
Szmytkowski, Cz. (1989). Z. Phy. D- Atoms, Molecules and Clusters 13, 69-73.
Swadia, M., Thakar, Y., Vinodkumar, M., and Limbachiya, C. (2017). Eur. Phys. J. D 71, 1-5.
Stokes, P. W., Foster, S. P., Casey, M. J. E., Cocks, D. G., Gonzalez-Magana, O., de Urquijo, J., Garcia, G., Brunger, M. J., White, R. D. (2021). J. Chem. Phys. 154, 084306.
Vinodkumar, M., Limbachiya, C., Barot, M., Barot, A., and Swadia, M. (2014). Int. J. Mass Spectrom. 360, 1-7.
Zecca, A., Karwasz, G., and Brusa, R. (1991). Phys. Rev. A 45, 2777.
Zecca, A., Chiari, L., Garcia, G., Blanco, F., Trainotti, E., Brunger, M. J. (2011). New J. Phys. 13, 063019.